Title
Metabolic and Intracellular Signaling Mechanisms of Hair Follicle Stem Cell Activation

Author
MirandaSalmeron, Matilde

Publication Date
2020

Peer reviewed|Thesis/dissertation

UNIVERSITY OF CALIFORNIA

Los Angeles

Metabolic and Intracellular Signaling Mechanisms of Hair Follicle Stem Cell Activation

A dissertation submitted in partial satisfaction of the requirements for the degree Doctor of Philosophy in Molecular Biology

by

Matilde Miranda

2020

ABSTRACT OF THE DISSERTATION

Metabolic and Intracellular Signaling Mechanisms

of Hair Follicle Stem Cell Activation

by

Matilde Miranda

Doctor of Philosophy in Molecular Biology

University of California, Los Angeles, 2020

Professor William Edward Lowry, Chair

The hair follicle is considered a mini-organ which makes it a useful model for studying regenerative processes and cross-tissue interactions due to its unique populations of cell types and specialized pools of adult stem cells. Hair itself is a defining feature of the skin organ and is critical for external protection, thermoregulation, sweat and pheromone relays, and social interactions. In the bulge niche, hair follicle stem cells (HFSCs) oscillate between activation and quiescence to create the hair cycle. This process is cyclically and dynamically maintained throughout a coated animal's lifetime, requiring precise temporal and spatial control of the HFSC niche. However, a complete inventory of the mechanisms underlying hair follicle homeostasis remains unclear. Herein I will briefly explain the current dogma of signaling pathways regulating HFSCs. But, the novelty of my work will go on to further describe the synergistic – yet understudied – roles of metabolic control and canonical G-protein coupled receptors (GPCR) and signaling in modulating downstream genes facilitating HFSC biology. The data out of these projects of course will yield new avenues for the development of

metabolic/pharmacological compounds alike for regenerative medicine and equally important molecular management of adult stem cell homeostasis.

The dissertation of Matilde Miranda is approved.

Heather R. Christofk

Brigitte Gomperts

Dana Leanne Jones

David Walker

William Edward Lowry, Committee Chair

University of California, Los Angeles

2020

This dissertation is dedicated to

My loving family, through thick and thin:

Julio Cesar Miranda, PhD; Matilde Salmeron Miranda, and Mauricio Miguel Miranda

TABLE OF CONTENTS

ACKNOWLEDGEMENTS

One of my sources of energy has – and always will be – the communities of people that I consider mentors, colleagues, peers, family, and friends. Though I consider myself to be a massive introvert, I treasure good company. Whether that is amongst lab/grad program/cohort/dodgeball mates, the past several years have been rich with relationships that have been sources of support during everything that life has (sometimes literally) thrown my direction.

Firstly, my family have instilled in me a fierce desire to be better and change the world. As a child of immigrants, this sort of pressure was overwhelming at times, but it is also the same reason for my unwavering resilience. Their love is strong. To Mom and Dad, thank you for all the sacrifices for sending Mauricio and me to get high quality education, and also teaching us discipline along the way with equally important life and karate lessons. To Gerald(ine), for being my sister, for being the one who picked me up and took me to school as a kid, only to then help take me to school once more when I moved to UCLA Graduate Housing 6 years ago. To Julio, for being my big brother, for showing me how to be tough yet playful; I will never forget Tiger Cruise on the naval carrier and all the activities we did to understand (or try to understand) why you were always on a fancy boat. Finally, to the Betanco family, who have literally been my second family before PhD was even an idea in my head. For letting me rest when I have visited the past 6 years. For feeding me when I have been too stressed to eat. For treating me like I was your own daughter. Having twice the amount of family love is rare in this day and age and I hold it all close to my heart.

I always like to tell people that I selected UCLA and the Lowry Lab out of a gut feeling. During the interview process, I was looking for somewhere where I could be happy; cutting-edge research was a given at all the institutions I was considering. I was lucky enough to learn during my undergraduate research experience that a good mentor and good community make me happy, and in turn more productive about work and achieving my goals. I remember Bill's personable demeanor during my interview weekend (even if he got my name wrong at first) but what struck me the most was that he personally reached out after the interview to dispel any hesitations I had about choosing the Molecular Biology program at UCLA. That really cemented it for me. This was someone that cared deeply and could see my potential, even if I wasn't aware of it myself. I will now admit here that Dr. William Edward Lowry was in my top three reasons for choosing UCLA for grad school.

Bill Lowry is a mentor that is remarkably kind, and I believe that is what also allows him to be brilliant. His open-door policy is not restricted to just for project discussions, but also for matters of the heart. He is a mentor that has built me up when I frequently felt down and out. Bill is unabashedly human and has taught me to own that part of myself, as good scientists are humans at their core. I am beyond grateful for having a mentor that permitted me the space to grow in science alongside my personal journey as an independent young woman.

So, I'll come clean. I already said I am a massive introvert, but I really love being surrounded by good people. Bill does a remarkable job choosing people that eventually become part of the lab family. Another thing I know is that the way to my heart is through my stomach. I will fondly remember how the lab would lunch together almost

every day. Our gatherings almost always revolved around food: Korean Barbecue, DineLA, birthday cake celebrations, potluck holiday parties, etc. People may come and go over the years, but there is something very special when you are able to share a meal with like-minded people. Perhaps that is the secret to having a good lab environment. Bill might be on to something...

Thank you to my dodgeball family, for busting my nose (accidentally) *the very first time* I played as an adult. I have not missed a season playing the West LA league since that fateful day six years ago. It was truly a rite of passage, as a newcomer to LA and grad school. Fun fact: It was both picture day and my first day in the Lowry Lab the day after my injury. The rest is history. My heart goes out to my marvelous teammates...to many that have turned into marvelous friends. Hope to see you all on the court again soon!

Thank you to my “MBI Kidz” cohort for the endless laughs, dank memes, and fierce camaraderie since our famous games of Never-Have-I-Ever way back in first year. It fills my heart that many of you are going to fantastic places to keep being remarkable scientists and quality humans.

Thank you to the GPB and MBI programs, for seeing value in faculty/student community. Interacting with my colleagues/peers throughout the years helped me find guidance and then pay it forward when it was time. I am grateful that you taught me the importance of self-care, even if that means admitting my vulnerabilities to let myself grow with grace.

Coming to Los Angeles has helped me find my people in many ways and with many groups. Thank you for the wonderful laughs and memories that I will cherish

forever. My world is better because of these relationships. Thank you for the adventures. I am so excited for the next chapter of my science and life journey. I hope I do not come off as dramatic by saying my dreams are coming true. I promise to take full advantage of these opportunities to make lasting impacts in many contexts.

The work presented here is made possible by numerous funding mechanisms. My first two years were sponsored by the National Science Foundation Bridge to the Doctorate Program. For years 3-5, my funding source was the National Science Foundation Graduate Research Fellowship. My final year of graduate studies was funded by the UCLA Graduate Division Eugene V. Cota-Robles Fellowship.

VITA

EDUCATION

University of California, Los Angeles 2016

Ph.D. Candidate, Molecular Biology (Cell and Developmental Biology)

San Francisco State University 2014

B.S., *magna cum laude*, Cell and Molecular Biology

RESEARCH EXPERIENCE

University of California, Los Angeles 2015 - present

Graduate Student Researcher; Advisor: William E. Lowry, PhD

San Francisco State University 2011-2014

Undergraduate Student Researcher; Advisor: Laura W. Burrus, PhD

PUBLICATIONS

Miranda MM, Avila I, Esparza J, Shwartz Y, Krall A, Christofk H, Hsu YC, Berdeaux R, and Lowry WE. Defining the mechanism of GPCR/cAMP/Creb signaling in HFSC activation. **In preparation, submitted (2020).**

Miranda MM and Lowry WE. Hip to the Game: YAP/TAZ is required for nonmelanoma skin cancers. *The EMBO Journal* (2018) e99921.

Miranda MM, Christofk H, Jones DL, Lowry WE. Topical inhibition of the electron transport chain can stimulate the hair cycle. *Journal of Investigative Dermatology* (2017).

Flores A, Schell J, Krall AS, Jelinek D, **Miranda MM**, Grigorian M*, et al.* ...Lowry WE. Lactate dehydrogenase activity drives hair follicle stem cell activation. *Nat Cell Biol* (2017) 19:1017-26.

Miranda MM, Galli LM, Enriquez M, Szabo LA, Gao X, Hannoush RN, Burrus LW. Identification of the WNT1 residues required for palmitoylation by Porcupine. *FEBS Letters* (2014), Volume 588, Issue 24, 4815-4824.

SELECTED HONORS AND AWARDS

UCLA Eugene V. Cota-Robles Graduate Fellowship	2019-2020
UCLA Edward A. Bouchet Graduate Honor Society Nominee	2019
UCLA MBI Teaching Excellence Award Nominee	2018
UCLA GPB Bioscience Fellowship Incentive Award	2018
Notre Dame High School Women of Impact - 30 under 30 Honoree	2018
UCLA GPB Bioscience Fellowship Incentive Award	2017
NSF Emerging Researchers National First Place Oral Presentation	2017
UCLA GPB Bioscience Fellowship Incentive Award	2016
Kenneth I. Shine Fellowship Recipient	2016
National Science Foundation Graduate Research Fellow	2015-2019
Ford Foundation Predoctoral Fellowship Recipient (declined)	2015
National Science Foundation Bridge to the Doctorate Scholar	2014-2020
Magna Cum Laude	2014

INTELLECTUAL PROPERTY

Utility Patent Application, Based on U.S. Provisional Application No.: 62/672,935

Title: COMPOSITIONS AND METHODS FOR MODULATING HAIR GROWTH

Filing Date: May 17, 2019

Inventor(s): William E. Lowry *et al.*

Patent Cooperation Treaty (PCT) Based on U.S. Provisional Application No.: 62/566,031

Title: COMPOSITIONS AND METHODS FOR MODULATION HAIR GROWTH

Filing Date: September 29, 2018

Inventor(s): William E. Lowry *et al.*

Chapter 1: Introduction

Molecular Mechanisms Regulating Hair Follicle Stem Cell Activation

Skin Architecture

The skin is a sophisticated multilayer organ, comprised of stratified epithelium to provide a barrier from external damage. The skin is necessary for protection from external stressors, thermoregulation, mechanosensation, and important in social communications. In mammals, skin barrier formation occurs during embryonic development and is a result of a milieu of cell types interacting together to provide appropriate cues for the stratification and specialization[1] of skin layer types prior to birth. This results in the established anatomy of the skin: outer epidermis, the underlying dermis, and hypodermis layers. The epidermis is the outermost layer of the skin and its primary function is to function as a barrier from injuries/infections and to retain water. The epidermis is stratified, where the most basal layer contains stem cells that function for optimal cell turnover to maintain the skin barrier. Underneath, the dermis is primarily made up of fibroblasts, the cells responsible for generating various types of collagen and other elastic fibers for extracellular matrix function and skin elasticity. Lastly, the hypodermis (a.k.a subcutaneous fat later) acts as a cushion and insulation layer, containing fat deposits that can also be used for energy.

The hair follicle is an intricate structure that also helps maintain the skin barrier. Hair follicles are densely innervated[2], further aiding in mechanosensory function of the skin through piloerectile movements, especially in the context of social communication. Hair fibers are some of the main physiological features in people that can be fully manipulated without painful side effects. Thus, maintenance of the hair follicle – or lack thereof – extends past physiological effects, greatly impacting psychological and social status to underscore the need for many applications in clinical settings.

The Hair Cycle

The hair follicle has fascinated biologists for decades. At its core, it is a regenerating biological system[3]. The hair follicle appendage undergoes cyclical bouts of rest and growth across a coated organism's lifetime (Figure 1)[4-6]. Hair follicles contain adult stem cells that can replenish cell turnover to regulate homeostasis or repair upon wound healing[7]. The bulge was recognized as a "hot spot" as early as 1876 by the researcher Unna whom theorized this area was where the hair shaft continued to grow; in 1903 the researcher Stöhr deemed the area the "bulge".

Adult stem cells located near the base of the follicle captured researchers' interests because of a nucleotide analog pulse-chase experiments, where slow-cycling cells retained signal better, i.e. did not dilute out the nucleotide label through multiple mitotic cycles[8]. It is important to highlight researchers did not find these cells at the hair bulb, but adjacent to the arrector pili muscle in a specialized niche where these unique cells remained relatively undifferentiated for periods upwards of 14 months in murine follicles[9]. These cells also exist in a similar area in human skin[10].

These unique label-retaining cells – coined hair follicle stem cells (HFSCs) – are multipotent epithelial stem cells that permanently reside in a region called the "bulge" and are responsible for producing a hair shaft *de novo* with every round of the hair cycle[8]. Even so, HFSs are more quiescent than other epidermal cells[9]; homeostasis in other skin tissues are maintained by resident stem cells independently of HFSC behaviors. However, during acute injury, HFSCs possess the remarkable ability to generate all skin tissue lineages for successful wound healing[7].

In the telogen (rest) phase of the hair cycle, HFSCs are dormant and no active hair growth is observed. Upon telogen-to-anagen transition (also known as anagen onset), the transit-amplifying cells of the bulge differentiate and begin to create a dynamic structure at the base of the hair follicle called the matrix, which will eventually produce a new hair shaft. In the anagen (growth) phase, bulge stem cells rapidly proliferate and migrate downwards to generate the outer root sheath, the adjacent inner root sheath, and the complete structure of the hair shaft that protrudes out to lay flat on the top layer of the epidermis. The catagen (regression) phase then follows with reduced proliferation and increased apoptosis of the base of the follicle below the bulge, diminishing overall hair follicle size back to that normally observed in telogen. Another telogen (rest) phase occurs, beginning the cycle of hair follicle stem cell quiescence and prospective activation once more. Although the bulge is the source of cells that ultimately become hair, a notable structure to highlight is the dermal papilla (DP). The DP is a structure mesenchymal in origin and function, where these cells help relay signals influencing the hair cycle to the adjacent HFSC niche[11, 12].

In a normal human scalp, a great majority of follicles are in the anagen phase – and remain in such a state for several decades of life[13]. This significantly differs from the murine hair cycle, where follicles remain in anagen for approximately two weeks prior to catagen and telogen anew[14]. Activation of hair follicle stem cells coincides with other dermal events, such as subcutaneous adipose expansion, melanocyte proliferation, and dermal thickening[15]. There is also evidence that HFSC activation is heterogenous, and that hair cycling is a result of a two-step mechanism of stem cell activation for the hair cycle to be complete[16]. Indeed, two distinct HFSC populations

exist in the bulge – quiescent HFSCs and primed HFSCs; primed HFSCs are the first set of stem cells to activate in telogen-to-anagen transition to regeneration the lower half of hair follicle undergoing anagen. Quiescent HFSCs do not contribute to hair growth at the peak of anagen.

The hair follicle has long been a classic model to study crosstalk between tissue types, resident adult stem cell pools, and mechanisms regulating stem cell homeostasis – especially during regeneration (i.e. hair cycling). Delays in anagen entry are observed in hair loss disorders such as alopecia[17]. Many signaling pathways coalesce in the stem cell niche to mitigate proper hair follicle appendage form and function, and emerging research on hair loss disorders focus on the interplay of these cell-extrinsic cues. These types of questions usually rely on mouse modes for an intact HFSC niche platform. In addition, HFSCs can be isolated via FACS with the surface markers CD34 and CD49f (alpha6 integrin), though additional markers can be used to further refine subpopulations in this pool of adult stem cells[18] to further investigate the molecular shifts necessary for stem cell state. Here, I report on a handful of signaling pathways that are implicated in maintaining proper hair cycling.

Hair Loss Disorders

Hair loss is unfortunately a common condition that affects men and women alike. Hair loss is the result of an amalgam of abnormal states: hormonal imbalance, age, level of stress, immune condition, genetics – just to name a few. While hair loss itself is not physiologically painful, it can greatly affect well-being and quality of life.

Telogen effluvium is a temporary phenomenon characterized by excessive shedding and prolonged telogen. It is usually caused by some shock to the system, anecdotally from extreme stress and/or trauma[19]. Androgenetic alopecia (a.k.a male/female pattern hair loss) is the most common type of hair loss and is caused by dysfunctional mesenchymal cells (specialized fibroblasts) at the base of the hair follicle, in the DP. Pathologically, it resembles hair follicle aging – complete with hair follicle miniaturization, prolonged telogen, and transdermal elimination of the entire follicular unit[20, 21]. The presumed mechanism of this type of hair loss due to high activity of 5α-reductase, the enzyme responsible for converting testosterone into dihydrotestosterone (DHT). An accumulation of DHT acts as an allosteric inhibitor towards the androgen receptor, blocking any testosterone and negating HFSC activation via stunted DP signaling. This induces cell senescence, shrinking of the DP, prolonged telogen, shortening telogen, and progressive follicular atrophy to yield macroscopic hair loss[22-24].

Alopecia areata (a.k.a spot baldness) is largely attributed to misguided inflammatory attacks (i.e. reactive T cell infiltration into the hair follicle) against anagen hair follicles, with its severity ranging from singular patches of hair loss to universal loss of hair across the skin (alopecia totalis). Chronic inflammation will render HFSCs dormant and arrested in telogen. Clinical treatments to alleviate this inhibitory phenotype include local/systemic steroids or immunomodulatory therapeutics to restore hair growth. On the other hand, resident macrophages adjacent to the hair follicle can provide morphogens and growth factors that stimulate cell proliferation and thus, HFSC

activation and anagen as a wounding response to minor skin organ trauma (hair plucking, scratching).

Anagen hair follicles are massive sources of proliferating cells, making them sensitive to genotoxic stressors from therapies such as chemotherapy and radiotherapy. Due to the nature of these treatments to target fast-growing cells (as those found in cancer), this same systemic treatment has many unfortunate consequences for other healthy populations of fast-dividing cell populations – like those found in the epidermis, hair follicle root, and gastrointestinal tract. Hair follicles will undergo a swift catagen phase to reset back to telogen. Depending on the severity of the treatment(s), the following anagen cycle may be able to replenish hair shafts loss in the process.

To date, only two FDA-approved drugs are available for treating hair loss, but their end results have been reported as variable and temporary. Minoxidil (brand name Rogaine) was the first FDA-approved medication for alleviating androgenetic alopecia. Developed in the 1950s, it was initially used for targeting potassium channels for the treatment of hypertension. In regards to hair growth, its mechanism of action is poorly understood – but a popular hypothesis is that the drug is able to increase blood flow that can go on to feed and nourish proliferating cells involved in anagen induction. There is also evidence that minoxidil may work by inhibiting HIF-degrading enzyme, activating growth factor signaling via VEGF[25]. Finasteride (brand name Propecia) and dutasteride appeared on the market later on, and these pharmaceuticals function to inhibit 5α-reductase activity and allow for reversal of DHT-affiliated balding.

Signaling Pathways Regulating the Hair Cycle

The HFSC niche is highly specialized, full of stimuli acting on the micro- or macro- level(s) of the environment. As such, the hair follicle is a hub of cell types that appropriately respond to/influence a milieu of signaling mechanisms. Appropriate understanding of activating or inhibitory cues is therefore key to developing and advancing technical and clinical methods to modulate HFSC activity and subsequent hair regeneration.

Two of the most well-known – and opposing – signaling pathways regulating HFSC activity are the Wnt/β-catenin/Lef1 and BMP pathways. In simple terms, activated Wnt signaling promotes HFSC activation while BMP promotes quiescence by suppressing HFSC activity. BMP signaling also works in concert with NFATc1 to maintain quiescence in HFSCs[26, 27]. Anagen (re)entry is achieved by antagonizing active BMP signaling to cease NFATc1 transcription. Interestingly, a recent report implicated Sirt7 can directly modulate Nfatc1 signaling in HFSCs poised for telogen-to-anagen transition[28].

Next, the TGF-β signaling pathway is activated early in the hair cycle[29, 30] which may work in concert with other activatory pathways in HFSCs to reach a threshold of signals necessary for reach telogen-to-anagen transition of the hair cycle. This signaling pathway can be broadly described as positive-feedback modulator of hair cycle progression towards anagen.

Endocrinology - Hormones and the Hair Cycle

Androgens very obviously regulate hair growth, most notably during puberty and during the onset of old age[31]. Systemic hormones are another layer of the regulatory networks in HFSCs. Androgens also hold the power to override many paracrine signaling factors that influence proper hair cycling; this is quite notable in pregnant mammalian females[32]. Indeed, one report has found that androgens have the power to inhibit Wnt signaling in HFSCs, thus promoting quiescence[33]. Many components of the hair follicle unit express androgen receptors (ARs), and to varying degrees of sensitivity across a human body. Unsurprisingly, androgen-sensitive follicles (and subsequently more ARs) are widely reported in beard/pubis areas as opposed to androgen-insensitive follicles (with less ARs) in nonbalding scalp[31]. Even localization of ARs in skin various with epidermal locations, perhaps influencing hair patterning that is closely tied to social perceptions. As previously described, androgenetic alopecia is characterized by hair follicle miniaturization and can be hereditary. On the other end of the spectrum, hyperandrogenism causes excessive male-pattern hair growth, regardless of sex. Of note, DP cells have androgen receptors and will be the primary cell type responding to such circulating extrinsic stimuli.

Neurobiology: Adrenergic Signaling and the Hair Cycle

Hair follicle innervation fluctuates with the hair cycle; the isthmus and bulge area of hair follicles are the most densely innervated area upon telogen-to-anagen transition and early anagen[2, 34, 35]. In fact, prominent expression of β_2-adrenoreceptors have been observed adjacent to HFSCs. Furthermore, the β_2-adrenoreceptor agonist

isoproteranol promotes hair cycle progression in mouse skin cultures. Sympathetic nerves allow for the mechanosensory functions of the hair follicle[36]. The influence of sympathetic nerve stimulation in HFSC activity is also observed at the clinical levels, where patients taking "beta blockers" experience temporary alopecia until cessation of treatment. Additionally, several cases of hypertrichosis (hair overgrowth) have been reported in cases of patients subjected to thoracic surgery and consequential nerve hyperactivity. Upon sympathetic nerve stimulation, norepinephrine is released to act on the HFSC niche, where it stimulates anagen progression via hedgehog signaling[37].

In the skin, the arrector pili muscle (APM) and hair follicle form a unit. Cold temperature stimuli trigger contraction of the APM, physically pulling the hair follicle erect. Goosebumps are a direct result of such actions; APMs directly attach to and entangle the HFSC bulge for stimulation (Figure 3)[38]. Aside from thermoregulation, the reason(s) behind this phenomenon remains to be determined. Perhaps this sympathetic adjustment is to facilitate stem cell modulation from adrenergic inputs; APM synapses are indeed necessary for HFSC innervation and local norepinephrine delivery[37]. Furthermore, RNA-sequencing data from our collaborators at the Hsu lab at Harvard generously shared the information that this occurs via the adrenergic receptor Adrb2, highly enriched in murine HFSCs in telogen[37]. Indeed, genetic ablation of Adrb2 in HFSCs significantly extended telogen, implicating loss of Adrb2 with upregulation in quiescence mechanisms, uncovering the novelty of quiescence signaling pathways under neuronal control. As such, sympathetic nerves serve a dual mode of function in the bulge: 1) facilitate piloerecton; 2) facilitate intracellular signaling

cascades modulating hair growth. The idea of other signaling mechanisms acting in concert with this regulatory circuit remains to be seen.

Metabolic Control of HFSC Function

One can think of cancer and stem cells as two sides of the same coin. For a growing number of years, the link between metabolism and cell fate has captured researchers' interests for its dual ability to prospectively control stem cell behavior and malignant cancer transformation[39, 40]. The current thinking is that most adult tissue cells heavily rely on oxidative phosphorylation to meet their energetic demands, especially in highly proliferative cells[41]. This changes in cancer metabolism if one considers the "Warburg effect" where cancer relies on increased metabolism of glucose to lactate; a "quick and dirty" energy source. While HFSCs have been shown to be a cancer cell of origin for squamous cell carcinoma (SCC)[42], the bioenergetics allow for homeostasis and SCC transformation remain to be elucidated. In conjunction with a former labmate's thesis work[43], I expanded on the basal metabolic profile of HFSCs to show that maintenance of a glycolytic state (Figure 2) is critical for facilitating a quick response to activation stimuli to generate a new hair cycle[10, 44, 45].

The G-protein-coupled Receptor Signaling Pathway

G-protein-coupled receptors (GPCRs) are a large diverse family of cell surface receptors that mediate a number of cellular actions – sometimes through second-messenger signaling – in tissue homeostasis and cancer[46]. They are involved in a variety of fundamental cell processes like proliferation, migration, differentiation, and cell

survival (cite). Controlling GPCR signaling for homeostatic purposes or even as a preventative effort is an understudied avenue of anti-cancer and drug discovery work.

Upon ligand binding, the GPCR becomes activated and undergoes a conformational change (heterotrimeric protein). In canonical GPCR signaling (Figure 4), activated Gα can then interact with the effector adenylate cyclase (AC), which results in effector activation and initiation of a second-messenger cascade (via cAMP). cAMP subsequently activates protein kinase A (PKA) which is then able to phosphorylate CREB, thereby facilitating its nuclear translocation and gene target expression.

G-protein-Coupled Receptors and Adult Stem Cells/HFSCs

A subset of GPCRs, known as Leucine-rich repeating-containing G-protein-coupled receptor (Lgr) proteins, are known to regulate stem cell identity. Lgr proteins were initially discovered to function extensively for embryonic development but were later on discovered to be prevalent in maintaining adult stem cell populations. They are now widely used as adult stem cells markers for various epithelial adult stem cells, such as ones found in intestinal crypts and hair follicle stem cells. However, since many adult stem cells can be the cell of origin for certain cancers, Lgr proteins can also be used to study aberrant signaling properties (cite). Apart from that, Lgr proteins have also been linked to regulating the hair cycle and HFSCs, where Lgr5 marks frequently cycling, long-lived HFSCs[47] and usually marks the lower portion of the bulge. A recent report also implicated that Spondin, the Lgr4/5/6 ligand, is also upregulated upon telogen-to-anagen transition[48] and can be used as an exogenous factor to drive the hair cycle[49]. R-Spondins can also mediate Wnt signaling, but GPCR/CREB involvement in

this process is unknown. We would like to further study how GPCR/CREB signaling fine tunes the balance between self-renewal and differentiation in adult stem cells, chiefly in hair follicle stem cells, and if they regulate epithelial cancer development[50].

Hair follicle appendages are highly proliferative tissues with the ability to withstand external injuries; disruption of this process – either by external injury, depilation, disease, medical treatments, etc. – often leads to clinical hair loss. This makes them an ideal model for studying extrinsic and intrinsic cues necessary for stem cell maintenance and overall organ homeostasis. By using the mouse follicle as a model system, we have been able to delve further into distinguishing the molecular networks fundamental for optimal homeostasis. With the eve of uncovering multiple molecular pathways regulating HFSC activity[51-53], there is great promise for development of novel therapies and improve current treatment strategies in alleviating physiological hair loss, and even go on to direct tissue engineering of human hair follicles. Understanding the precise inputs of intra- and inter-cellular signaling pathways for their adult stem cell populations can therefore be extended to other populations in the body. Here we contribute to the current dogma in the skin/hair biology field by introducing the distinct yet complementary roles of metabolic control and GPCR/cAMP/Creb-dependent signaling in HFSC activation.

Summary of Chapters

My graduate work can be split into two main themes: studying metabolic control of HFSC activation and investigating the role of GPCR/cAMP/Creb signaling in HFSC homeostasis. Chapters 1 and 2 are publications that complement each other due to their central message of promoting glycolysis for HFSC activation. In Chapter 1, this is through making the chase that Ldh is necessary for hair cycling; deletion of this gene in HFSCs ablates any hair growth and the hair follicle itself persists in the telogen stage indefinitely. This project was underway upon my acceptance into the Lowry Lab. I assisted with data analysis, performed assays, and developed a method for quantifying macroscopic hair cycle stage; my involvement warranted authorship. Chapter 2 was my first independent lab project and first, first-author publication as a graduate student. Here, we took the idea of glycolysis and HFSC activation more downstream, looking at how electron transport chain (ETC) inhibition may function to ramp up glycolytic process, facilitating the shift to activation and hair growth. In other words, ETC inhibition created a backup of lactate that can be used for HFSCs for activation and subsequent hair cycling. Our approach here was relatively simple yet robust due to topical pharmacological manipulations of Complex I or Complex III. This yielded prominent hair growth and an accelerated hair growth in both young, telogen-stage male mice and 24-month-old aged female mice. We believe that transient ETC inhibition is sufficient for HFSC activation, regardless of HFSC age. However, the effect of chronic mitochondrial modulation in HFSC activation is not known and warrants further study. Chapter 3 shifted my curiosity towards a more mechanistic approach in HFSC homeostasis. There is extensive data on classic developmental signaling pathways in the regulation of adult

stem cells like HFSCs, but an absolute dearth when the idea of GPCR signaling is brought up in such a context. This struck us as odd since GPCRs are one of the largest classes of receptors in cell biology and of great interest for novel drug discovery. A few papers were able to set the stage that GPCR signaling may regulate adult stem cells, especially in the context where abrogation of GPCR signaling in epidermal stem cells led to basal cell carcinogenesis[50]. With this in mind, we sought to test if canonical GCPR/cAMP/Creb drives hair follicle cycling at various points of the signaling cascade. We are happy to report we may have identified upstream and downstream components in this circuit that award HFSC activation and have recently submitted a manuscript to the Journal of Investigative Biology to share our findings.

Figures

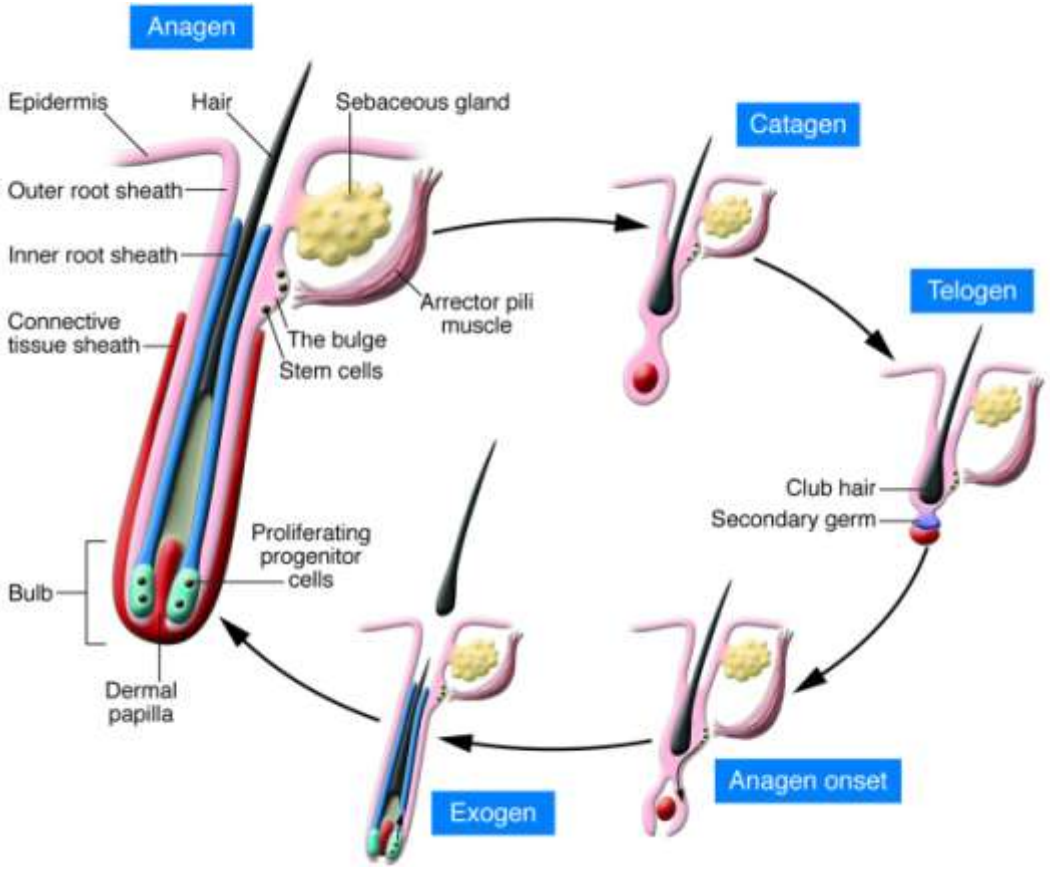

Adapted from Cotsarelis, 2006

Figure 1. **The Hair Cycle**. While the interfollicular epidermis self-renews and maintains the outermost epidermal layers, hair follicle stem cells (HFSCs) in a region termed the "bulge", drive the hair cycle. The hair follicle appendage undergoes three phases: growth (anagen), regression (catagen), and rest (telogen) throughout a coated animals' lifetime. These cyclical bouts of destruction and regeneration require precise temporal and spatial control of the bulge niche.

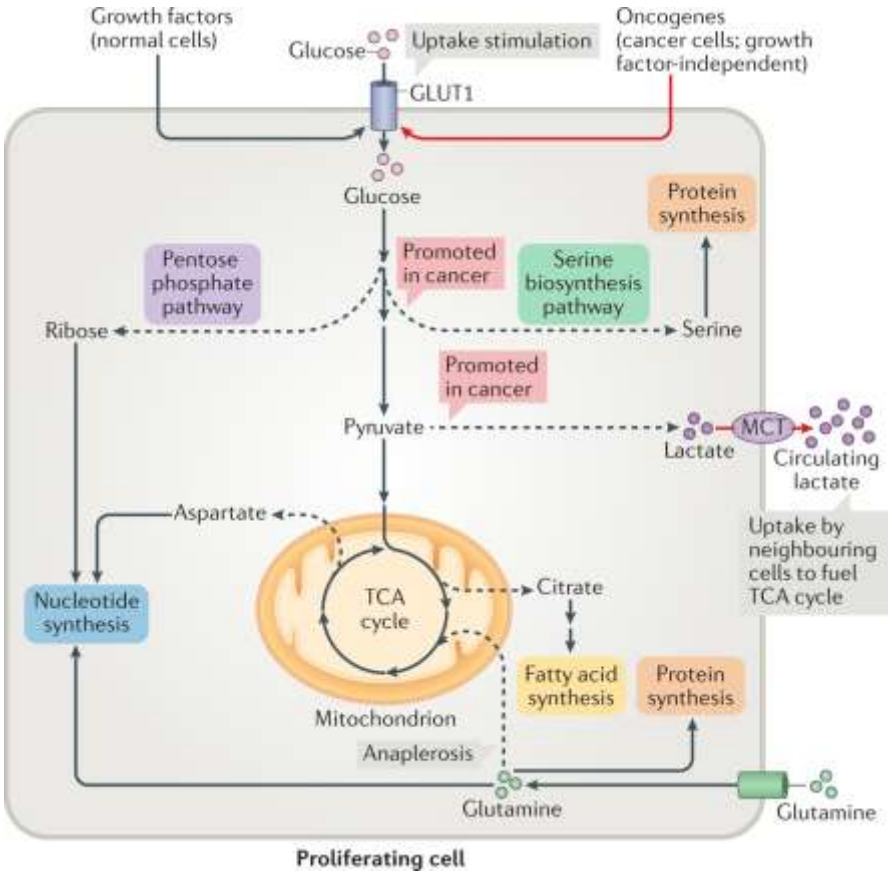

Adapted from Zhu and Thompson, 2019.

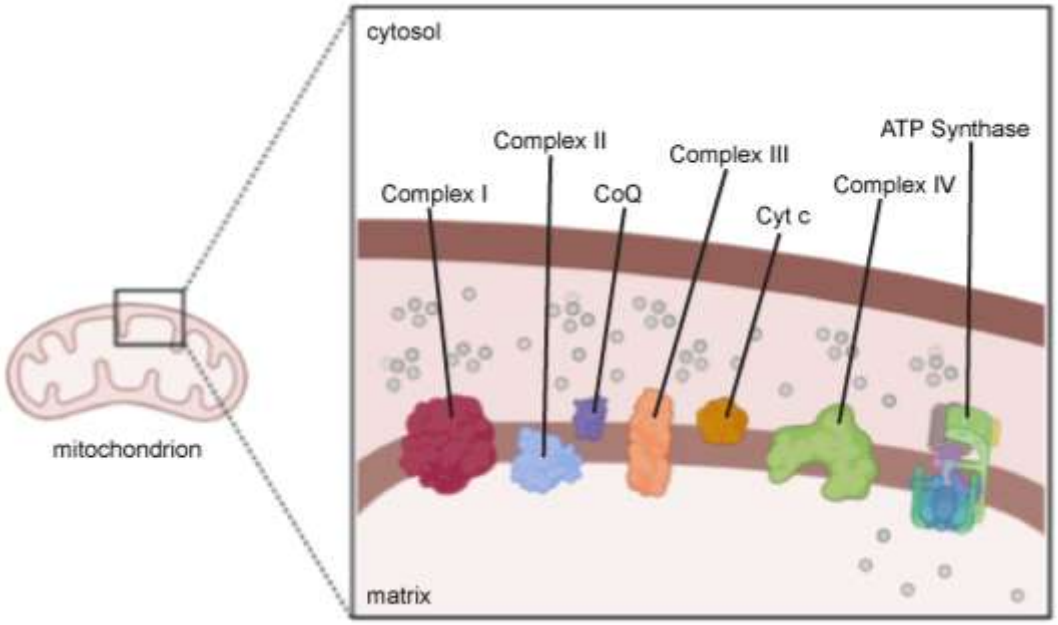

Figure 2. **Glycolysis and ETC for Metabolic Control of HFSCs**. Cellular metabolism is the crux of all biological activities. Cellular bioenergetics in adult stem cells have not been studied extensively, though many rely on glycolysis as opposed to oxidative metabolism normally powering differentiated cells. Adult stem cells require specific metabolic states to maintain stemness. HFSCs heavily rely on glycolysis in for homeostasis; HFSC activation is dictated by glycolysis. Electron transport chain (ETC) inhibition is another method to promote glycolysis and HFSC activation, particularly through Complex I and Complex III inhibition.

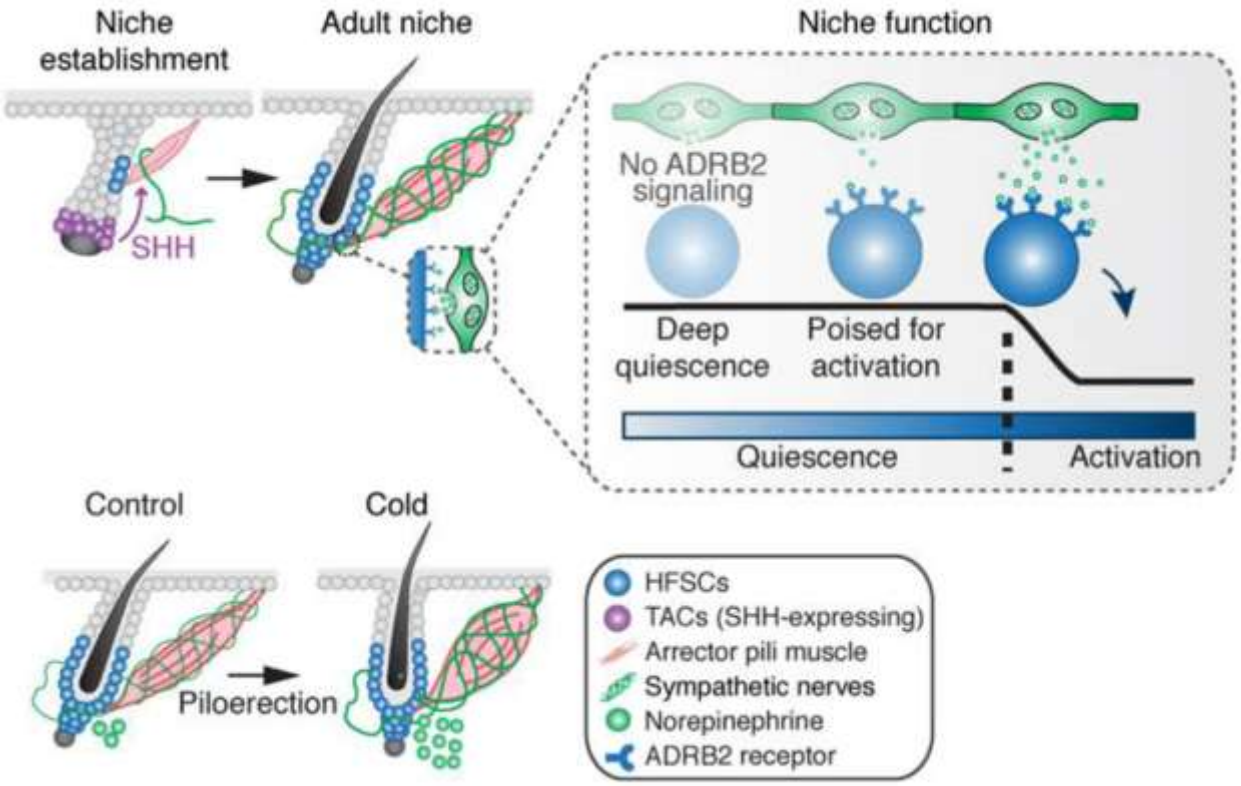

Adapted from Shwartz et al, 2020

Figure 3. **Adrenergic signaling relays norepinephrine to promote HFSC activation**. The arrector pili muscle (APM) and sympathetic nerves form a niche that directly influences hair follicle stem cells (HFSCs) via the adrenergic receptor Adrb2. Sympathetic nerves form synapses at the hair follicle bulge and signal through norepinephrine to modulate metabolic state of HFSCs necessary for cycling between activation and quiescence.

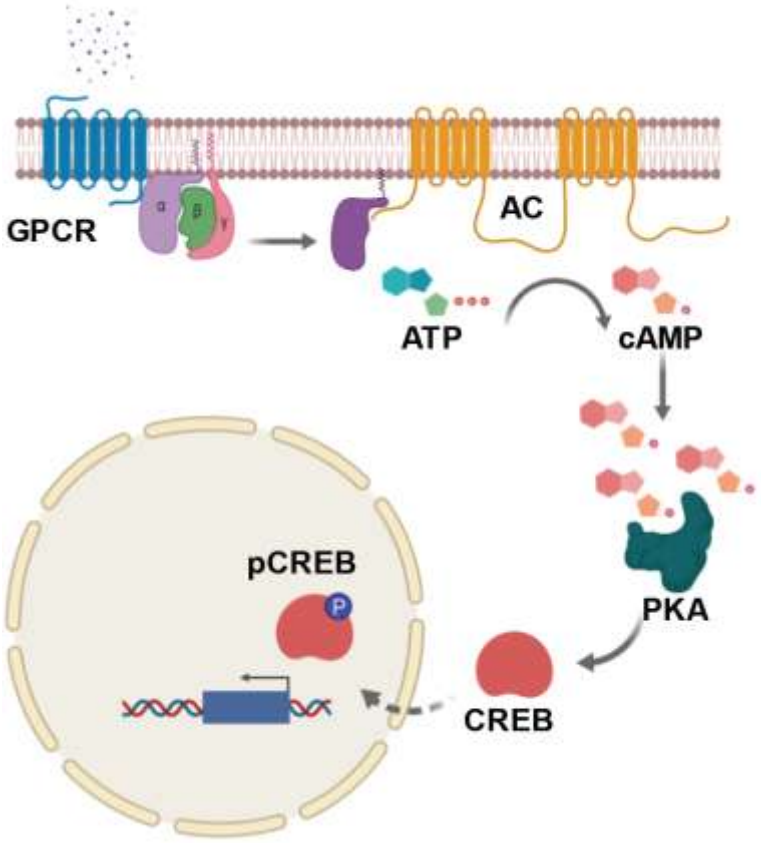

Figure 4. **The classical GPCR/cAMP/Creb-dependent intracellular signaling pathway in adult stem cell modulation**. G-protein-coupled-receptors (GPCRs) are the largest family of cell surface receptors that mediate numerous intracellular signaling pathways important for physiological and pathological processes. In canonical GPCR signaling, ligand(s) bind to the extracellular receptor, where activated intracellular subunit Gα can then interact with the effector adenylate cyclase (AC), resulting in effector activation and initiation of a second-messenger cascade (via cAMP). Increased intracellular levels of cAMP subsequently activate protein kinase A (PKA) which is then able to phosphorylate CREB, thereby facilitating its nuclear translocation and gene target expression.

References

1. Wang, X., E.E. Tredget, and Y. Wu, *Dynamic signals for hair follicle development and regeneration.* Stem cells and development, 2012. **21**(1): p. 7-18.
2. Botchkarev, V.A., et al., *Hair cycle-dependent plasticity of skin and hair follicle innervation in normal murine skin.* Journal of Comparative Neurology, 1997. **386**(3): p. 379-395.
3. Schneider, M.R., R. Schmidt-Ullrich, and R. Paus, *The hair follicle as a dynamic miniorgan.* Current Biology, 2009. **19**(3): p. R132-R142.
4. Paus, R. and G. Cotsarelis, *The biology of hair follicles.* New England journal of medicine, 1999. **341**(7): p. 491-497.
5. Stenn, K., et al., *What controls hair follicle cycling?* Experimental dermatology, 1999. **8**(4): p. 229-236.
6. Alonso, L. and E. Fuchs, *The hair cycle.* Journal of cell science, 2006. **119**(3): p. 391-393.
7. Ito, M., et al., *Stem cells in the hair follicle bulge contribute to wound repair but not to homeostasis of the epidermis.* Nature medicine, 2005. **11**(12): p. 1351-1354.
8. Cotsarelis, G., T.-T. Sun, and R.M. Lavker, *Label-retaining cells reside in the bulge area of pilosebaceous unit: implications for follicular stem cells, hair cycle, and skin carcinogenesis.* Cell, 1990. **61**(7): p. 1329-1337.
9. Morris, R.J., et al., *Capturing and profiling adult hair follicle stem cells.* Nature biotechnology, 2004. **22**(4): p. 411-417.
10. Adachi, K., et al., *Human hair follicles: metabolism and control mechanisms.* J Soc Cosmet Chem, 1970. **21**: p. 901-924.
11. Blanpain, C. and E. Fuchs, *Epidermal homeostasis: a balancing act of stem cells in the skin.* Nature reviews Molecular cell biology, 2009. **10**(3): p. 207-217.
12. Soma, T., et al., *Hair-inducing ability of human dermal papilla cells cultured under Wnt/β-catenin signalling activation.* Experimental dermatology, 2012. **21**(4): p. 307-309.

13. Lee, J. and T. Tumbar. *Hairy tale of signaling in hair follicle development and cycling*. in *Seminars in cell & developmental biology*. 2012. Elsevier.
14. Müller-Röver, S., et al., *A comprehensive guide for the accurate classification of murine hair follicles in distinct hair cycle stages.* Journal of investigative dermatology, 2001. **117**(1): p. 3-15.
15. Hsu, Y.-C., L. Li, and E. Fuchs, *Emerging interactions between skin stem cells and their niches.* Nature medicine, 2014. **20**(8): p. 847-856.
16. Greco, V., et al., *A two-step mechanism for stem cell activation during hair regeneration.* Cell stem cell, 2009. **4**(2): p. 155-169.
17. Courtois, M., et al., *Ageing and hair cycles.* British Journal of Dermatology, 1995. **132**(1): p. 86-93.
18. Cotsarelis, G., *Gene expression profiling gets to the root of human hair follicle stem cells.* The Journal of clinical investigation, 2006. **116**(1): p. 19-22.
19. Ito, T., *Hair follicle is a target of stress hormone and autoimmune reactions.* Journal of dermatological science, 2010. **60**(2): p. 67-73.
20. Matsumura, H., et al., *Hair follicle aging is driven by transepidermal elimination of stem cells via COL17A1 proteolysis.* Science, 2016. **351**(6273).
21. Lei, M. and C.-M. Chuong, *Aging, alopecia, and stem cells.* Science, 2016. **351**(6273): p. 559-560.
22. Ceruti, J.M., G.J. Leirós, and M.E. Balañá, *Androgens and androgen receptor action in skin and hair follicles.* Molecular and cellular endocrinology, 2018. **465**: p. 122-133.
23. Garza, L.A., et al., *Bald scalp in men with androgenetic alopecia retains hair follicle stem cells but lacks CD200-rich and CD34-positive hair follicle progenitor cells.* The Journal of clinical investigation, 2011. **121**(2): p. 613-622.
24. Itami, S., et al., *Mechanism of action of androgen in hair follicles.* Journal of dermatological science, 1994. **7**: p. S98-S103.
25. Houschyar, K.S., et al., *Molecular mechanisms of hair growth and regeneration: Current understanding and novel paradigms.* Dermatology, 2020: p. 1-10.

26. Plikus, M.V. and C.-M. Chuong, *Macroenvironmental regulation of hair cycling and collective regenerative behavior.* Cold Spring Harbor perspectives in medicine, 2014. **4**(1): p. a015198.
27. Keyes, B.E., et al., *Nfatc1 orchestrates aging in hair follicle stem cells.* Proceedings of the National Academy of Sciences, 2013. **110**(51): p. E4950-E4959.
28. Li, G., et al., *SIRT 7 activates quiescent hair follicle stem cells to ensure hair growth in mice.* The EMBO Journal, 2020: p. e104365.
29. Oshimori, N. and E. Fuchs, *The harmonies played by TGF-β in stem cell biology.* Cell stem cell, 2012. **11**(6): p. 751-764.
30. Oshimori, N., D. Oristian, and E. Fuchs, *TGF-β promotes heterogeneity and drug resistance in squamous cell carcinoma.* Cell, 2015. **160**(5): p. 963-976.
31. Randall, V.A. *Hormonal regulation of hair follicles exhibits a biological paradox*. in *Seminars in cell & developmental biology*. 2007. Elsevier.
32. Alonso, L.C. and R.L. Rosenfield, *Molecular genetic and endocrine mechanisms of hair growth.* Hormone Research in Paediatrics, 2003. **60**(1): p. 1-13.
33. Leiros, G.J., A.I. Attorresi, and M.E. Balaña, *Hair follicle stem cell differentiation is inhibited through cross-talk between Wnt/β-catenin and androgen signalling in dermal papilla cells from patients with androgenetic alopecia.* British Journal of Dermatology, 2012. **166**(5): p. 1035-1042.
34. Botchkarev, V.A., et al., *Hair cycle-dependent changes in adrenergic skin innervation, and hair growth modulation by adrenergic drugs.* Journal of investigative dermatology, 1999. **113**(6): p. 878-887.
35. Peters, E., et al., *Hair growth-modulation by adrenergic drugs.* Experimental dermatology, 1999. **8**(4): p. 274-281.
36. Paus, R., et al. *Neural mechanisms of hair growth control*. in *Journal of Investigative Dermatology Symposium Proceedings*. 1997. Elsevier.
37. Shwartz, Y., et al., *Cell Types Promoting Goosebumps Form a Niche to Regulate Hair Follicle Stem Cells.* Cell, 2020. **182**(3): p. 578-593. e19.
38. Fujiwara, H., et al., *The basement membrane of hair follicle stem cells is a muscle cell niche.* Cell, 2011. **144**(4): p. 577-589.

39. Ying, Q.-L., et al., *The ground state of embryonic stem cell self-renewal.* Nature, 2008. **453**(7194): p. 519-523.
40. Zhu, J. and C.B. Thompson, *Metabolic regulation of cell growth and proliferation.* Nature reviews Molecular cell biology, 2019. **20**(7): p. 436-450.
41. Shyh-Chang, N. and H.-H. Ng, *The metabolic programming of stem cells.* Genes & development, 2017. **31**(4): p. 336-346.
42. White, A.C., et al., *Defining the origins of Ras/p53-mediated squamous cell carcinoma.* Proceedings of the National Academy of Sciences, 2011. **108**(18): p. 7425-7430.
43. Flores, A., et al., *Lactate dehydrogenase activity drives hair follicle stem cell activation.* Nature cell biology, 2017. **19**(9): p. 1017-1026.
44. Miranda, M., et al., *Topical Inhibition of the Electron Transport Chain Can Stimulate the Hair Cycle.* The Journal of investigative dermatology, 2018. **138**(4): p. 968.
45. Son, M.J., et al., *A novel and safe small molecule enhances hair follicle regeneration by facilitating metabolic reprogramming.* Experimental & molecular medicine, 2018. **50**(12): p. 1-15.
46. Dorsam, R.T. and J.S. Gutkind, *G-protein-coupled receptors and cancer.* Nature reviews cancer, 2007. **7**(2): p. 79-94.
47. Barker, N., S. Tan, and H. Clevers, *Lgr proteins in epithelial stem cell biology.* Development, 2013. **140**(12): p. 2484-2494.
48. Smith, A.A., et al., *Activating hair follicle stem cells via R-spondin2 to stimulate hair growth.* Journal of Investigative Dermatology, 2016. **136**(8): p. 1549-1558.
49. Li, N., et al., *Exogenous R-spondin1 induces precocious telogen-to-anagen transition in mouse hair follicles.* International journal of molecular sciences, 2016. **17**(4): p. 582.
50. Iglesias-Bartolome, R., et al., *Inactivation of a Gα s–PKA tumour suppressor pathway in skin stem cells initiates basal-cell carcinogenesis.* Nature cell biology, 2015. **17**(6): p. 793-803.

51. Chen, C.-L., et al., *Functional complexity of hair follicle stem cell niche and therapeutic targeting of niche dysfunction for hair regeneration.* Journal of Biomedical Science, 2020. **27**(1): p. 1-11.
52. Lin, S.-J., et al., *Hair Follicle Stem Cells and Hair Regeneration.* Cell Engineering and Regeneration, 2020: p. 265-296.
53. Millar, S.E., *Molecular mechanisms regulating hair follicle development.* Journal of Investigative Dermatology, 2002. **118**(2): p. 216-225.

Chapter 2

Lactate Dehydrogenase Activity Drives Hair Follicle Stem Cell Activation

nature cell biology

Lactate dehydrogenase activity drives hair follicle stem cell activation

Aimee Flores[1,2,3], John Schell[1], Abigail S. Krall[5], David Jelinek[1], Matilde Miranda[1], Melina Grigorian[6], Daniel Braas[5,7], Andrew C. White[8], Jessica L. Zhou[9], Nicholas A. Graham[5,9], Thomas Graeber[5,10], Pankaj Seth[11], Denis Evseenko[12], Hilary A. Coller[1,2,3,13,14], Jared Rutter[4,15], Heather R. Christofk[2,5,7,13,14,16] and William E. Lowry[1,2,3,13,16]

Although normally dormant, hair follicle stem cells (HFSCs) quickly become activated to divide during a new hair cycle. The quiescence of HFSCs is known to be regulated by a number of intrinsic and extrinsic mechanisms. Here we provide several lines of evidence to demonstrate that HFSCs utilize glycolytic metabolism and produce significantly more lactate than other cells in the epidermis. Furthermore, lactate generation appears to be critical for the activation of HFSCs as deletion of lactate dehydrogenase (Ldha) prevented their activation. Conversely, genetically promoting lactate production in HFSCs through mitochondrial pyruvate carrier 1 (Mpc1) deletion accelerated their activation and the hair cycle. Finally, we identify small molecules that increase lactate production by stimulating Myc levels or inhibiting Mpc1 carrier activity and can topically induce the hair cycle. These data suggest that HFSCs maintain a metabolic state that allows them to remain dormant and yet quickly respond to appropriate proliferative stimuli.

The hair follicle is able to undergo cyclical rounds of rest (telogen), regeneration (anagen) and degeneration (catagen). The ability of the hair follicle to maintain this cycle depends on the presence of the hair follicle stem cells, which reside in the bulge (Fig. 1). At the start of anagen, bulge stem cells are activated by signals received from the dermal papilla, which at that stage abuts the bulge area[1,2]. These stem cells exit the bulge and proliferate downwards, creating a trail that becomes the outer root sheath. Bulge stem cells are capable of giving rise to all the different cell types of the hair follicle. The ability of HFSCs to maintain quiescence and yet become proliferative for a couple days before returning to quiescence is unique in this tissue, and the precise mechanism by which these cells are endowed with this ability is not fully understood. While significant effort has produced a wealth of knowledge on both the transcriptional and epigenetic mechanisms by which HFSCs are maintained and give rise to various lineages[3,4], little is known about metabolic pathways in the hair follicle or adult stem cells *in vivo*.

Considering the fact that there are essentially no published data on metabolic states of any cell in the hair follicle, a detailed study of metabolism was necessary to understand the nature of HFSCs and their progeny. Several previous studies employed genetic disruption of the mitochondrial electron transport chain in the epidermis by deletion under the control of a pan-epidermal keratin promoter and found that mitochondrial function was essential for maintenance of the follicle[5–8]. However, these studies did not explore the metabolic requirements for specific cell types within the tissue, nor did they explore a role for glycolytic metabolism. In this study, we present methods to study the metabolism of HFSCs *in vivo*, and provide evidence that these cells take advantage of a distinct mode of metabolism not found in their progeny. In the process, we also define small molecules that can take advantage of the unique metabolism of HFSCs to ignite the hair cycle in otherwise quiescent follicles.

RESULTS

Numerous studies have uncovered unique gene expression signatures in HFSCs versus other follicle cells or cells of the interfollicular epidermis[9–12]. Many of these signatures are regulated by transcription factors that were later shown to play important roles in HFSC

[1]Department of Molecular Cell and Developmental Biology, UCLA, 90095, USA. [2]Eli and Edythe Broad Center for Regenerative Medicine, UCLA, 90095, USA. [3]Molecular Biology Institute, UCLA, 90095, USA. [4]Department of Biochemistry, University of Utah, 84322, USA. [5]Department of Molecular and Medical Pharmacology, UCLA, 90095, USA. [6]Stanford School of Medicine, Stanford University, 94305, USA. [7]UCLA Metabolomics Center, UCLA, 90095, USA. [8]School of Veterinary Medicine, Cornell University, 14853, USA. [9]Mork Family Department of Chemical Engineering, University of Southern California, 90089, USA. [10]Crump Institute for Molecular Imaging, UCLA, 90095, USA. [11]Division of Interdisciplinary Medicine and Biotechnology, Beth Israel Deaconess Cancer Center, Harvard Medical School, 02215, USA. [12]Broad Center for Regenerative Medicine, University of Southern California, 90089, USA. [13]Jonsson Comprehensive Cancer Center, UCLA, 90095, USA. [14]Department of Biological Chemistry, UCLA, 90095, USA. [15]Howard Hughes Medical Institute, 20815, USA. [16]Correspondence should be addressed to H.R.C. or W.E.L. (e-mail: HChristofk@mednet.ucla.edu or blowry@ucla.edu)

Received 29 September 2016; accepted 19 June 2017; published online 14 August 2017; DOI: 10.1038/ncb3575

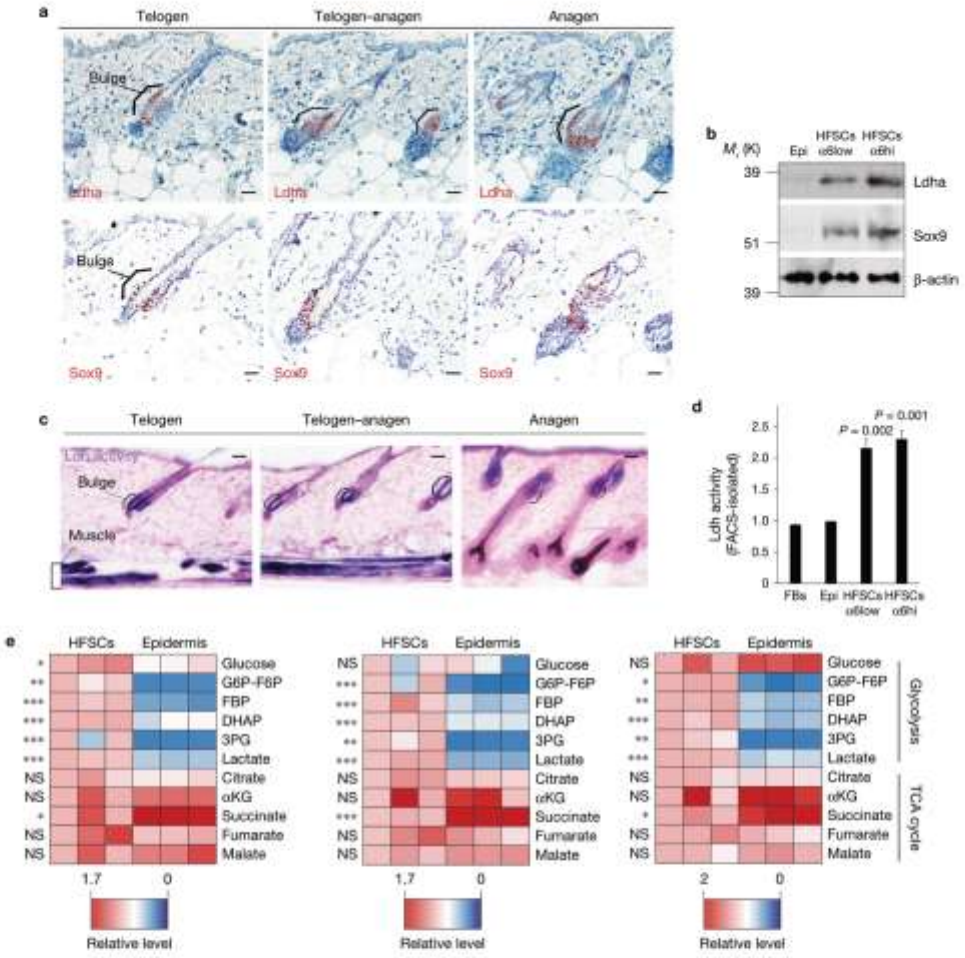

Figure 1 Lactate dehydrogenase activity is enriched in HFSCs. (**a**) IHC staining for Ldha expression across the hair cycle shows Ldha protein confined to the HFSC niche, the bulge, indicated by the bracket. IHC staining for Sox9 on serial sections demarcates the HFSC population. Scale bars, 20 μm. (**b**) Immunoblotting on FACS-isolated HFSC populations (α6low/Cd34$^+$ and α6hi/Cd34$^+$) versus total epidermis (Epi) shows differential expression of Ldha in the stem cell niche. Sox9 is a marker of HFSCs, and β-actin is a loading control. (**c**) Colorimetric assay for Ldh enzyme activity in the epidermis shows highest activity in the bulge (brackets) and subcuticular muscle layer (bracket). This activity is enriched in the bulge across different stages of the hair cycle. Activity is indicated by purple colour; pink is a nuclear counterstain. Note also that developing hair shafts in pigmented mice show strong deposits of melanin as observed here; hair shafts never displayed any purple stain indicative of Ldh activity. Scale bars, 50 μm. (**d**) Ldh activity in sorted cell populations, measured using a plate-reader-based assay, also shows the highest Ldh activity in two separate HFSC populations (α6hi/Cd34$^+$ and α6low/Cd34$^+$) compared with epidermal cells (Epi) and fibroblasts (FBs). Each bar represents the average signal for each cell type where $n=9$ mice pooled from 3 independent experiments. Shown as mean ± s.e.m. Paired *t*-test was performed, $P<0.05$ shown for each cell type versus epidermal cells. (**e**) HFSCs and epidermal cells were isolated during telogen (day 50) by FACS, and metabolites were extracted and analysed by LC–MS. Heatmaps show relative levels of glycolytic and TCA cycle metabolites from cells isolated from different mice in independent experiments with cells from three animals in each. G6P-F6P, glucose-6-phosphate and fructose-6-phosphate; FBP, fructose-bisphosphate; DHAP, dihydroxyacetone phosphate; 3PG, 3-phosphoglycerate; and αKG, alpha-ketoglutarate. Asterisks indicate significant difference in metabolite levels between epidermal cells and HFSCs. For (**e**) paired *t*-test was performed; $^*P<0.05$; $^{**}P<0.01$; $^{***}P<0.001$); NS, $P>0.05$; $n=9$ mice pooled from 3 independent experiments. Unprocessed original scans of blots are shown in Supplementary Fig. 6.

homeostasis[13]. Lactate dehydrogenase is most commonly encoded by the *Ldha* and *Ldhb* genes in mammals, the protein products of which form homo- or hetero-tetramers to catalyse the NADH-dependent reduction of pyruvate to lactate and NAD$^+$-dependent oxidation of lactate to pyruvate[14]. By immunostaining, Ldha appeared to be enriched in quiescent HFSCs *in situ* (telogen) (Fig. 1a), and

immunohistochemistry (IHC) with an antibody that recognizes both Ldha and Ldhb showed that only Ldha appears to be localized to the HFSC niche (Supplementary Fig. 1a).

HFSCs are known to go through successive rounds of quiescence (telogen) punctuated by brief periods of proliferation correlating with the start of the hair cycle (telogen–anagen transition)[4,15]. Proliferation or activation of HFSCs is well known to be a prerequisite for advancement of the hair cycle. IHC analysis also showed that Ldha expression was enriched in HFSCs ($Sox9^+$) at three stages of the hair cycle (Fig. 1a). Consistently, immunoblotting of lysates from sorted cells showed strong expression of Ldha in the basal HFSCs ($\alpha6hi/CD34^+$), and suprabasal ($\alpha6lo/CD34^+$) HFSC populations relative to total epidermis (Fig. 1b)[9] (the sorting strategy is outlined in Supplementary Fig. 1b).

To determine whether Ldha expression patterns correlate with activity of the Ldh enzyme, we used a colorimetric-based enzymatic assay to assess Ldh activity capacity *in situ*. Typically performed on protein lysates or aliquots with a plate reader[16], we adapted the Ldh activity assay to work *in situ* on frozen tissue sections. Note that since both the *in situ* and *in vitro* Ldh activity assays employ use of excess substrate (lactate), the results from these assays reflect the capacity for Ldh activity, and not the steady-state activity.

Applying this assay to skin samples demonstrated that Ldh activity capacity was significantly higher in HFSCs, consistent with the expression pattern of Ldha (Fig. 1c). Furthermore, Ldh activity was enriched in HFSCs across the hair cycle (Fig. 1c). As a control, assays conducted without the enzymatic substrate (lactate) or on acid-treated tissue yielded zero activity (Supplementary Fig. 1c). To further validate these results, we sorted epidermal populations, generated cell lysates on the sorted cells, and performed a similar colorimetric-based enzymatic assay on the sorted cell lysates, which also showed increased Ldh activity in HFSCs (Fig. 1d). To better characterize the metabolism of HFSCs, we performed metabolomics analysis on sorted populations from mouse skin by liquid chromatography–mass spectrometry (LC–MS) (Fig. 1e). Several glycolytic metabolites, including glucose/fructose-6-phosphate, fructose-bisphosphate, dihydroxyacetone phosphate, 3-phosphoglycerate and lactate, were routinely higher in HFSCs relative to total epidermis across three independent experiments (isolated from different mice on different days). Conversely, most TCA cycle metabolites were not consistently different between the epidermis and HFSCs (Fig. 1e). Collectively these results suggest that while all cells in the epidermis use the TCA cycle extensively to generate energy, HFSCs also have increased Ldha expression, Ldh activity and glycolytic metabolism.

Measuring metabolism across the hair cycle therefore would capture any dynamic changes that occur in HFSCs that correlate with activation or quiescence. Analysis of RNA-seq data from HFSCs isolated during either telogen or the telogen–anagen transition demonstrated not only that *Ldha* is the predominant *Ldh* isoform expressed in HFSCs (Fig. 2c), but it is also induced during the telogen–anagen transition (Fig. 2a,b) (NIHGEOGSE67404 and GSE51635). To confirm that the cells analysed by RNA-seq were indeed either in telogen or the telogen–anagen transition, important markers of this transition were assessed including the Shh and Wnt pathways (*Gli1, 2, 3, Lef1, Axin1, Axin2* and *Ccnd1*) as well as proliferation markers (*Ki-67, Pcna* and *Sox4*) (Supplementary Fig. 2a).

The *in vitro* Ldh activity assay on lysates from sorted HFSCs uncovered a modest induction of Ldh activity correlating with the telogen–anagen transition (Fig. 2d). Hair cycle staging was validated by Ki-67 immunostaining to determine HFSC activation (Supplementary Fig. 2b). Additionally, measurements of steady-state metabolites extracted from sorted HFSCs showed an increase in lactate in HFSCs as they enter the telogen–anagen transition, and then decrease again in anagen as HFSCs return to quiescence (Fig. 2e).

To determine whether Ldh activity is functionally related to the ability of HFSCs to remain quiescent or to activate at the start of a hair cycle, we deleted *Ldha* specifically in the HFSCs. Taking advantage of mice with floxed alleles of *Ldha*[17], this enzyme was deleted in HFSCs by crossing to mice bearing the *K15-CrePR* allele[11], known to be inducible by mifepristone specifically in HFSCs. Deletion of *Ldha* in HFSCs was initiated by administration of mifepristone during telogen (day 50) and led to a typically mosaic recombination of the floxed alleles across the backskin[11,18]. Mice with HFSC-specific deletion of *Ldha* failed to undergo a proper hair cycle, with most follicles remaining in telogen across at least 33 pairs of littermates 3–4 weeks after mifepristone treatment (Fig. 3a). A complete list of transgenic animals including birth date, sex and genotype is provided in Supplementary Table 1.

Histology showed that wild-type hair follicles entered into the telogen–anagen transition typically by day 70, and this was accompanied by typical expansion of the hypodermis below (Fig. 3b). However, in backskin with deletion of *Ldha*, the hypodermis did not expand, and the telogen–anagen transition was severely abrogated (Fig. 3b). In areas of strong phenotypic penetrance, Ldh activity was severely abrogated in the HFSC compartment (Fig. 3c), demonstrating that the *Ldha* allele is critically important for Ldh activity in HFSCs and consistent with the fact that isoform a of *Ldh* is expressed at the highest level. Quantification of hair cycle progression across numerous animals indicated that most follicles lacking *Ldha* remained in telogen (Fig. 3d).

In addition, to confirm the phenotypes, we also deleted *Ldha* with an independent HFSC-specific Cre strategy. *Lgr5-CreER* has been used for lineage tracing in a variety of adult stem cell models, and has been shown to mark cells with high regenerative capacity, including HFSCs[19]. *Lgr5-CreER;Ldha*$^{fl/fl}$ mice, treated with tamoxifen at postnatal day 50 prior to a synchronized hair cycle, also failed to activate anagen across at least 20 littermate pairs (Fig. 3g). *In situ* Ldh assay and metabolomics confirmed the successful deletion of *Ldha* in these animals (Fig. 3h,i).

We also monitored the effect of loss of Ldha activity in $K15^+$ cells over a six-month period and found that deletion of *Ldha* led to a mosaic, but permanent block of HFSC activation in some portions of the backskin (Supplementary Fig. 3a). These data confirm that Ldh activity is required for HFSC activation, and is not simply a marker of HFSCs. A closer look at these long-term *Ldha* deletions showed that *Ldha*-null HFSCs continued expressing typical markers, but lacked Ldh activity, and failed to initiate new hair cycles, while those follicles that escaped deletion continued to express Ldha and to cycle normally (Supplementary Fig. 3b,c).

After sorting HFSCs from animals with or without *Ldha* deletion, LC–MS-based metabolomics analysis demonstrated that lactate levels, as well as levels of other glycolytic metabolites, were strongly

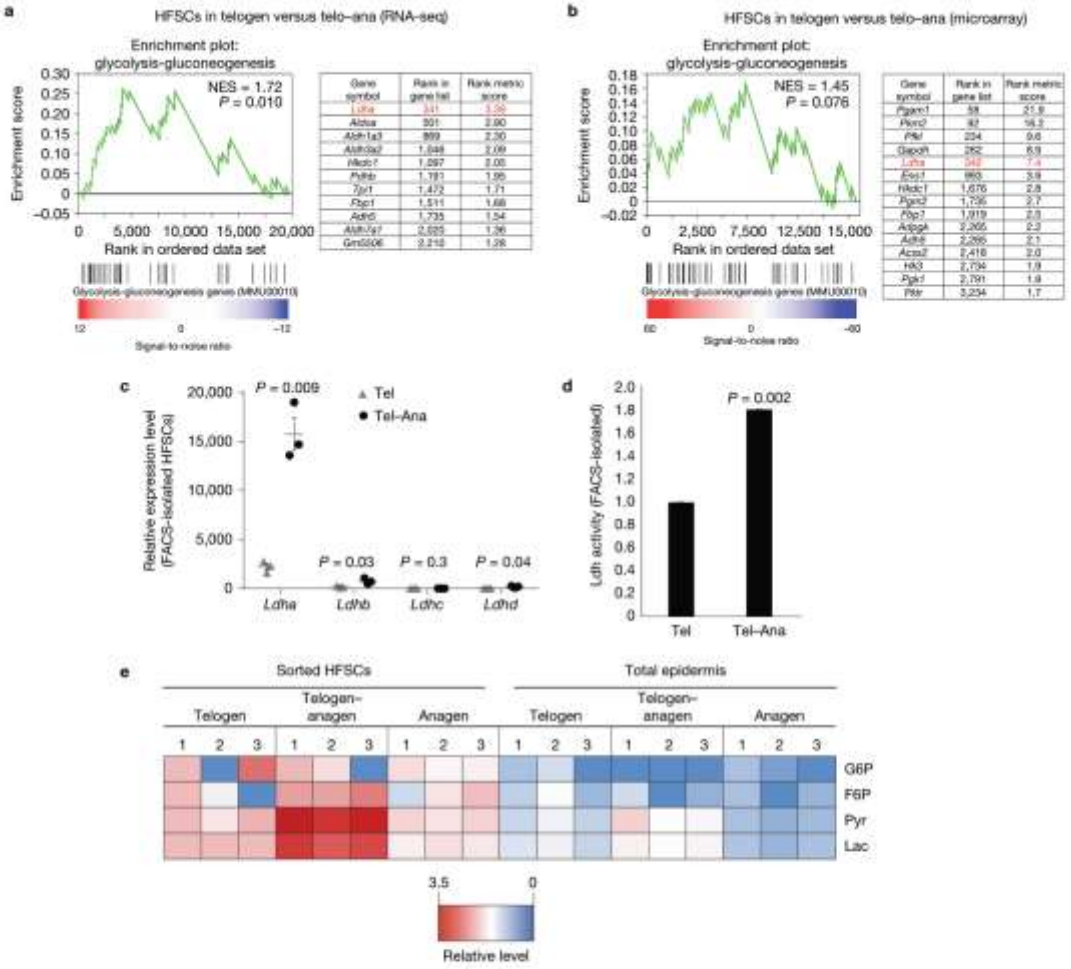

Figure 2 Ldh activity increases during HFSC activation. (**a**) Gene set enrichment analysis (GSEA) on RNA-seq transcriptome data from HFSCs versus total epidermis shows enrichment for glycolysis-related genes in HFSCs (normalized enrichment score (NES) = 1.72). (**b**) GSEA on microarray transcriptome data from HFSCs versus total epidermis shows enrichment for glycolysis-related genes in HFSCs (NES = 1.45). Results were generated from three mice of each condition. (**c**) RNA-seq data from HFSCs sorted during telogen or telogen–anagen transition (Tel–Ana) show induction of *Ldha*[35]. Data represent the average of three separate animals at each time point ($n=3$), and subjected to Student's *t*-test for significance ($P<0.05$). (**d**) Ldh activity in sorted stem cell populations, measured using a plate-reader-based assay, shows elevated Ldh activity as stem cells become activated in telogen–anagen transition. Each bar represents the average signal for each condition where $n=9$ mice pooled from 3 independent experiments. Shown as mean ± s.e.m. Paired *t*-test was performed, $P<0.05$. (**e**) Heatmap showing relative levels of glycolytic and TCA cycle metabolites extracted from quiescent (Telogen, day 50), activated (Telogen–Anagen, day 70) and HFSCs that have returned to the quiescent state (Anagen, day 90). Pyr, pyruvate; Lac, lactate. Data shown were generated from $n=3$ animals per time point in 3 independent experiments.

reduced in the absence of Ldha (Fig. 3e), functional evidence that the targeting strategy was successful. The fact that glycolytic metabolites upstream of lactate were also suppressed suggests that HFSCs could be adapting their metabolism to account for the loss of Ldh activity. Immunostaining for markers of HFSC activation and proliferation indicated a failure of HFSC activation. Ki-67 and pS6 have been clearly demonstrated to be abundant in the HFSC niche at the start of the hair cycle[39], and both of these markers were absent in *Ldha*-deleted backskin (Fig. 3f). Immunostaining for Ldha also confirmed successful deletion of this protein, while staining for Sox9, a marker of HFSCs, indicated that these cells remained in their niche, but just failed to activate in the absence of Ldha (Fig. 3f). Induction of the hair cycle is also thought to be regulated by signalling from the Shh, Wnt and Jak–Stat pathways.

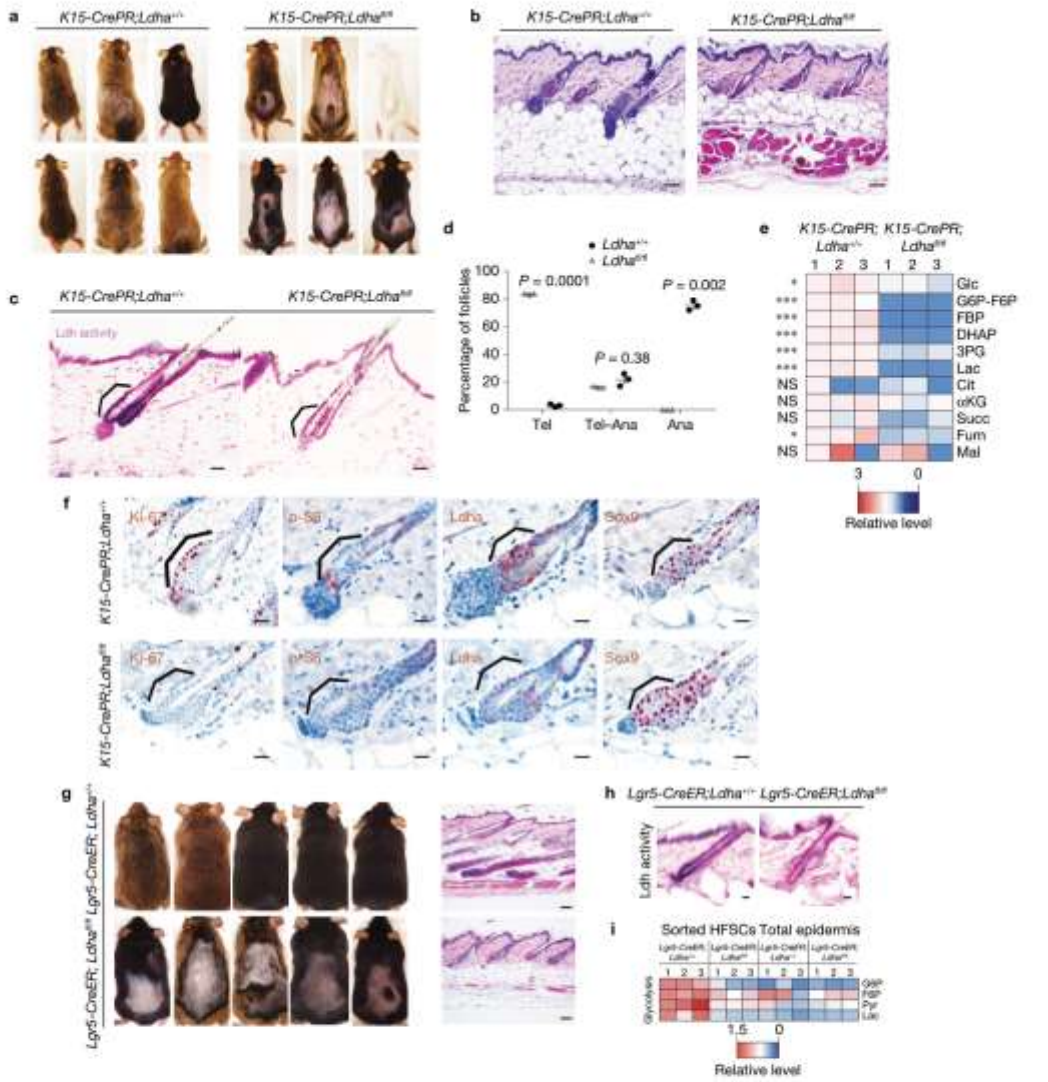

Figure 3 Deletion of Ldha blocks HFSC activation. (**a**) *Ldha*$^{+/+}$ animals enter the hair cycle synchronously around day 70 as measured by shaving and observation beginning at day 50. *K15-CrePR;Ldha*$^{\Delta/\Delta}$ animals treated with mifepristone show defects in anagen entry. Results are representative of at least 33 animals of each genotype. (**b**) Skin pathology showing that *K15-CrePR;Ldha*$^{\Delta/\Delta}$ animals remained in telogen. Scale bars, 50 μm. (**c**) Ldh enzyme activity assay showed that *K15-CrePR;Ldha*$^{\Delta/\Delta}$ animals lacked this activity in the HFSCs (indicated by bracket). Scale bars, 20 μm. (**d**) Graph showing percentage of follicles in telogen, telogen–anagen transition and anagen in *K15-CrePR;Ldha*$^{+/+}$ mice versus *K15-CrePR;Ldha*$^{\Delta/\Delta}$ mice ($n = 225$ follicles from 3 mice per genotype). Shown as mean ± s.e.m. Paired *t*-test was performed, $P < 0.05$. (**e**) Heatmap showing relative levels of glycolytic and TCA cycle metabolites extracted from *Ldha*$^{+/+}$ HFSCs and *Ldha*$^{\Delta/\Delta}$ HFSCs and measured by LC–MS. Asterisks indicate significant difference in metabolite levels between genotypes. For **e**, paired *t*-test was performed; $^{*}P < 0.05$; $^{***}P < 0.001$; NS, $P > 0.05$; $n = 9$ mice pooled from 3 independent experiments. (**f**) Immunohistochemistry staining for Ki-67, a marker of proliferation, is absent in *Ldha*$^{\Delta/\Delta}$ HFSCs. Phospho-S6, a marker in HFSCs at the beginning of a new hair cycle, is absent in *Ldha*$^{\Delta/\Delta}$ HFSCs. Staining for Ldha protein shows specific deletion in HFSCs. Brackets indicate bulge. Staining for Sox9 shows that HFSCs are still present in the *Ldha*-deleted niche. Scale bars, 20 μm. (**g**) Animals with *Ldha* deletion in their HFSCs as controlled by *Lgr5-CreER* show profound defects in the entry into anagen. Right, skin pathology showing that *Lgr5-CreER;Ldha*$^{\Delta/\Delta}$ animals mostly remained in telogen. Scale bars, 100 μm. Results are representative of at least 12 animals of each genotype. (**h**) Ldh enzyme activity assay in the epidermis shows that *Lgr5-CreER;Ldha*$^{\Delta/\Delta}$ animals lacked this activity in the HFSCs. Scale bars, 20 μm. (**i**) LC–MS analysis of metabolites from the indicated mice. Data were generated from $n = 3$ animals per condition pooled from 3 independent experiments.

We assayed each of these by IHC in normal or *Ldha*-deletion follicles and found that in general these pathways were not activated in *Ldha*-null HFSCs that failed to enter a telogen–anagen transition (Supplementary Fig. 3d).

To determine whether induction of lactate production could affect HFSC activation or the hair cycle, we crossed *K15-CrePR* animals to those floxed for mitochondrial pyruvate carrier 1 (*Mpc1*) (*K15-CrePR;Mpc1*$^{fl/fl}$). Mpc1, as a heterodimer with Mpc2, forms the mitochondrial pyruvate carrier MPC, a transporter on the inner mitochondrial membrane required for pyruvate entry into the mitochondria[21]. Loss of function of Mpc1 has been shown to drive lactate production through enhanced conversion of pyruvate to lactate by Ldh[22].

In animals with *Mpc1* deletion in HFSCs, we observed a strong acceleration of the ventral and dorsal hair cycles with all the typical features of a telogen–anagen transition (Fig. 4a) ($n = 12$ littermate pairs). Mifepristone-treated *K15-CrePR;Mpc1*$^{fl/fl}$ animals were the only ones to show any signs of dorsal anagen by day 70. Western blotting on sorted HFSCs validated the loss of Mpc1 protein (Fig. 4b). Importantly, purified HFSCs lacking *Mpc1* showed a strong induction of Ldh activity (Fig. 4c). Quantification of the dorsal hair cycle across three pairs of littermates showed a strong induction of anagen in backskin lacking *Mpc1* (Fig. 4d, right), and histology showed that the anagen induction was normal in appearance with a typical hypodermal expansion (Fig. 4d). Immunostaining demonstrated the induction in *Mpc1*-null HFSCs of various markers of hair cycle activation such as Ki-67 and pS6, while Sox9 expression was unaffected (Fig. 4e). Long-term deletion of *Mpc1* did not lead to aberrant follicles or exhaustion of HFSCs as judged by pathology and staining for Sox9 (Supplementary Fig. 4a). Furthermore, deletion of *Mpc1* with *Lgr5-CreER* showed a very similar phenotype as deletion with *K15-CrePR* (Fig. 4f,g), validating the fact that deletion of this protein in HFSCs leads to their activation ($n = 12$ pairs of littermates). Finally, immunofluorescence for the *Ires-GFP* of the *Lgr5-CreER* transgene along with Ki-67 and lineage tracing with K15-CrePR;Mpc1$^{fl/fl}$;lsl-Tomato mice also demonstrated that the HFSCs were indeed proliferative following induction of Mpc1 deletion by tamoxifen or mifepristone (Supplementary Fig. 4b).

On the other hand, deletion of *Mpc1* in the top of the follicle (infundibulum, sebaceous gland progenitors) and a limited number of interfollicular cells with *Lgr6-CreER* (ref. 23) did not appear to affect the hair cycle (*Lgr6-CreER;Mpc1*$^{fl/fl}$) ($n = 10$ littermate pairs) or general skin homeostasis over at least 2 months (Supplementary Fig. 4c). Ldh activity assay on Lgr6$^+$ cells sorted from wild-type or deletion skin demonstrated that the *Mpc1* deletion was effective (Supplementary Fig. 4d). Together, these results indicate that increasing lactate production through the blockade of pyruvate into the TCA cycle has a strong effect on the ability of HFSCs, but not other cells in the hair follicle, to become activated to initiate a new hair cycle.

UK-5099 is a well-established pharmacological inhibitor of the mitochondrial pyruvate carrier and is known to promote lactate production as a result in various settings[24]. Topical treatment of animals in telogen (day 50) with UK-5099 led to a robust acceleration of the hair cycle, as well as minor hyperproliferation of the interfollicular epidermis (Fig. 5a). Quantification of the hair cycle across at least 6 pairs of animals (vehicle versus UK-5099) indicated a strong acceleration of the hair cycle, in as few as 6–9 days (Fig. 5b). Similar to genetic deletion of *Mpc1*, pharmacological blockade of the mitochondrial pyruvate carrier by UK-5099 for 48 h during telogen promoted increased Ldh activity in HFSCs and the interfollicular epidermis, consistent with increased capacity for lactate production (Fig. 5c). Finally, metabolomic analysis demonstrated that topical application of UK-5099 increases total levels of lactate in sorted HFSCs (Fig. 5d).

Because alteration of lactate production in HFSCs appeared to regulate their activation, we attempted to identify other small molecules that could take advantage of these findings to induce the hair cycle. *Ldha* is known to be transcriptionally regulated by Myc, which has been shown to play an important role in HFSC activation and the hair cycle[25–27]. RNA-seq on sorted HFSCs indicated that Myc is induced during the telogen–anagen transition (Fig. 6a). Western blotting for both c-Myc and n-Myc in sorted HFSCs versus total epidermis showed a strong increase in Myc protein in the nuclei of HFSCs (Fig. 6b).

Taking advantage of a molecule with the robust ability to promote Myc expression through binding of GP130 and activation of Jak/Stat signalling, we topically treated mice for 48 h to determine the effect of RCGD423 on Stat signalling and Myc expression. We found that RCGD423 induced levels of both c-Myc and n-Myc as well as Ldha (Fig. 6c), consistent with activation of Stat3 signalling leading to induction of Myc and Ldha protein expression. *In vitro* measurement of Ldh activity on lysates from total epidermis showed an increase in activity by RCGD423 (Fig. 6d). *In situ* staining for Ldh activity showed a strong induction following treatment with RCGD423 in both the epidermis and even in the dermis, as expected with topical treatment (Fig. 6e). LC–MS-based metabolomics on epidermis isolated from vehicle or RCGD423 showed a large increase in lactate as well, even after just 48 h (Fig. 6f).

RCGD423 binds to GP130, a co-receptor for Jak–Stat signalling, and activates Stat3. We found that Stat3 was activated in HFSCs by RCGD423 after topical treatment by immunostaining with phospho-Stat3 antibody (Fig. 6g). This also correlated with induction of Ki-67 in HFSCs in the same tissue (Fig. 6g). IHC for pStat1 and pStat5 suggested that RCGD423 does not dramatically affect these other Stat family members (Supplementary Fig. 5). Topical treatment of animals in telogen (day 50) with RCGD423 led to a robust acceleration of the hair cycle (Fig. 6h), as well as minor hyperproliferation of the interfollicular epidermis.

DISCUSSION

Together, these data demonstrate that the production of lactate, through Ldha, is important for HFSC activation, and that HFSCs may maintain a high capacity for glycolytic metabolism at least in part through the activity of Myc. Our data also demonstrate that a genetic or pharmacological disruption of lactate production can be exploited to regulate the activity of HFSCs. It is possible that these results have implications for adult stem cells in other tissues. In an accompanying manuscript, the Rutter laboratory describes a role for Mpc1 in adult intestinal stem cells[28]. Consistent with data presented here on HFSCs, deletion of Mpc1 led to an increase in the ability of intestinal stem cells to form organoids.

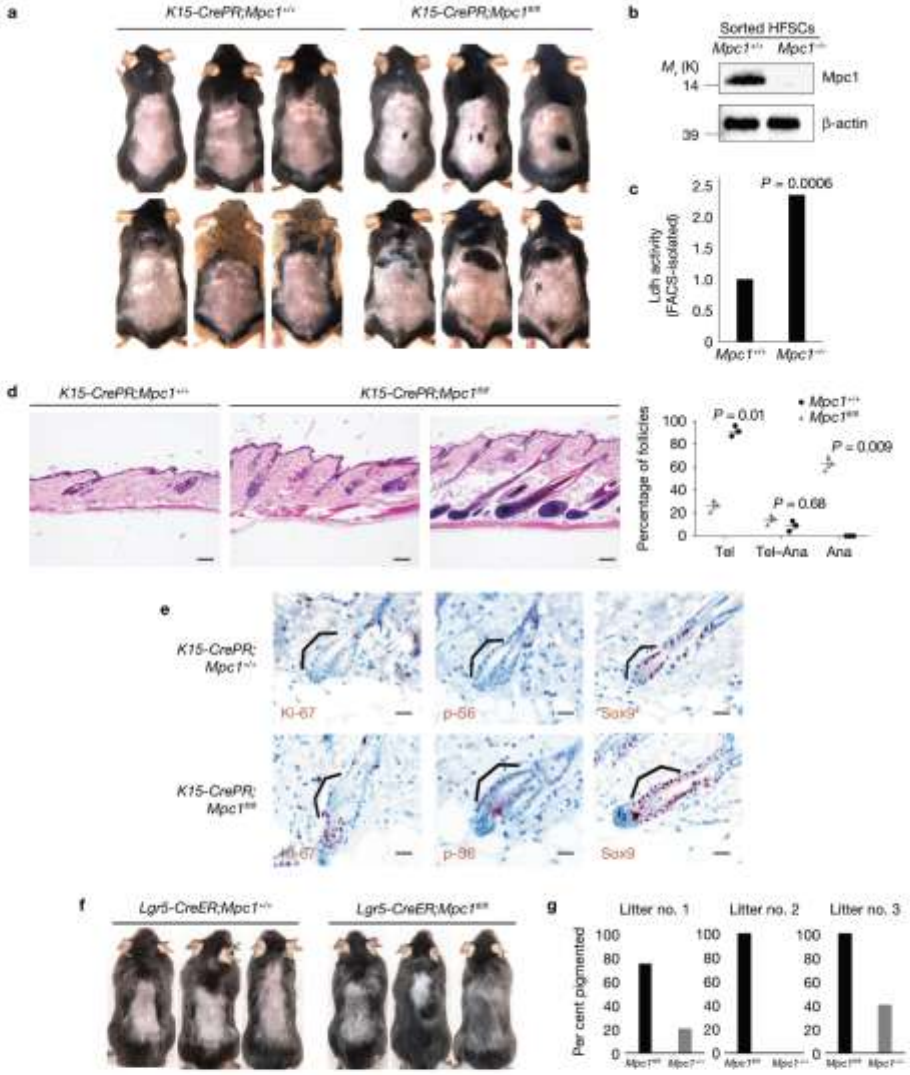

Figure 4 Deletion of Mpc1 increases lactate production and accelerates the activation of HFSCs. (**a**) *Mpc1*$^{-/-}$ animals show pigmentation and hair growth, consistent with entry into the anagen cycle at 8.5 weeks, whereas *Mpc1*$^{+/+}$ animals do not show dorsal pigmentation and hair growth this early. Animals shown are representative of at least 12 animals of each genotype. (**b**) FACS isolation of HFSC bulge populations in *Mpc1*$^{+/+}$ versus *Mpc1*$^{-/-}$ mice followed by western blotting shows successful deletion of Mpc1 protein in the stem cell niche. β-actin is a loading control. (**c**) Plate-reader assay for Ldh activity on sorted HFSC populations shows elevated activity in *Mpc1*$^{-/-}$ HFSCs compared with *Mpc1*$^{+/+}$ HFSCs. Each bar represents the average signal for each genotype where $n=9$ mice pooled from 3 independent experiments. Shown as mean ± s.e.m. Paired *t*-test was performed, $P<0.05$. (**d**) Histology on wild-type versus Mpc1 deletion skin shows induction of anagen in absence of Mpc1. Scale bars, 100 μm. Quantification of phenotype at right shows percentage of dorsal follicles in telogen, telogen–anagen transition and anagen in *Mpc1*$^{+/+}$ mice versus *Mpc1*$^{-/-}$ mice ($n=250$ follicles from 3 mice per genotype). Shown as mean ± s.e.m. Paired *t*-test was performed, $P<0.05$. (**e**) Immunohistochemistry staining for Ki-67, a marker of proliferation that is active in HFSCs only at the beginning of a new hair cycle, is present in *Mpc1*$^{-/-}$ HFSCs only at 8.5 weeks, consistent with their accelerated entry into a new hair cycle. Phospho-S6, another marker that is active in HFSCs only at the beginning of a new hair cycle, is present in *Mpc1*$^{-/-}$ HFSCs. Staining for Sox9 shows that HFSCs are present in the Mpc1-deleted niche. Images taken at ×60 magnification. (**f**) Deletion of Mpc1 in mice bearing the *Lgr5-CreER* allele shows strong induction of the hair cycle. Results are representative of at least 9 animals per genotype. (**g**) Quantification of pigmentation in the indicated genotypes across three independent litters ($n=5$ mice per genotype). Unprocessed original scans of blots are shown in Supplementary Fig. 6.

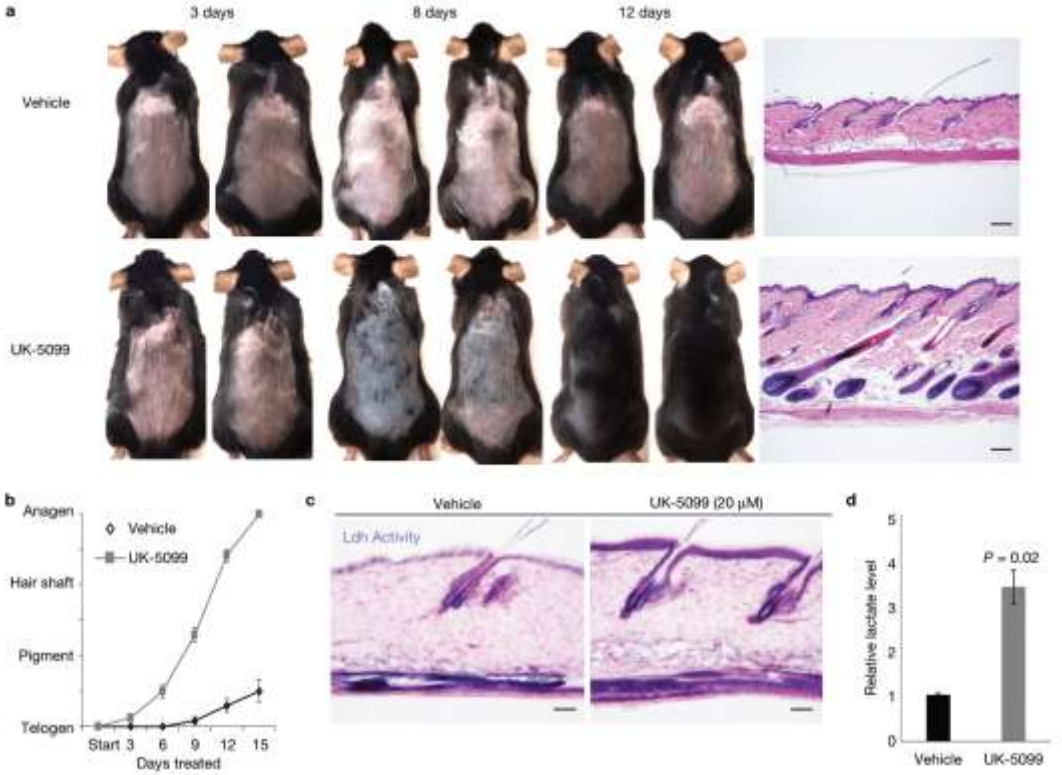

Figure 5 Pharmacological inhibition of Mpc1 promotes HFSC activation. (**a**) Animals treated topically with UK-5099 (20 μM) show pigmentation and hair growth, indicative of entry into anagen, after 8 days of treatment. Full anagen, indicated by a full coat of hair, is achieved after 14 days of treatment. Mice treated topically with vehicle control do not show pigmentation nor hair growth even after 12 days of treatment. Right, skin pathology showing that UK-5099 animals enter an accelerated anagen at 8 weeks typified by down growth of the follicle and hypodermal thickening, while vehicle control-treated animals showed neither and remained in telogen. Images shown are representative of at least 14 mice from 7 independent experiments. Scale bars, 100 μm. (**b**) Graph showing time to observed phenotype in vehicle- versus UK-5099-treated mice. $n = 6$ mice per condition. Shown as mean ± s.e.m. (**c**) Ldh enzyme activity assay in the epidermis shows strong activity in HFSCs in vehicle control- and UK-5099-treated animals. Ldh enzyme activity also seen in interfollicular epidermis of UK-5099-treated animals. Ldh activity is indicated by purple stain; pink is nuclear fast red counterstain. Scale bars, 50 μm. (**d**) Metabolomic analysis of lactate on HFSCs isolated from UK-5099-treated skin for 48 h; each bar represents the average signal for each condition where $n = 9$ mice pooled from 3 independent experiments. Shown as mean ± s.e.m. Paired *t*-test was performed, $P < 0.05$.

Previous work showed that haematopoietic stem cells (HSCs) show higher glycolytic activity, but disruption of glycolysis in the HSCs led to activation of their cycling[29–32], contrary to what we find with HFSCs. While the distinction could be biological, there are technical reasons for potential discrepancies as well. First, there are no Cre transgenic lines that can delete genes specifically in HSCs, as opposed to HFSCs ($K15^+$ or $Lgr5^+$). Second, to block glycolysis in HSCs, the previous study deleted the PDK enzyme, which would only indirectly regulate glycolysis, whereas here we deleted the Ldh enzyme specifically. In addition, HSCs and HFSCs are functionally distinct in that HFSCs cycle only at well-defined moments (telogen–anagen transition), while the timing of HSC activation is not as well established or synchronized. Instead, we hypothesize that increased glycolytic rate in HFSCs allows them to respond quickly to the barrage of cues that orchestrate the onset of a new hair cycle. This has also been proposed to be the case for neural stem cells solely on the basis of RNA-seq data[33], but as of yet no *in vivo* functional evidence exists to confirm this possibility.

The fact that small molecules could be used to promote HFSC activation suggests that they could be useful for regenerative medicine. This is not only the case for hair growth, but potentially for wound healing as well. While HFSCs do not normally contribute to the interfollicular epidermis, in a wound setting, HFSCs migrate towards the wound site and make a contribution, as measured by lineage tracing[34]. Whether activation of Ldh enzyme activity by Mpc1 inhibition (UK-5099) or Myc activation (RCGD423) can promote wound healing will be the subject of intense effort going forward. □

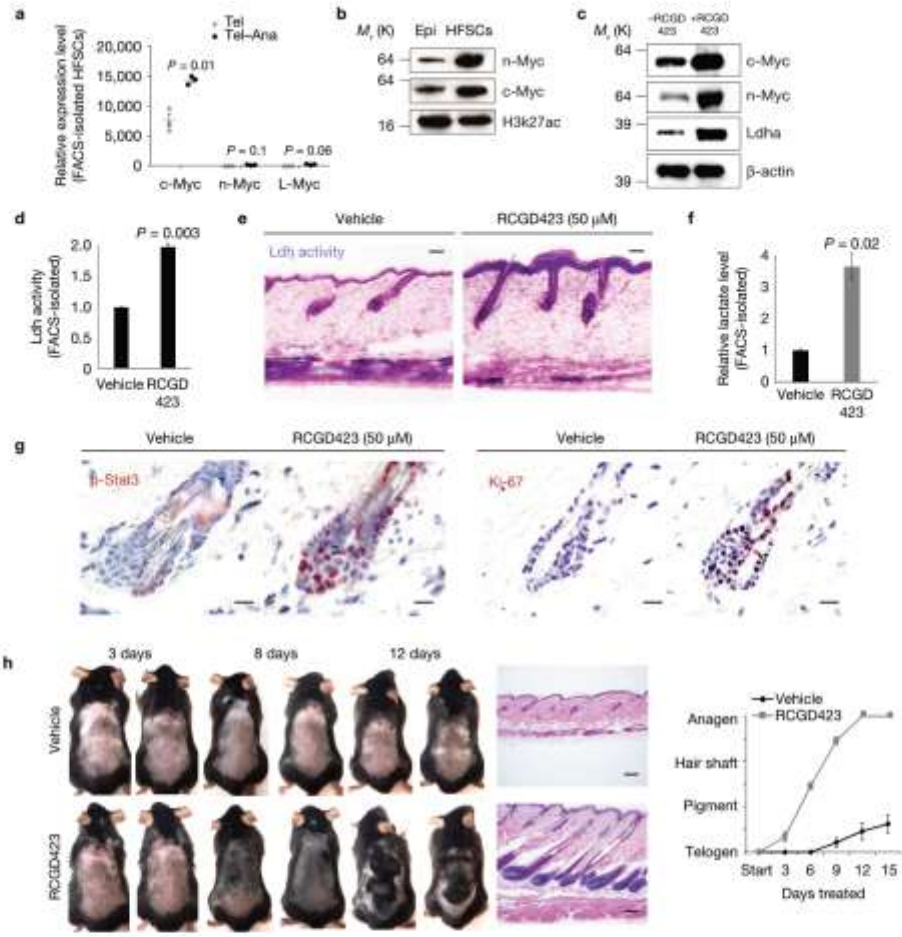

Figure 6 Stimulation of Myc levels promotes HFSC activation. (**a**) RNA-seq data from sorted HFSCs in telogen and telogen-anagen transition[15]. $n = 3$ mice per time point. Shown as mean ± s.e.m. Paired *t*-test was performed, $P < 0.05$. (**b**) Nuclear protein fractions show expression of n-Myc and c-Myc in HFSCs compared with epidermal cells. H3k27ac is a loading control for nuclear proteins. (**c**) Total protein preparations from skin treated with two topical doses of RCGD423 (50 μM) show increased c-Myc, n-Myc and Ldha protein levels compared with animals that received two topical doses of vehicle control. β-actin is a loading control. (**d**) Plate-reader assay for Ldh enzyme activity in the epidermis. Each bar represents the average signal for each condition where $n = 9$ mice pooled from 3 independent experiments. Shown as mean ± s.e.m. Paired *t*-test was performed, $P < 0.05$. (**e**) Ldh enzyme activity assay in the epidermis in vehicle control- and RCGD423-treated animals. Scale bars, 50 μm. (**f**) Metabolomic analysis of lactate on HFSCs isolated from RCGD423-treated skin for 48 h. Each bar represents the average signal for each condition where $n = 9$ mice pooled from 3 independent experiments. Shown as mean ± s.e.m. Paired *t*-test was performed, $P < 0.05$. (**g**) Immunohistochemistry staining for Ki-67 and phospho-Stat3, a downstream marker of RCGD423 activity. Scale bars, 20 μm. (**h**) Animals treated with RCGD423 (50 μM) show pigmentation and hair growth, indicative of entry into anagen, after 5 doses. Images shown are representative of at least 14 mice from 7 independent experiments. Scale bars, 100 μm. Quantification of phenotype showing time to observed phenotype in vehicle- versus RCGD423-treated mice. $n = 6$ mice per condition. Shown as mean ± s.e.m. Unprocessed original scans of blots are shown in Supplementary Fig. 6.

METHODS

Methods, including statements of data availability and any associated accession codes and references, are available in the online version of this paper.

Note: Supplementary Information is available in the online version of the paper

ACKNOWLEDGEMENTS

We would like to acknowledge the significant technical support of M. Neebe, J. Cinkornpumin and A. Liu on this project. We are also particularly grateful to members of the Banerjee laboratory for guidance and development of the Ldh activity assay. A.F. and A.C.W. were supported by a fellowship from the Eli and Edythe Broad Center for Regenerative Medicine at UCLA. A.C.W. and M.G. were supported by a fellowship from the Tumor Cell Biology programme

at UCLA (NIH). A.C.W. was also supported by a training grant from CIRM. D.J. was supported by awards from a New Idea Award from the Leukemia Lymphoma Society, the Jonsson Comprehensive Cancer Center, the UCLA Clinical Translational Science Institute UL1TR000124, the Prostate Cancer SPORE at UCLA P50 CA092131, and the Eli & Edythe Broad Center for Regenerative Medicine & Stem Cell Research. N.A.G. is a postdoctoral trainee supported by the UCLA Scholars in Oncologic Molecular Imagining program (NCI/NIH grant R25T CA098010). A.S.K. was supported by a UCLA Dissertation Year Fellowship. H.A.C. was supported by National Institute of General Medical Sciences R01-GM081686 and R01-GM0866463. J.R. was supported by NIH (RO1GM094232). H.R.C. was supported by a Research Scholar Grant, RSG-16-111-01-MPC, from the American Cancer Society and the Eli & Edythe Broad Center of Regenerative Medicine and Stem Cell Research at UCLA and Rose Hills Foundation Research Award. W.E.L. was supported by NIH-NIAMS (5R01AR57409), an Impact award from CTSI and the Jonsson Comprehensive Cancer Foundation, and The Gaba Fund through the Eli & Edythe Broad Center of Regenerative Medicine at UCLA.

AUTHOR CONTRIBUTIONS

A.F., J.S., A.S.K., D.J., M.M., M.G. and D.B. performed experiments. A.F., A.S.K., J.L.Z., N.A.G. performed analysis and compiled data. P.S., D.E. and J.R. provided key reagents essential to the work. T.G. and H.A.C. provided important insight and advice. H.R.C. and W.E.L. provided oversight and were financially responsible for the work. A.F., H.R.C. and W.E.L. were responsible for assembling the figures and writing the manuscript.

COMPETING FINANCIAL INTERESTS

The use of RCGD423 to promote hair growth is covered by a provisional patent application filed by UC Regents and this technology has been licensed by Carthronix LLC. W.E.L. is a member of the board of advisers and a shareholder of Carthronix LLC. None of the work in this study was supported by Carthronix. The use of UK-5099 to promote hair growth is covered by a separate provisional patent filed by UC Regents with W.E.L. and H.R.C. as inventors.

Published online at http://dx.doi.org/10.1038/ncb3575
Reprints and permissions information is available online at www.nature.com/reprints
Publisher's note: Springer Nature remains neutral with regard to jurisdictional claims in published maps and institutional affiliations.

1. Hsu, Y. C., Pasolli, H. A. & Fuchs, E. Dynamics between stem cells, niche, and progeny in the hair follicle. *Cell* **144,** 92–105 (2011).
2. Morris, R. J. & Potten, C. S. Highly persistent label-retaining cells in the hair follicles of mice and their fate following induction of anagen. *J. Invest. Dermatol.* **112,** 470–475 (1999).
3. Fuchs, E. The tortoise and the hair: slow-cycling cells in the stem cell race. *Cell* **137,** 811–819 (2009).
4. Fuchs, E., Merrill, B. J., Jamora, C. & DasGupta, R. At the roots of a never-ending cycle. *Dev. Cell* **1,** 13–25 (2001).
5. Kloepper, J. E. *et al.* Mitochondrial function in murine skin epithelium is crucial for hair follicle morphogenesis and epithelial-mesenchymal interactions. *J. Invest. Dermatol.* **135,** 679–689 (2015).
6. Hamanaka, R. B. & Chandel, N. S. Mitochondrial metabolism as a regulator of keratinocyte differentiation. *Cell. Logist.* **3,** e25456 (2013).
7. Hamanaka, R. B. *et al.* Mitochondrial reactive oxygen species promote epidermal differentiation and hair follicle development. *Sci. Signal.* **6,** ra8 (2013).
8. Baris, O. R. *et al.* The mitochondrial electron transport chain is dispensable for proliferation and differentiation of epidermal progenitor cells. *Stem Cells* **29,** 1459–1468 (2011).
9. Blanpain, C., Lowry, W. E., Geoghegan, A., Polak, L. & Fuchs, E. Self-renewal, multipotency, and the existence of two cell populations within an epithelial stem cell niche. *Cell* **118,** 635–648 (2004).
10. Tumbar, T. *et al.* Defining the epithelial stem cell niche in skin. *Science* **303,** 359–363 (2004).
11. Morris, R. J. *et al.* Capturing and profiling adult hair follicle stem cells. *Nat. Biotech.* **22,** 411–417 (2004).
12. Trempus, C. S. *et al.* Enrichment for living murine keratinocytes from the hair follicle bulge with the cell surface marker CD34. *J. Invest. Dermatol.* **120,** 501–511 (2003).
13. Nguyen, H., Rendl, M. & Fuchs, E. Tcf3 governs stem cell features and represses cell fate determination in skin. *Cell* **127,** 171–183 (2006).
14. Fromm, H. J. The nature of pyruvate involved in the enzymic formation of L-lactate in the rabbit-muscle lactate dehydrogenase reaction. *Biochim. Biophys. Acta* **99,** 540–542 (1965).
15. Paus, R., Muller-Rover, S. & Botchkarev, V. A. Chronobiology of the hair follicle: hunting the 'hair cycle clock'. *J. Invest. Dermatol. Symp. Proc.* **4,** 338–345 (1999).
16. Chan, F. K., Moriwaki, K. & De Rosa, M. J. Detection of necrosis by release of lactate dehydrogenase activity. *Methods Mol. Biol.* **979,** 65–70 (2013).
17. Xie, H. *et al.* Targeting lactate dehydrogenase-a inhibits tumorigenesis and tumor progression in mouse models of lung cancer and impacts tumor-initiating cells. *Cell Metab.* **19,** 795–809 (2014).
18. White, A. C. *et al.* Defining the origins of Ras/p53-mediated squamous cell carcinoma. *Proc. Natl Acad. Sci. USA* **108,** 7425–7430 (2011).
19. Jaks, V. *et al.* Lgr5 marks cycling, yet long-lived, hair follicle stem cells. *Nat. Genet.* **40,** 1291–1299 (2008).
20. Kellenberger, A. J. & Tauchi, M. Mammalian target of rapamycin complex 1 (mTORC1) may modulate the timing of anagen entry in mouse hair follicles. *Exp. Dermatol.* **22,** 77–80 (2013).
21. Bricker, D. K. *et al.* A mitochondrial pyruvate carrier required for pyruvate uptake in yeast, *Drosophila*, and humans. *Science* **337,** 96–100 (2012).
22. Schell, J. C. *et al.* A role for the mitochondrial pyruvate carrier as a repressor of the Warburg effect and colon cancer cell growth. *Mol. Cell* **56,** 400–413 (2014).
23. Snippert, H. J. *et al.* Lgr6 marks stem cells in the hair follicle that generate all cell lineages of the skin. *Science* **327,** 1385–1389 (2010).
24. Patterson, J. N. *et al.* Mitochondrial metabolism of pyruvate is essential for regulating glucose-stimulated insulin secretion. *J. Biol. Chem.* **289,** 13335–13346 (2014).
25. Wang, N. *et al.* The expression and role of c-Myc in mouse hair follicle morphogenesis and cycling. *Acta Histochem.* **114,** 199–206 (2012).
26. Bull, J. J. *et al.* Ectopic expression of c-Myc in the skin affects the hair growth cycle and causes an enlargement of the sebaceous gland. *Br. J. Dermatol.* **152,** 1125–1133 (2005).
27. Zanet, J. *et al.* Endogenous Myc controls mammalian epidermal cell size, hyperproliferation, endoreplication and stem cell amplification. *J. Cell Sci.* **118,** 1693–1704 (2005).
28. Schell, J. C. *et al.* Control of intestinal stem cell function and proliferation by mitochondrial pyruvate metabolism. *Nat. Cell Biol.* http://dx.doi.org/10.1038/ncb3583 (2017).
29. Hsu, P. & Qu, C. K. Metabolic plasticity and hematopoietic stem cell biology. *Curr. Opin. Hematol.* **20,** 289–294 (2013).
30. Harris, J. M. *et al.* Glucose metabolism impacts the spatiotemporal onset and magnitude of HSC induction *in vivo*. *Blood* **121,** 2483–2493 (2013).
31. Takubo, K. *et al.* Regulation of glycolysis by Pdk functions as a metabolic checkpoint for cell cycle quiescence in hematopoietic stem cells. *Cell Stem Cell* **12,** 49–61 (2013).
32. Simsek, T. *et al.* The distinct metabolic profile of hematopoietic stem cells reflects their location in a hypoxic niche. *Cell Stem Cell* **7,** 380–390 (2010).
33. Shin, J. *et al.* Single-cell RNA-Seq with waterfall reveals molecular cascades underlying adult neurogenesis. *Cell Stem Cell* **17,** 360–372 (2015).
34. Ito, M. *et al.* Stem cells in the hair follicle bulge contribute to wound repair but not to homeostasis of the epidermis. *Nat. Med.* **11,** 1351–1354 (2005).
35. Wang, L., Siegenthaler, J. A., Dowell, R. D. & Yi, R. Foxc1 reinforces quiescence in self-renewing hair follicle stem cells. *Science* **351,** 613–617 (2016).

METHODS

Mice. Several of the animal strains came from Jackson Labs (*K15-CrePR*, *Lgr5-CreER* and *Lgr6-CreER*), while others were generated in the Rutter (*Mpc*$^{fl/fl}$) and Seth laboratories[17] (*Ldha*$^{fl/fl}$) and maintained under conditions set forth by IUCUC and UCLA ARC. For experiments that include analysis of the telogen stage of the hair cycle, animals were harvested at postnatal day 50, for telogen–anagen transition animals were harvested at day 70, and for anagen animals were harvested at postnatal day 90. For experiments that include analysis of transgenic animals, *K15-CrePR* animals were shaved and treated by injection of mifepristone and *Lgr5-CreER* and *Lgr6-CreER* animals were shaved and treated with tamoxifen (10 mg ml^{-1} dissolved in sunflower seed oil, 2 mg per day for 3 days) during telogen (postnatal day 50), and monitored for hair regrowth following shaving. For Figs 5 and 6, wild-type C57BL/6J animals were shaved at postnatal day 50 and treated topically with Transderma Pho Gel Ultramax Base (TR220) (vehicle), UK-5099 (Sigma PZ0160) (20 μM) or RCGD423 (50 μM) for the indicated periods of time. Both male and female animals were used in this study in approximately equal numbers with no apparent difference in phenotype between genders. All animal experiments were performed in compliance with ethical guidelines and approved by the UCLA Animal Research Committee (ARC) according to IACUC guidelines in facilities run by the UCLA Department of Laboratory Animal Medicine (DLAM).

Histology, immunostaining and immunoblotting. Tissues were isolated from the indicated genotypes and embedded fresh in OCT compound for frozen tissue preparations, or fixed overnight in 4% formalin and embedded in paraffin. For frozen tissue, sectioning was performed on a Leica 3200 Cryostat, and the sections were fixed for 5 min in 4% paraformaldehyde. Paraffin-embedded tissue was sectioned, de-paraffinized and prepared for histology. All sections prepared for staining were blocked in staining buffer containing appropriate control IgG (goat, rabbit and so on). Immunohistochemistry was performed on formalin-fixed paraffin-embedded tissue with citrate or Tris buffer antigen retrieval with the following antibodies: Ki-67 (Abcam ab16667, 1:50), p-S6 (Cell Signaling CST2215, 1:50), Sox9 (Abcam ab185230, 1:1,000), Ldha (Abcam ab47010, 1:100), Ldh (Abcam ab125683, 1:100), p-Stat3 (Abcam ab68153, 1:200), p-Stat1 (Abcam ab109461, 1:200), p-Stat5 (Abcam ab32364; 1:50), Gli3 (Abcam ab6050; 1:100), β-catenin (Abcam ab32572; 1:500). The DAKO EnVision+ HRP Peroxidase System (Dako K400911-2) and Dako AEC Substrate Chromogen (Dako K346430-2) was used for detection. Images were collected on an Olympus BX43 Upright Microscope and Zeiss Model Axio Imager M1 Upright Fluorescence Microscope. Protein samples for western blots and enzymatic assays were extracted from FACS-sorted epidermal populations in RIPA lysis buffer (Pierce) with Halt protease and phosphatase inhibitors (Thermo-Fisher) and precipitated in acetone for concentration. The following antibodies were used: β-actin (Abcam ab8227; 1:1,000), β-actin (Santa Cruz sc-47778; 1:1,000), c-Myc (Abcam ab32072; 1:1,000), n-Myc (Santa Cruz sc-53993; 1:200), H3K27Ac (Abcam ab177178; 1:200), Mpc1 (Sigma HPA045119).

Cell isolation and FACS. Whole dorsal and ventral mouse skin was excised and floated on trypsin (0.25%) for 1 h at 37° or overnight at 4°. The epidermis was separated from dermis by scraping and epidermal cells were mechanically dissociated using a pipette. Epidermal cells were filtered with a 70 μM cell strainer into 20% BCS, collected at 300*g* and washed twice with PBS. The cells were then filtered through a 40 μM cell strainer and stained for FACS processing with CD34 Monoclonal Antibody (RAM34), FITC, eBioscience (catalogue no. 11-0341-82) and CD49d (Integrin alpha 4) Monoclonal Antibody (R1-2), PE, eBioscience (catalogue no. 12-0492-81). The gating strategy is shown in Supplementary Fig. 1b. Cells were sorted using BD FACSAria high-speed cell sorters. Single-positive and double-positive populations were collected into 20% BCS, RIPA lysis buffer (Thermo Scientific, Pierce), or 80% methanol for enzymatic assays, western blots or mass spectrometry analyses respectively.

Cell lines. No cell lines were used in this study.

Plate-reader Ldh assay. Ldh activity was determined in cell lysates by measuring the formation of soluble XTT formazan in direct relation to production of NADH over time at 475 nm at 37 °C using a Synergy-MX plate reader (Biotek Instruments). Lysates were prepared in RIPA Buffer (Thermo Scientific Pierce). Protein content was determined using the BCA Protein Assay Kit (Thermo Scientific Pierce). Ten micrograms of protein was used per well. The staining solution contained 50 mM Tris buffer pH 7.4, 150 μM XTT (Sigma), 750 μM NAD (Sigma), 80 μM phenazine methosulfate (Sigma) and 10 mM of substrate lactate (Sigma). Ldh activity was determined in cell lysates by measuring the change in absorbance of their common substrate or product, NADH, over time at 340 nm at 25 °C using a Synergy-MX plate reader (Biotek Instruments).

***In situ* Ldh assay.** Cryostat sections of mouse skin were briefly fixed (4% formalin for 5 min), washed with PBS pH 7.4, and then incubated with the appropriate solution for LDH activity. Staining medium contained 50 mM Tris pH 7.4, 750 μM NAD (Sigma), 80 μM phenazine methosulfate (Sigma), 600 μM nitrotetrazolium blue chloride (Sigma), 10 mM $MgCl_2$ (Sigma) and 10 mM of the substrate lactate (Sigma). Slides were incubated with staining medium at 37 °C until they reached the desired intensity, then counterstained using Nuclear Fast Red (Vector) and mounted using VectaMount (Vector). Control reactions were performed by using incubation medium that lacked the substrate mixture or NAD.

Mass spectrometry-based metabolomics analysis. The experiments were performed as described in ref. 17. To extract intracellular metabolites, FACS-sorted cells were briefly rinsed with cold 150 mM ammonium acetate (pH 7.3), followed by addition of 1 ml cold 80% methanol on dry ice. Cell suspensions were transferred into Eppendorf tubes and 10 nmol D/L-norvaline was added. After rigorously mixing, the suspension was pelleted by centrifugation (18,000*g*, 4 °C). The supernatant was transferred into a glass vial, metabolites dried down under vacuum, and resuspended in 70% acetonitrile. For the mass spectrometry-based analysis of the sample, 5 μl was injected onto a Luna NH2 (150 mm × 2 mm, Phenomenex) column. The samples were analysed with an UltiMate 3000RSLC (Thermo Scientific) coupled to a Q Exactive mass spectrometer (Thermo Scientific). The Q Exactive was run with polarity switching (+3.50 kV/−3.50 kV) in full scan mode with an m/z range of 65–975. Separation was achieved using A) 5 mM NH_4AcO (pH 9.9) and B) ACN. The gradient started with 15% A) going to 90% A) over 18 min, followed by an isocratic step for 9 min and reversal to the initial 15% A) for 7 min. Metabolites were quantified with TraceFinder 3.3 using accurate mass measurements (≤3 ppm) and retention times. Normalized metabolite data are available at figshare.com (https://doi.org/10.6084/m9.figshare.c.3801271).

Statistics and reproducibility. Experiments were performed on male and female animals in approximately equal numbers with no apparent difference in phenotype between sexes. All phenotypes described are representative of a minimum of $n = 3$ littermate pairs as indicated in the description of each experiment. For analysis of the hair regrowth phenotype no statistical measure was used to determine the sample size beforehand, nor were statistics used to measure effects, as the results were essentially positive or negative as represented in the figures. The results described include data from all treated animals. Investigators were not blinded to allocation during the experimental data collection. Experiments were not randomized. All results shown are representative images from at least three independently treated animals, and genotyping was performed both before and after animal treatment for confirmation. For graphs, all comparisons are shown by Student's two-tailed unpaired *t*-test and all graphs, bars or lines indicate mean and error bars indicate standard error of the mean (s.e.m.).

Data availability. Previously published transcriptomics data that were reanalysed here are available under accession code GSE67404 and GSE51635 (refs 35,36). Normalized metabolite data are available at figshare.com (https://doi.org/10.6084/m9.figshare.c.3801271). All other data supporting the findings of this study are available from the corresponding author on reasonable request.

36. White, A. C. *et al.* Stem cell quiescence acts as a tumour suppressor in squamous tumours. *Nat. Cell Biol.* **16**, 99–107 (2014).

nature cell biology

DOI: 10.1038/ncb3575

In the format provided by the authors and unedited.

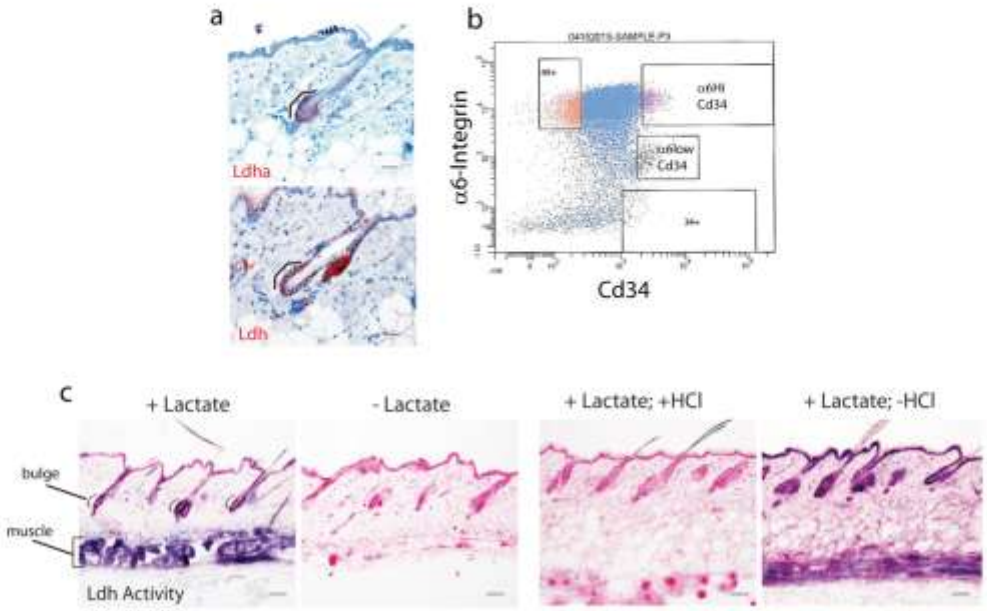

Supplementary Figure 1 Validation of key reagents and assays **a**, top, IHC with antibody recognizing specifically Ldha (same as used in Fig 1a). bottom, IHC with antibody recognizing multiple isoforms of Ldh protein. Scale bars indicate 20 micrometers. **b**, the sorting strategy employed to isolate two populations of cells from the bulge. This particular sort was used to isolate the protein samples shown by western blot in Fig 1b. **c**, Validation of colorimetric Ldh enzyme activity assay. The highest Ldh enzyme activity was observed in HFSC bulge and in the muscle. Activity indicated by purple stain; pink color is nuclear fast red counterstain. In absence of substrate lactate there was no detectable activity (purple stain). **right**, Additional validation of colorimetric Ldh enzyme activity assay. Enzyme activity inhibited by treating skin with HCl before addition of staining solution with substrate lactate. No Ldh activity (purple stain) detected. Skin in which enzyme activity is not inhibited by Hydrochloric Acid (HCl) shows highest Ldh enzyme activity in HFSC bulge and in the muscle. Scale bars indicate 50 micrometers.

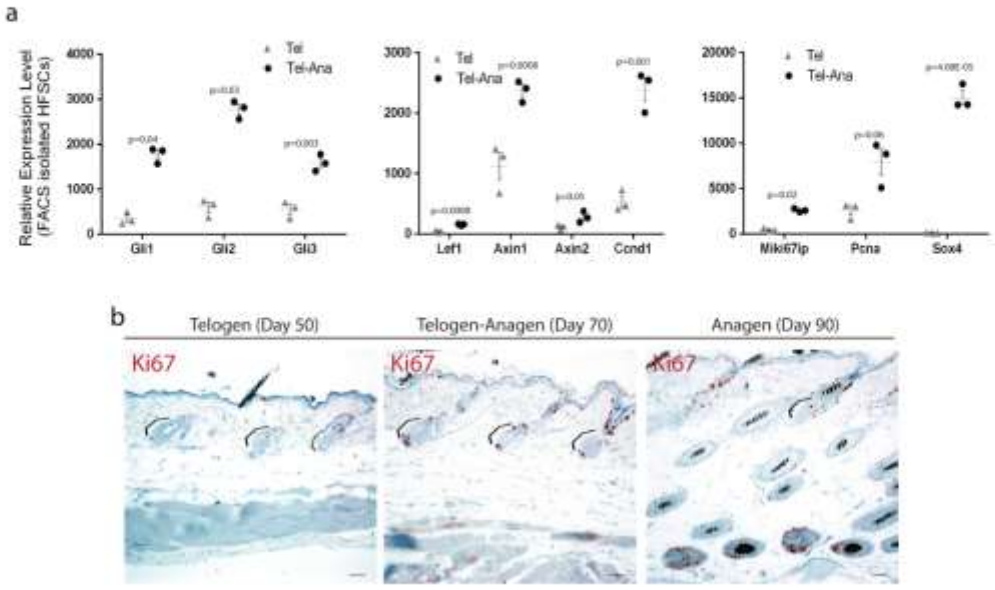

Supplementary Figure 2 Validation of hair cycle stage **a**, Analysis of RNA-seq data to validate that HFSCs in telogen-anagen transition were in fact in such a transition. The telogen-anagen transition is known to be driven by Shh (Gli factors are targets) and Wnt (Lef1, Axin, Ccnd1 are targets) signaling, and correlate with increased proliferation (Ki67 and Pcna). In addition, Sox4 was previously identified as a regulator of the telogen-anagen transition. n=3 mice per timepoint. Shown as mean ± SEM. Paired t-test was performed, $p < 0.05$. **b**, staining for Ki-67 marks dividing cells during various stages of the hair cycle. Brackets indicate the HFSC niche. Scale bars indicate 100 micrometers.

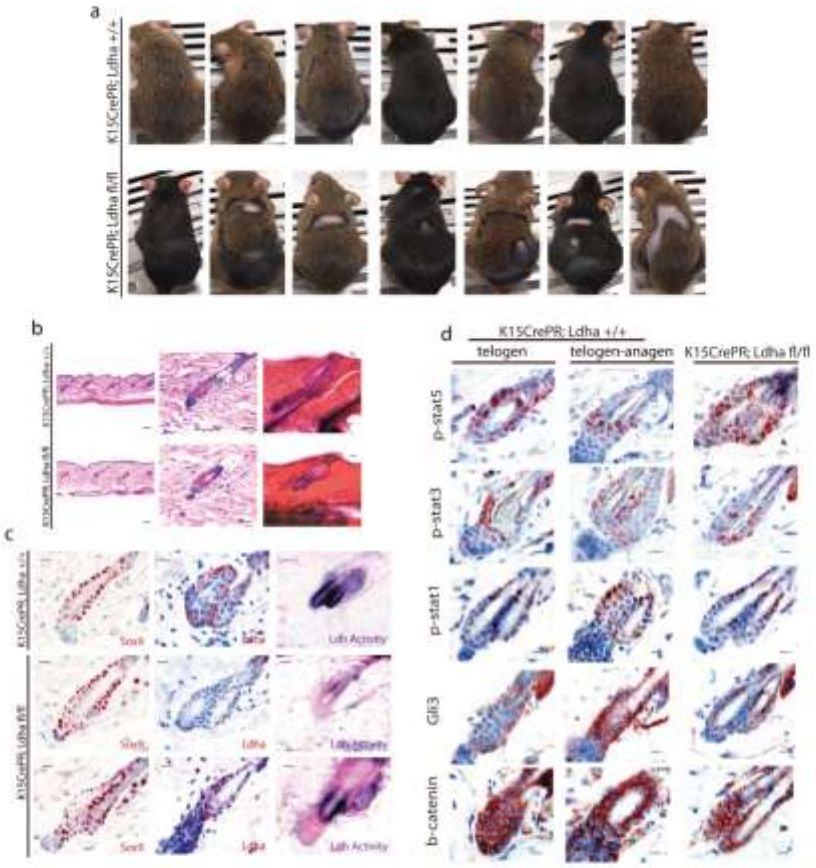

Supplementary Figure 3 Long term deletion of Ldha in HFSCs **a**, *K15CrePR;Ldha*$^{fl/fl}$ animals treated with Mifepristone during telogen (day 50) were allowed to develop for 6 months. None of the *K15CrePR;Ldha*$^{fl/fl}$ mice showed complete hair regrowth, compared to control animals that all grew their hair coats back completely. Images are representative of at least 12 animals per genotype. **b**, Histological examination of the long term *K15CrePR;Ldha*$^{fl/fl}$ mice showed that Ldha-null HFSCs remained in telogen while WT HFSCs went through anagen and then returned to telogen. This is apparent from thick sections (50 micron, right) that show an increased number of club hairs in the WT relative to *Ldha*-null follicles. Scale bars indicate 100 micrometers (left), and 20 micrometers (middle and right). **c**, IHC for HFSC marker Sox9 showed that deletion of *Ldha* from HFSCs does not affect their presence in the bulge even after 6 months. In addition, IHC and Ldh activity assay demonstrate that the deletion of *Ldha* was sustained. Because of the mosaicism of the deletion, in some portions of *K15CrePR;Ldha*$^{fl/fl}$ skin *Ldha* was not deleted. Shown on the bottom row is tissue from hair bearing skin in the *K15CrePR;Ldha*$^{fl/fl}$ mice where *Ldha* was still expressed, showing that new hair growth in *K15CrePR;Ldha*$^{fl/fl}$ mice was due to lack of deletion of *Ldha* caused by the mosaic approach used to mediate Cre recombination. Scale bars indicate 20 micrometers. **d**, To determine how various signaling pathways previously linked to the hair cycle are affected by loss of *Ldha* in HFSCs, we performed IHC for markers that indicate activity of these pathways in telogen and telogen-anagen transition. Note that pStat5 appears to be suppressed in normal telogen-anagen transition, and this does not seem to occur in *Ldha*-null HFSCs. pStat1 and pStat3 did not seem to be affected by loss of *Ldha*. Expression of Gli3, a target of Shh signaling, is typically induced in an activated hair germ derived from HFSCs, but *Ldha*-null HFSCs do not make an active hair germ. Activation of the Wnt pathway is indicated by nuclear localization of β-catenin, and very little nuclear β-catenin was detected in Ldha-null HFSCs. Scale bars indicate 6 micrometers.

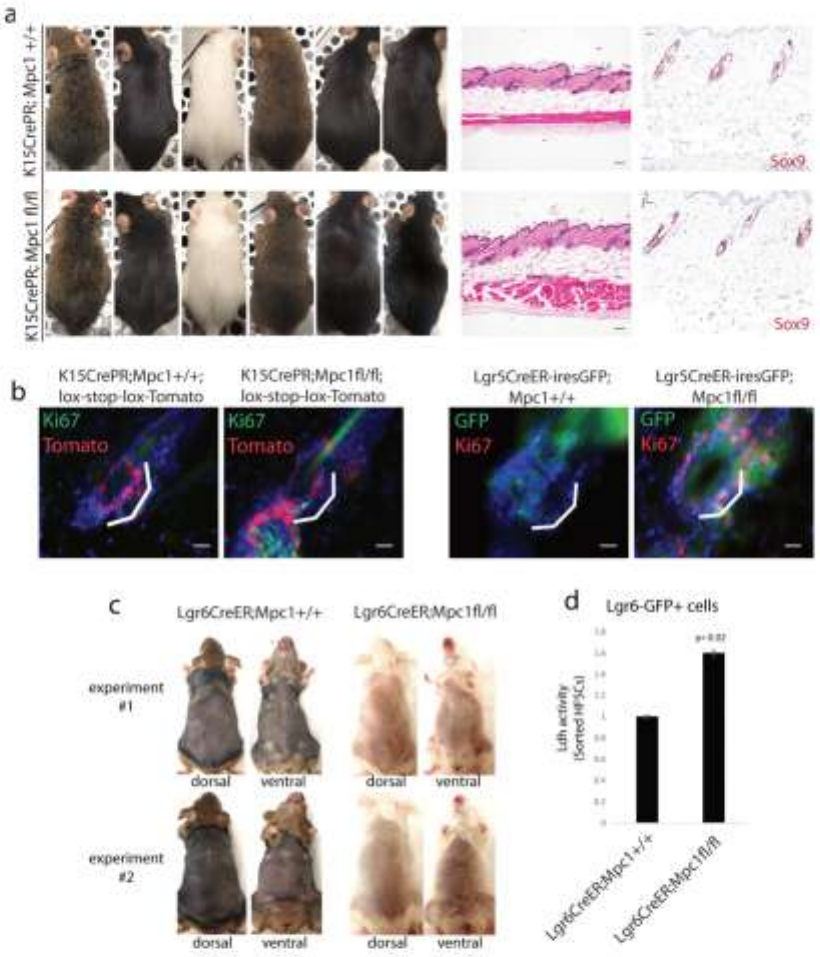

Supplementary Figure 4 Long term deletion of Mpc1 in HFSCs **a**, Six months after initiation of deletion of Mpc1 in HFSCs (*K15CrePR;Mpc1fl/fl*), mice lacking Mpc1 show no deleterious effects as measured by the hair cycle (left), pathology (middle, H and E), or staining for HFSCs (right, Sox9). Scale bars indicate 100 micrometers in middle panel, and 50 micrometers in right panel. Images are representative of at least 12 animals per genotype. **b**, To demonstrate that the deletion of Mpc1 promotes proliferation specifically in HFSCs, we used *K15CrePR;Ldha*$^{fl/fl}$ mice bearing a lox-stop-lox-Tomato allele to look at K15+ HFSCs and proliferation with and without Mpc1 deletion (left). In addition, we took advantage of the ires-GFP within the *Lgr5CreER* allele to stain for Ki-67 and GFP and look for co-localization with and without Mpc1 deletion (right). White brackets denote bulge area. Scale bars represent 20 micrometers. **c**, Deletion of *Mpc1* in mice bearing the *Lgr6CreER* allele shows no premature induction of the hair cycle. **d**, Ldh activity assay on sorted HFSCs from either control or *Lgr6CreER* mediated *Mpc1* deletion mice showed increased activity in cells lacking Mpc1. n=6 mice per genotype pooled from 2 independent experiments. Shown as mean ± SEM. Paired t-test was performed, $p < 0.05$.

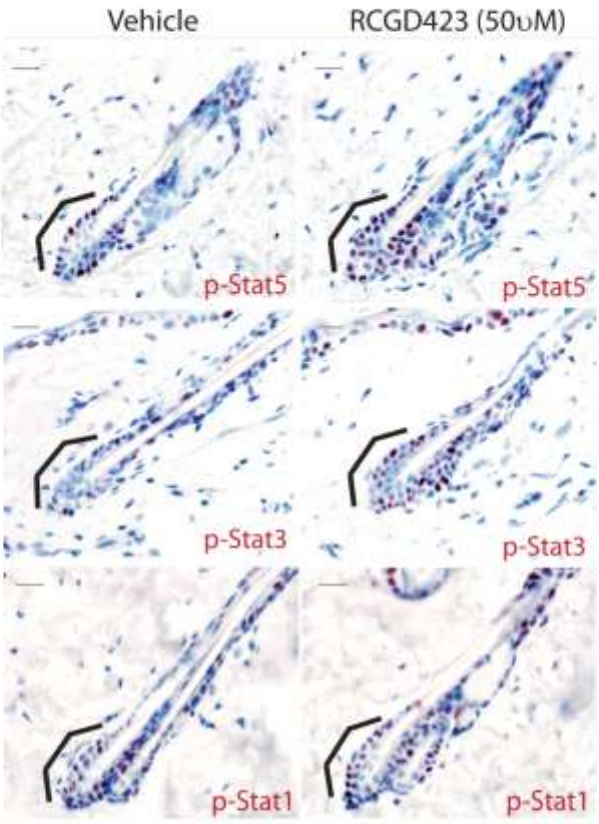

Supplementary Figure 5 Stimulation of Jak-Stat signaling and the hair cycle. RCGD423 was applied topically to shaved mice at day 50. 48 hours after treatment, the skin was harvested and prepared for IHC. IHC with the indicated antibodies demonstrates relative activity of Stat signaling in vehicle vs RCGD423 treated skin. Scale bars indicate 20 micrometers.

Fig1

Fig 4

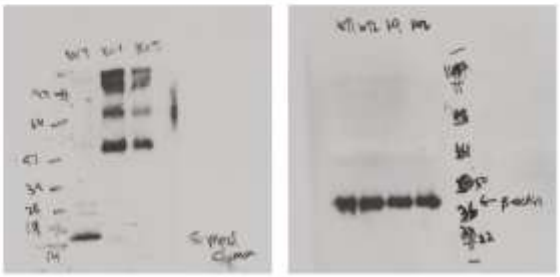

Fig 6

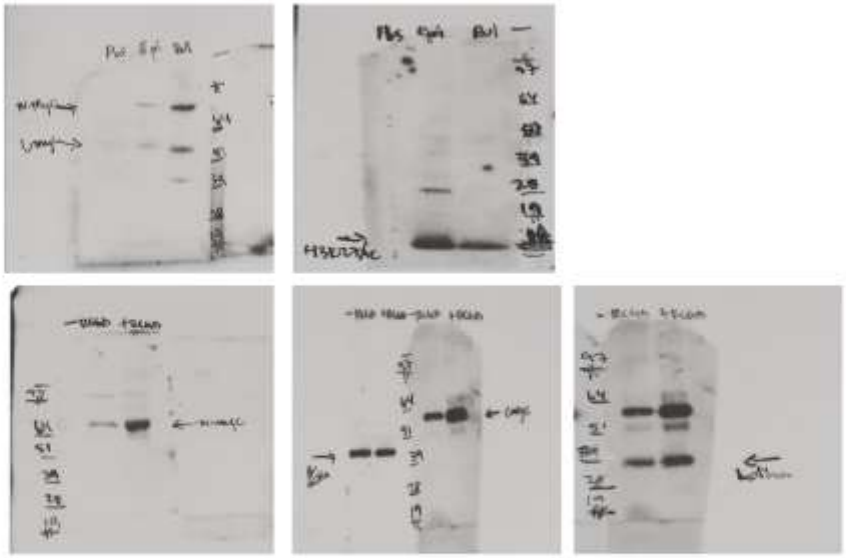

Supplementary Figure 6 Unprocessed Blots. Unprocessed scans of the blots shown in Figures 1, 4, 6 are shown.

Supplementary Table Legend

Supplementary Table 1 Presented is an inventory of mice that are described in Figures 1-6 (and Supplementary Figures 1-5), including age, sex, and genotype.

Chapter 3

Topical Inhibition of the Electron Transport Chain Can Stimulate the Hair Cycle

Topical Inhibition of the Electron Transport Chain Can Stimulate the Hair Cycle

Journal of Investigative Dermatology (2017) ■, ■–■; doi:10.1016/j.jid.2017.10.021

TO THE EDITOR

Enormous effort over the last 3 decades has identified a number of signaling pathways that act on hair follicle stem cells (HFSCs) to promote both quiescence as well as activation (Chan et al., 2004; DasGupta and Fuchs, 1999; Kimura-Ueki et al., 2012; Ming Kwan et al., 2004; Paus and Foitzik, 2004; Plikus et al., 2008; Sugawara et al., 2010; Vauclair et al., 2005; Zhang et al., 2006). With respect to intrinsic mechanisms of HFSC regulation, less is known about the cellular metabolism of individual cell types in the epidermis. In general, it has been presumed that somatic cells use mostly the electron transport chain (ETC) to produce energy from pyruvate that was generated by the uptake and processing of glucose, while early embryonic and cancer cells are thought to also rely on production of lactate from pyruvate. We recently demonstrated that HFSCs balance the production of energy through the ETC with the production of lactate as well (Flores et al., 2017). Previous efforts to define metabolic activities in the epidermis focused on measurements of enzyme activities on entire follicles (Hamanaka et al., 2013; Kloepper et al., 2015). In addition, several studies used transgenic models targeting the entire epidermis (including the follicle) for deletion of ETC components (Hamanaka et al., 2013; Kloepper et al., 2015). Those studies suggested that genetic blockade of the ETC leads to degeneration of the follicle. It is less clear whether inhibition of ETC complexes, as opposed to genetic ablation of ETC, would affect cell metabolism or fate decisions.

In the study by Flores et al. (2017), we deleted Ldha specifically in HFSCs and found that blocking lactate production prevented activation of HFSCs. In addition, deletion of a protein required to transport pyruvate into mitochondria (Mpc1) in HFSCs led to the increase of lactate production and acceleration of HFSC activation (Flores et al., 2017). Therefore, we hypothesized that pharmacological ETC inhibition would promote HFSC activation because of increased production of lactate.

To determine whether manipulation of ETC activity could affect HFSC activation, we used topical application of various inhibitors of ETC components during a resting phase of the hair cycle. At postnatal day 50, the HF is in telogen, a resting phase where the stem cells of the follicle are quiescent until the start of the next hair cycle at day 70–80 (Greco et al., 2009; Muller-Rover et al., 2001; Paus and Foitzik, 2004). Rotenone, phenformin, and antimycin A are all established inhibitors of Complex I and Complex III, respectively (Graeber et al., 1976). Animals were shaved at postnatal day 47 and treated with the indicated compounds or vehicle on the shaved area every 48 hours for the indicated duration. After 3–4 treatments (8–12 days), animals treated with ETC inhibitors began to show signs of hair cycle activation macroscopically, judged by pigmentation of the skin in black mice, whereas vehicle-treated mice did not show significant pigmentation for at least 20 days (Figure 1a and Supplementary Figure S1a online). As defined previously, the epidermis of murine skin becomes pigmented upon induction of the hair cycle, which is indicative of the generation of melanocytes injecting pigment (melanin) into the keratinocytes, which go on to make the hair shaft, as well as those in the interfollicular epidermis. Therefore, the induction of pigmentation observed after 8–12 days in ETC inhibitor–treated mice was most likely indicative of hair cycle activation induced by this treatment.

To demonstrate that the pigmentation induced by ETC inhibition was in fact due to changes in HFSC activation, tissue was harvested and subjected to pathology. Histological analysis showed that follicles in back skin treated with ETC inhibitors underwent a normal telogen-to-anagen transition (Figure 1b and Supplementary Figure S1b). These findings were in contrast to previous studies showing that transgenic abrogation of the ETC led to HF degeneration (Kloepper et al., 2015).

To determine whether the hair cycle induction driven by ETC inhibition was typical, we measured the thickness of each layer of skin across different stages of treatment. As shown in Figure 1c, all of the ETC inhibitors increased the thickness of the epidermis, dermis, and particularly the hypodermis, suggesting an expansion of the adipocytes. Analysis of ETC-inhibited skin showed an increase in Ki67 in HFSCs a week after treatment, evidence of HFSC activation in response to ETC inhibition (Figure 1d and Supplementary Figure S1d). To determine whether application of the ETC inhibitors promoted inflammation, which could cloud interpretation of hair cycle data, we assessed various markers of chemokine response and the presence of inflammatory immune cells after treatment. We found no evidence of significant inflammation by these measures in response to ETC inhibition (Supplementary Figure S1d).

To determine the effect on cellular metabolism of ETC inhibition by rotenone, phenformin, and antimycin A, we performed two measures of metabolic pathways. First, we quantified lactate dehydrogenase activity on cells isolated from the epidermis treated with ETC inhibitors for 48 hours (Figure 2a). Next, we employed metabolomics on

Abbreviations: ETC, electron transport chain; HFSC, hair follicle stem cell

Accepted manuscript published online 26 October 2017; corrected proof published online XXX

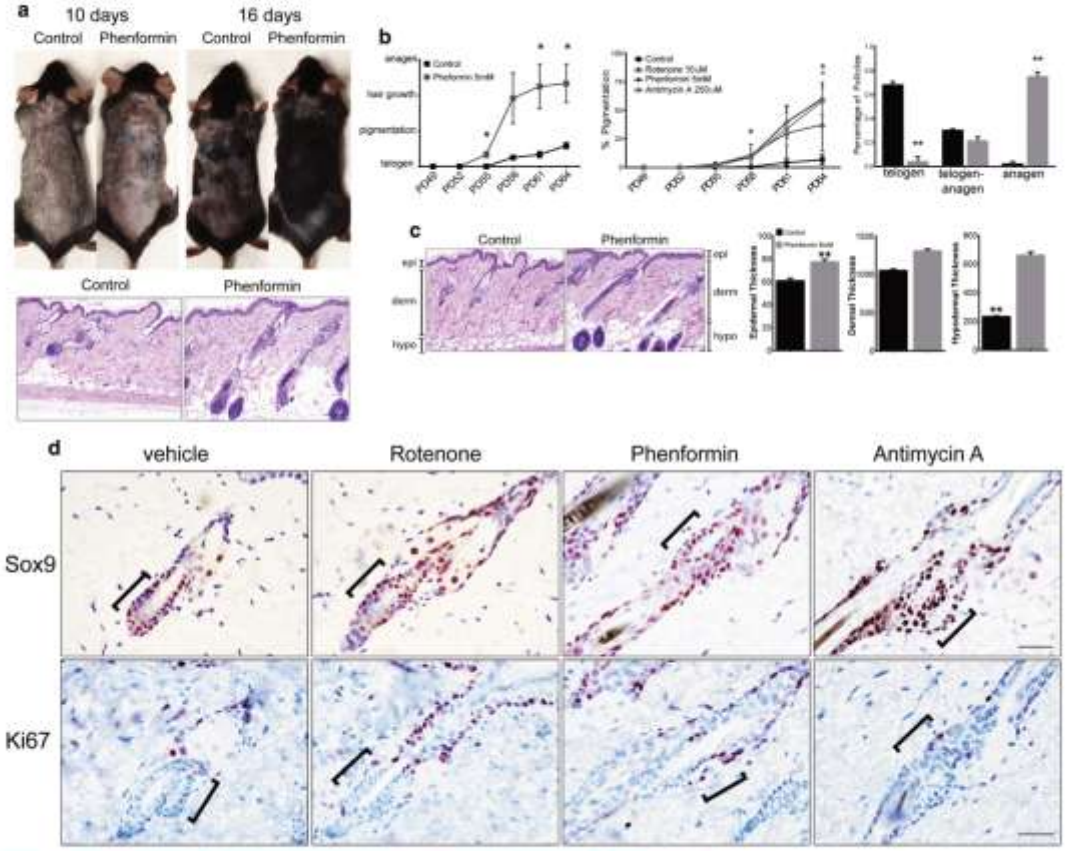

Figure 1. Topical treatment with electron transport chain (ETC) inhibitor can promote the hair cycle. (**a**) Mice were shaved at day 50 (telogen) and topically treated with phenformin (5 uM) every other day for 2–3 weeks. The image demonstrates new pigmentation and then hair growth in response to treatment with phenformin at 10 and 16 days, and hematoxylin and eosin staining confirms advancement of the hair cycle (bottom). (**b**) Top: quantification of macroscopic changes to the hair cycle in treatment and control. Bottom: quantification of changes to the hair cycle at the microscopic level. Quantification performed across 13 vehicle-treated and 9 phenformin-treated male mice. (**c**) Top: changes to the thickness of the epidermis, dermis, and hypodermis were assessed microscopically and quantified below. (**d**) Immunohistochemistry for a marker of hair follicle stem cells (HFSCs) (Sox9) and proliferation (Ki67) demonstrated that HFSCs became activated in response to ETC inhibition by phenformin, rotenone, and antimycin A. Scale bars for (**a**) and (**b**) = 50 μm. Scale bar for (**c**) = 25 μm.

sorted HFSCs with and without treatment for either 48 hours or 10 days. These analyses indicated an increase in Ldh activity and lactate levels, as well as several other glycolytic intermediates, in response to ETC inhibition by rotenone, phenformin, and antimycin A (Figure 2b). This is consistent with our previous data showing that deletion of Mpc1 in HFSCs blocked pyruvate entry into mitochondria, leading to increased levels of lactate (Flores et al., 2017).

As mice age, the hair cycle is known to become protracted, such that upon shaving, only portions of the back skin show regrowth of hair within 1–2 months. We treated various batches of aged mice (at least 17 months) for 30 days with ETC inhibitors to determine whether this metabolic manipulation could stimulate the hair cycle even in dormant follicles. We found that topical application of phenformin, rotenone, or antimycin A all led to more complete hair regrowth across the entire back skin on a time course similar to that of younger mice (Supplementary Figure S2a online). As in younger animals, treatment with these ETC inhibitors led to an increase in lactate pool levels, as measured by metabolomics (Supplementary Figure S2b). The results presented here describe a method to promote lactate production and subsequent hair cycle activation. Building on our previous genetic dissection of metabolism and HFSC activation, this work provides a relatively simply route to promote proliferation of HFSCs.

Animals

Wild-type male and female 49-day-old C57BL/6 mice were obtained from Jackson Laboratories (Bar Harbor, ME) for all topical experiments. All animals were maintained in University of California Los Angeles Division of Laboratory Medicine–approved pathogen-free barrier facilities and procedures were

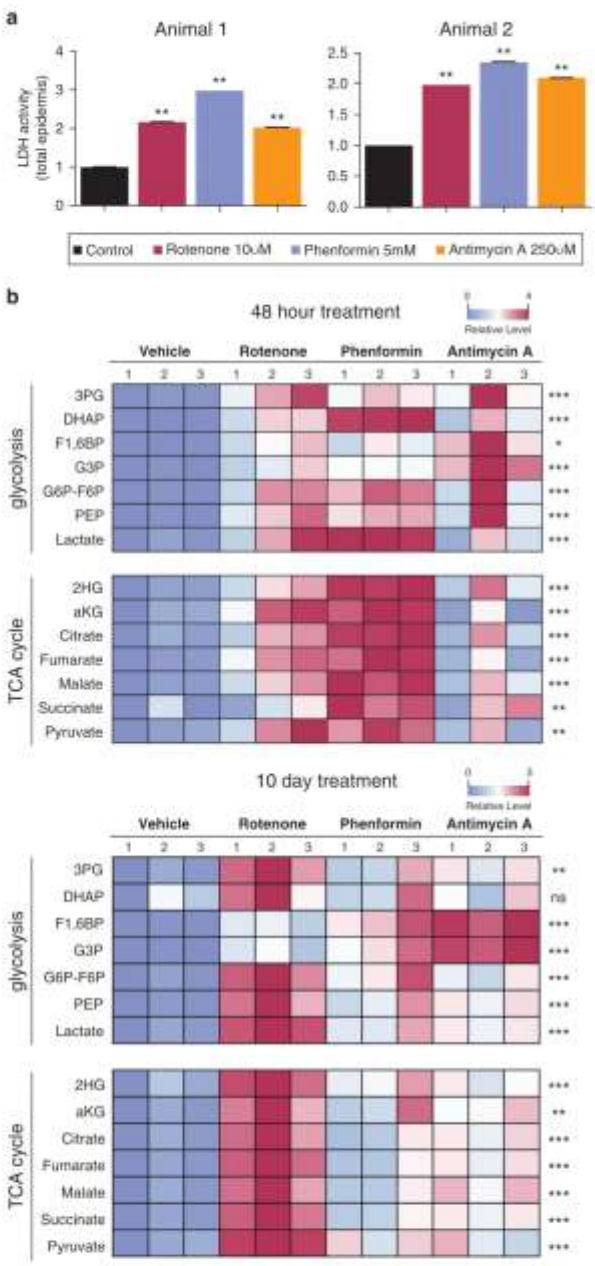

Figure 2. Topical electron transport chain (ETC) inhibition increases lactate production. (**a**) Mice were treated topically with the indicated ETC inhibitor for 48 hours. Total epidermis was isolated, lysed, and subjected to lactose dehydrogenase (LDH) activity assay. Relative LDH activity is presented as the rate of activity over 30 minutes in two different animals. (**b**) Mice were treated topically with ETC inhibitor for 48 hours (top) or 10 days (bottom). Total epidermis was isolated and metabolites were extracted and subjected to metabolomics. Heatmap indicates relative levels of metabolites related to glycolysis and the tricarboxylic acid (TCA) cycle.

performed using protocols that adhere to the standards of the University of California Los Angeles Animal Research Committee, Office of Animal Research Oversight, and the National Institutes of Health. Aged animals were acquired from a National Institute on Aging repository.

Topical inhibitor treatments

All drugs were suspended in DMSO and aliquoted at approximately fives times the half maximal inhibitory concentration for the purposes of penetrating the epidermal barrier upon in vivo application. Aliquots were then mixed with the appropriate volume of Premium Lecithin Organogel Base (Transderma Pharmaceuticals Inc., Coquitlam, BC, Canada) and topically applied onto the shaved dorsal skin of 49-day-old telogen-stage mice. Two experiment time points were used: acute treatment (two doses across 48 hours) or long-term studies (one dose three times a week for approximately 1.5 weeks). Full-thickness dorsal skin was collected for histological analysis, cryosectioning, RNA isolation, or epidermal stem cell isolation according to well-established FACS protocol.

Histology and immunostaining

A set of full-thickness skin samples were obtained from post-mortem tissue harvesting, fixed overnight in 4% paraformaldehyde, and then dehydrated for paraffin embedding and slide generation; hematoxylin and eosin staining was performed according to standard protocol. For immunohistochemistry, formalin-fixed, paraffin-embedded tissue slides were cleared and rehydrated through a series of ethanol washes. Antigen retrieval (20 minutes in pressure cooker, microwaved at 100 power) was performed with 10 mM citrate. Slides were incubated in hydrogen peroxide (30 minutes at 4°C) and then blocked with 10% goat serum/0.1% Tween for 1 hour at room temperature. Primary antibodies were added and incubated overnight. The following antibodies were used: rabbit Sox9 1:800 (Abcam, Cambridge, MA; 185667), rabbit Ki67 1:200 (Abcam 16667), phospho-EGFR 1:500 (Abcam 40815), IL-6 1:500 (Abcam 6672), and CD11b 1:250

(550282; BD Pharmingen, San Jose, CA). Sections were washed the following day with 0.1% phosphate buffered saline with Tween and incubated with rabbit secondary horseradish peroxidase–labeled polymer (Dako, Carpinteria, CA) for 1 hour at room temperature, and then quickly washed with 0.1% phosphate buffered saline with Tween and phosphate buffered saline. AEC chromogen (Dako) was used for the colometric development reaction. Slides were then briefly counterstained with hematoxylin, mounted with Faramount Aqueous Mounting Media (Dako), and sealed for subsequent visualization by light microscopy.

Hair cycle analysis

Hair cycles were assessed macroscopically by photographic documentation. A scale was established to grade hair cycle stage: 1) telogen (pink, white skin when dorsally shaved); 2) pigmentation (broad blue/gray pigment spots/patches on shaved dorsal area); 3) hair growth (dark pigmentation coupled with small patches of fur); and 4) anagen (dark, full patches of fur within dorsal area) in relation to number of doses and elapsed time of treatment. Hematoxylin and eosin–stained images of all treatment conditions were imaged at ×20 magnification to assess morphological changes in control and treated skin. Hair cycle stages were also evaluated by follicular morphology into respective telogen, telogen-to-anagen transition, or anagen categories. Additionally, the epidermis, dermis, and subcutaneous fat layers were independently measured via ImageJ software (National Institutes of Health, Bethesda, MD), with approximately 25 measurements/skin layer/animal. Scale was set at 1.68 micrometer/pixel for global layer measurements.

Lactate dehydrogenase plate reader metabolic assay

Protein lysate was obtained from cell pellets and resuspended in RIPA buffer with Halt protease and phosphatase inhibitors (Thermo Fisher Scientific, Waltham, MA). Staining solutions for lactate dehydrogenase were prepared with Tris buffer (pH 7.4), XTT, nicotinamide-adenine dinucleotide, phenazine methosulfate, substrate (lactate), and reagent-grade water and held at 37°C until use. Solution was added directly onto samples prepared in triplicate across a 96-well plate. A microplate reader held at 37°C measured 457-nm absorbances every 3 minutes across a 3-minute period to assess enzyme kinetics.

Metabolomics

The experiments were performed as described in Flores et al. (2017). Cells were washed with cold 150 mM ammonium acetate (pH 7.3), 1 ml cold 80% MeOH was added, and 10 nmol D/L-norvaline was added. After mixing and pelleting centrifugation, the supernatant was moved to glass vials, dessicated under vacuum, and resuspended in 70% acetonitrile. Five micrometers of sample were injected onto a Luna NH2 (150 mm × 2 mm; Phenomenex, Torrance, CA) column. Samples were analyzed by an UltiMate 3000RSLC (Thermo Scientific) coupled to a Q Exactive mass spectrometer (Thermo Scientific). The Q Exactive ran with polarity switching (+3.50 kV/−3.50 kV) in full scan mode with an m/z range of 65–975. Separation was performed using 5 mM NH_4AcO (pH 9.9) and acetonitrile. The gradient ran from 15% to 90% over 18 minutes, followed by an isocratic step for 9 minutes and reversal to the initial 15% for 7 minutes. Metabolites were quantified with TraceFinder 3.3 (Thermo Fisher Scientific) using accurate mass measurements (≤3 parts per million) and retention times.

Microscopy

Bright-field immunohistochemistry, hematoxylin and eosin–stained, and Nuclear Fast Red (Sigma, St Louis, MO)–stained images were captured using an Olympus BX51 light microscope (Olympus, Tokyo, Japan).

Statistical analysis

Data were analyzed and error bars represent standard error of the mean. An unpaired, two-tailed Student *t* test determined significance, with $P < 0.05$ considered statistically significant, denoted by asterisks (*$P < 0.05$, **$P < 0.01$, ***$P < 0.001$, ****$P < 0.0001$).

CONFLICT OF INTEREST

The authors state no conflict of interest.

ACKNOWLEDGMENT

We would like to acknowledge the efforts of technical staff of the Lowry lab, particularly Jessica Cinkornpumin, and of the Coller Lab, particularly David Jelinek. All metabolomics analyses were performed and initially processed by the UCLA Metabolomics Core Facility run by Daniel Braas. This work was supported by a training grant to MM (NSF Graduate Research Fellowship [2015203740]). In addition, this work was supported by both Innovation and GABA Fund awards from the Broad Center for Regenerative Medicine (UCLA) and the National Institutes of Health (DLL: R01AG040288).

Matilde Miranda[1,2], *Heather Christofk*[1,3], *D. Leanne Jones*[1,2,3] and *William E. Lowry*[1,2,3,*]

[1]*Molecular Biology Institute, University of California Los Angeles, Los Angeles, California, USA;* [2]*Department of Molecular Cell and Developmental Biology, University of California Los Angeles, Los Angeles, California, USA; and* [3]*Eli and Edythe Broad Center for Regenerative Medicine, University of California Los Angeles, Los Angeles, California, USA*

[*]*Corresponding author e-mail: blowry@ucla.edu*

SUPPLEMENTARY MATERIAL

Supplementary material is linked to the online version of the paper at www.jidonline.org, and at https://doi.org/10.1016/j.jid.2017.10.021.

REFERENCES

Chan KS, Sano S, Kiguchi K, Anders J, Komazawa N, Takeda J, et al. Disruption of Stat3 reveals a critical role in both the initiation and the promotion stages of epithelial carcinogenesis. J Clin Invest 2004;114:720–8.

DasGupta R, Fuchs E. Multiple roles for activated LEF/TCF transcription complexes during hair follicle development and differentiation. Development 1999;126:4557–68.

Flores A, Schell J, Krall AS, Jelinek D, Miranda M, Grigorian M, et al. Lactate dehydrogenase activity drives hair follicle stem cell activation. Nat Cell Biol 2017;19:1017–26.

Graeber GM, Marmor BM, Hendel RC, Gregg RO. Pancreatitis and severe metabolic abnormalities due to phenformin therapy. Arch Surg 1976;111:1014–6.

Greco V, Chen T, Rendl M, Schober M, Pasolli HA, Stokes N, et al. A two-step mechanism for stem cell activation during hair regeneration. Cell Stem Cell 2009;4:155–69.

Hamanaka RB, Glasauer A, Hoover P, Yang S, Blatt H, Mullen AR, et al. Mitochondrial reactive oxygen species promote epidermal differentiation and hair follicle development. Sci Signal 2013;6:ra8.

Kimura-Ueki M, Oda Y, Oki J, Komi-Kuramochi A, Honda E, Asada M, et al. Hair cycle resting phase is regulated by cyclic epithelial FGF18 signaling. J Invest Dermatol 2012;132:1338–45.

Kloepper JE, Baris OR, Reuter K, Kobayashi K, Weiland D, Vidali S, et al. Mitochondrial function in murine skin epithelium is crucial

for hair follicle morphogenesis and epithelial-mesenchymal interactions. J Invest Dermatol 2015;135:679–89.

Ming Kwan K, Li AG, Wang XJ, Wurst W, Behringer RR. Essential roles of BMPR-IA signaling in differentiation and growth of hair follicles and in skin tumorigenesis. Genesis 2004;39:10–25.

Muller-Rover S, Handjiski B, van der Veen C, Eichmuller S, Foitzik K, McKay IA, et al. A comprehensive guide for the accurate classification of murine hair follicles in distinct hair cycle stages. J Invest Dermatol 2001;117:3–15.

Paus R, Foitzik K. In search of the "hair cycle clock": a guided tour. Differentiation 2004;72:489–511.

Plikus MV, Mayer JA, de la Cruz D, Baker RE, Maini PK, Maxson R, et al. Cyclic dermal BMP signalling regulates stem cell activation during hair regeneration. Nature 2008;451:340–4.

Sugawara K, Schneider MR, Dahlhoff M, Kloepper JE, Paus R. Cutaneous consequences of inhibiting EGF receptor signaling in vivo: normal hair follicle development, but retarded hair cycle induction and inhibition of adipocyte growth in Egfr(Wa5) mice. J Dermatol Sci 2010;57:155–61.

Vauclair S, Nicolas M, Barrandon Y, Radtke F. Notch1 is essential for postnatal hair follicle development and homeostasis. Dev Biol 2005;284:184–93.

Zhang J, He XC, Tong WG, Johnson T, Wiedemann LM, Mishina Y, et al. BMP signaling inhibits hair follicle anagen induction by restricting epithelial stem/progenitor cell activation and expansion. Stem Cells 2006;24:2826–39.

Supplemental Figures

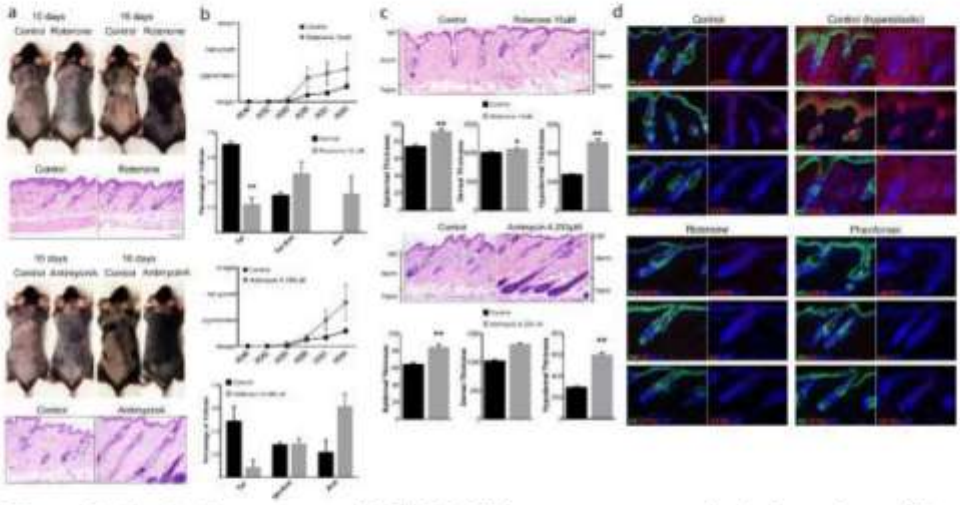

Figure S1. Topical treatment with ETC inhibitor can promote the hair cycle. a, Mice were shaved at day 50 (Telogen) and topically treated with antimycin A or Rotenone every other day for 2-3 weeks. The image demonstrates new pigmentation in response to treatment with either Rotenone or Antimycin A, and H and E staining confirms advancement of the hair cycle (BOTTOM). **b**, Top, quantification of macroscopic changes to the hair cycle in treatment and control. Bottom, quantification of changes to the hair cycle at the microscopic level. Quantification was performed with 13 vehicle treated, 11 Rotenone treated, and 9 Antimycin A treated male animals. **c**, Changes to the thickness of the epidermis, dermis and hypodermis were assessed microscopically (TOP) and quantified (BOTTOM). **d**, Immunolocalization was performed to detect evidence of inflammation due to topical application of ETC inhibitors. Both vehicle and ETC inhibitor treated skin was immunostained for phosphor-EGFR (chemokine receptor), CD11b (marker of macrophages), and IL6 (Chemokine). Vehicle treated skin from a wounded

animal with hyperplastic epidermis was used as a positive control for markers of inflammation. Scale bars indicate 50 micrometers.

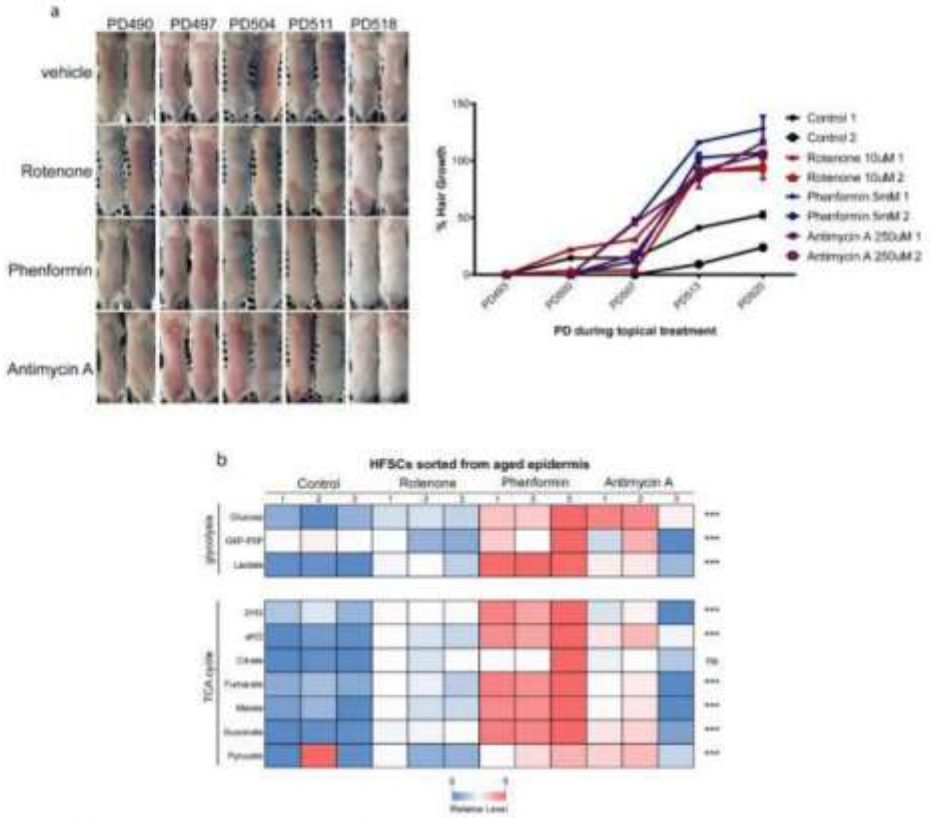

Figure S2. Treatment with ETC inhibitors can accelerate the hair cycle in aged mice. a, Female mice were shaved at 17 months of age and then treated with vehicle or the indicated ETC inhibitor every other day for up to 30 days. Images taken over time indicate the ETC inhibition promotes a more complete re-growth of hair after shaving in aged mice. Quantification of phenotype emergence from two pairs of animals are

presented on the right. Data shown are representative of three independent experiments with 10 mice each. **b**, Metabolites were isolated from sorted HFSCs from skin treated with ETC inhibitors at the end of the hair cycle experiment depicted in **a**. Heatmap shows relative levels of the indicated metabolites.

Chapter 4

Defining the Mechanism of GPCR/cAMP/Creb Signaling in HFSC Activation

THE JOURNAL OF INVESTIGATIVE DERMATOLOGY

Defining a role for GPCR/cAMP/Creb signaling in HFSC activation

Journal:	*Journal of Investigative Dermatology*
Manuscript ID	JID-2020-0755
Article Type:	Original Article
Date Submitted by the Author:	31-Aug-2020
Complete List of Authors:	Miranda, Matilde; University of California Los Angeles, MCDB Avila, Itzetl; University of California Los Angeles, MCDB Esparza, Jasmine; University of California Los Angeles, MCDB Shwartz, Juila; Harvard University, Department of Stem Cell and Regenerative Biology Hsu, Ya-Chieh; Harvard University Department of Chemistry and Chemical Biology, Harvard Stem Cell Insitute Berdeaux, Rebecca; The University of Texas Health Science Center at Houston John P and Katherine G McGovern Medical School, Integrative Biology and Pharmacology Lowry, William; UCLA, MCDB
Keywords:	Cell Biology, Hair Biology, Metabolomics, Stem Cells

Defining a role for GPCR/cAMP/Creb signaling in HFSC activation

Miranda M[1], Avila I[2], Esparza J[2], Shwartz Y, Hsu YC, Berdeaux R, and Lowry WE

1, Molecular Biology Institute, UCLA, Los Angeles, CA 90095

2, Department of Molecular Cell and Developmental Biology, UCLA, Los Angeles, CA 90095

3, Department of Biological Chemistry, DGSOM, UCLA, Los Angeles, CA 90095

4, Division of Dermatology, DGSOM, UCLA, Los Angeles, CA 90095

5, Broad Center for Regenerative Medicine, UCLA, Los Angeles, CA 90095

6, Jonsson Comprehensive Cancer Center, UCLA, Los Angeles, CA 90095

7, Integrative Biology and Pharmacology, University of Texas Health Science Center at Houston

8, Department of Stem Cell and Regenerative Biology, Harvard University and Harvard Stem Cell Institute, Cambridge, MA 02138

Correspondence:

William Lowry

615 Charles Young Drive South

Los Angeles, CA 90095

blowry@ucla.edu

Abstract

Manipulation of adrenergic signaling has been shown experimentally and clinically to affect hair follicle growth. Here we provide direct evidence that canonical cAMP/Creb signaling through adrenergic receptors can regulate HFSC activation and the hair cycle. We found that Creb activation is regulated through the hair cycle and coincides with HFSC activation. Both Isoproterenol and Procaterol, agonists of Adrenergic receptors show the capacity to activate HFSCs and the hair cycle in mice. Furthermore, deletion of Adrb2 receptor, which is thought to mediate sympathetic nervous system regulation of HFSCs, was sufficient to block HFSC activation. Downstream, stimulation of adenylyl cyclase with Forskolin, or inhibition of Phosphodiesterase to increase cAMP accumulation, or direct application of cAMP were each sufficient to promote HFSC activation and accelerate initiation of the hair cycle. Genetic induction of a DREADD allele demonstrated that GPCR/GαS stimulation specifically in HFSCs is sufficient for their activation and premature initiation of the hair cycle. Finally, we provide evidence that GPCR/Creb activation of HFSCs is through its ability to stimulate glycolytic metabolism, which was previously shown to stimulate HFSC activation.

Introduction

Skin is a classic model to study developmental biology and adult stem cells. The skin and hair protect animals from harmful environments but also require constant regeneration and maintenance throughout an animal's lifetime. While the interfollicular epidermis self-renews and maintains the outermost epidermal layers, hair follicle stem cells (HFSCs) located in a region termed the "bulge" drive the hair cycle(Lavker, Sun *et al.*, 2003; Morris and Potten, 1999). The hair follicle appendage undergoes a cycle consisting of three phases: growth (anagen), regression (catagen), and rest (telogen)(Fuchs, Merrill *et al.*, 2001). These cyclical bouts of destruction and regeneration require precise temporal and spatial control of the bulge niche. While most growth factor signaling pathways have been shown to act on HFSCs in this niche including Wnt, Tgfb, Bmp, Fgf etc(Plikus, 2012; Plikus, Mayer *et al.*, 2008), the role of canonical G-protein coupled receptors (GPCRs) and signaling downstream of these receptors has not been completely assessed.

G-protein-coupled receptors (GPCRs) are a large diverse family of cell surface receptors that mediate several cellular actions. GPCRs also represent a target protein for many pharmaceutical products on the market today. In addition, many adult stem cell populations are marked by expression of Lgr5, a seven-pass transmembrane receptor and therefore a potential GPCR(Carmon, Gong *et al.*, 2011). Therefore, it is conceivable that controlling GPCR signaling for homeostatic purposes is an understudied avenue to regulate stem cell biology. GPCRs coupled to GαS proteins are known to stimulate the activity of the effector protein Adenylyl Cyclase (AC), which regulate levels of a cyclic nucleotide, cAMP. cAMP is a signaling intermediate that can activate an enzyme called Protein Kinase A (Pka). Pka is known to phosphorylate and activate Cyclic AMP responsive element binding protein (Creb), which then translocates to the nucleus to drive expression of its target genes.

The role of Creb in regulating HFSC quiescence/activation is poorly understood. The only previous study to address the role of GPCR/GαS on the hair cycle showed that deletion of G-alpha-S or inhibition of Pka led to hyperactivation of the epidermis and a phenotype akin to Basal Cell Carcinoma(Iglesias-Bartolome, Torres *et al.*, 2015). This is an important issue as there is evidence that GPCR expression can be enriched in HFSCs. For instance, Lgr5 (also known as GPCR49 or Gpr49) is known to mark HFSCs, and activation of this receptor through its ligand R-spondin was shown to accelerate the hair cycle(Carmon, Gong *et al.*, 2011), but this was proposed to be due to signaling through the Wnt pathway.

Studies from the Paus group showed that sympathetic nerves appear to localize with the HFSC niche in mouse and human follicles potentially in a hair-cycle dependent manner and *ex vivo* activation of adrenergic receptor signaling accelerated hair growth(Botchkarev, Peters *et al.*, 1999; Cleale, Ingling *et al.*, 1998; Peters, Maurer *et al.*, 1999). In addition, cardiac patients taking beta-blockers, or antagonists of adrenergic receptors are known to suffer from temporary alopecia(Hathirat, Himathongkam *et al.*, 1980; Peters, Maurer *et al.*, 1999; Shelley and Shelley, 1985; Tatu, Elisei *et al.*, 2019). We recently demonstrated that sympathetic nerves innervate both the Arector Pili Muscle (APM) and directly on the HFSCs of the follicle(Shwartz, Gonzalez-Celeiro *et al.*, 2020). The APM is responsible for 'goosebumps' upon contraction and is permanently associated with the Bulge, or HFSC niche. We also showed that norepinephrine signaling in response to a cold environment through Adrb2 in HFSCs is directly responsible for receiving signals from the nervous system to drive contraction in the muscle, and for directly activating HFSCs to initiate a new hair cycle(Shwartz, Gonzalez-Celeiro *et al.*, 2020).

However, none of these studies directly demonstrated what types of signaling downstream of Adrenergic receptors are responsible for this effect. Adrenergic receptors are thought to signal canonically through Creb, but can also drive other pathways in a variety of settings. Here, we present evidence that a GPCR/GαS/AC/cAMP/Creb pathway directly acts on HFSCs by regulating cellular metabolism to promote their activation and thereby accelerate the hair cycle.

Results

Previous studies have shown that the human hair follicle is innervated by the sympathetic nervous system, and that stimulation by isoproterenol or procaterol, agonists of adrenergic receptor signaling, could promote activation of hair follicle growth(Botchkarev, Peters *et al.*, 1999; Cleale, Ingling *et al.*, 1998; Peters, Maurer *et al.*, 1999). These data were consistent with clinical observations that people taking "beta-blockers'" or adrenergic antagonist drugs displayed diminished keratinocyte proliferation and sporadic alopecia that subsided upon cessation of treatment(Shelley and Shelley, 1985). Here we sought to expand this work to uncover the mechanisms underlying these interesting observations. We started by repeating the previous work in a murine model of hair growth, by topically applying adrenergic receptor agonists isoproterenol or procaterol to mice during the second adult telogen, or resting phase of the hair cycle (day 50). At this stage, it is known that HFSCs remain quiescent and the hair cycle does not begin again until at least day 80-90. As shown in Figure 1A and Figure 1B, topical application of either isoproterenol or procaterol accelerated the onset of anagen, or hair growth, consistent with what the Paus group showed 20 years ago in *ex vivo* human follicles.

Adrenergic receptors typically signal through GαS and couple to adenylyl cyclase to cAMP levels and thereby activate cAMP-responsive binding factor (Creb) to initiate a transcriptional cascade in response to receptor signaling(Sun, McGarrigle *et al.*, 2007; Syrovatkina, Alegre *et*

al., 2016). However, the only previous related study suggested that loss of function of G□S instead would cause neoplasia akin to basal cell carcinoma(Iglesias-Bartolome, Torres *et al.*, 2015). Therefore, we measured the activity of cAMP/Creb signaling across the hair cycle in HFSCs by immunostaining with an antibody that recognizes the phosphorylated form of Creb. This analysis showed that Creb activation was negligible during telogen, and then strongly induced in the bulge and hair germ during the telogen-anagen period, coinciding with stimulation of proliferation as assessed by staining for Ki-67 (Fig 1C). Furthermore, upon quantification of pCreb-positive or Ki67-positive in various hair follicle compartments, we found the most active Creb and proliferative cells in the bulge and hair germ during the transition and anagen phase of the hair cycle (Figure 1D), suggesting Creb activation correlates with HFSC activation.

Because both isoproterenol and procaterol were both able to stimulate the hair cycle, we presumed that they were acting through adrenergic receptors(Botchkarev, Peters *et al.*, 1999; Cleale, Ingling *et al.*, 1998; Peters, Maurer *et al.*, 1999). To distinguish which of the four adrenergic receptors were possible in this context, we analyzed transcriptional data from both human and murine HFSCs. The Adrb2 receptor appeared from these studies to be the most likely candidate (Fig 1E and F). Crossing animals with floxed alleles for the Adrb2 gene with K15CrePR animals, we generated progeny with inducible loss of Adrb2 specifically in HFSCs. These animals showed a striking lack of both entry into anagen as well as Creb activation upon deletion of Adrb2 (Fig 1G). Quantification of the percentage of pCreb-positive or Ki67-positive cells in control and conditional knockouts (Fig 1G) revealed significant reduction in signal, suggesting a failure to activate Creb signaling and HFSCs upon deletion of Adrb2 in HFSCs. Therefore, we concluded that isoproterenol and procaterol were most likely stimulating the HFSCs in Fig 1A and B through a GPCR signaling specifically in HFSCs through the Adrb2 receptor.

The phosphorylation of Creb occurs through activation of Protein Kinase A (Pka) which is regulated by the concentration of cAMP(Meinkoth, Alberts *et al.*, 1993). cAMP is created through the activity of Adenylyl Cyclase (AC) downstream of GαS activation and can be then degraded through the action of Phosphodiesterase Enzymes (PDE) (Fig 2A)(Meinkoth, Alberts *et al.*, 1993). To understand whether the isoproterenol/procaterol effect was due to stimulation of GαS and thereby AC, we treated mice topically with forskolin, an established AC stimulating drug, and found an acceleration of the hair cycle (Fig 2B). To determine whether PDE inhibition is sufficient to activate pCreb and potentially affect the hair cycle, we topically treated mice during telogen with several PDE inhibitors we discovered in a previous study (#44, #61)(Cinkornpumin, Roos *et al.*, 2017) . Topical PDE inhibition during telogen appeared to strongly accelerate the hair cycle (Fig 2C). Because PDE inhibition is known to increase concentrations of cAMP, we also investigated whether directly increasing cAMP concentration through topical application could also affect the hair cycle. In fact, cAMP administration did indeed stimulate the hair cycle with a similar time course as PDE inhibition (Fig 2D and E).

Next, to determine the acute effect of elevated cAMP levels in the skin and confirm that each of the topically applied compounds having the expected effect on Creb stimulation, we performed immunohistochemistry (Fig 3A) for markers of cAMP signaling. Three treatments (over the course of one week) with each of the Creb simulating molecules led robust of pCreb signal in the treated epidermis and bugle niche, in addition to stimulating proliferation and and Creb targets (Fig 3A). Of note, staining for Sox9, a marker of HFSCs, did not uncover any dramatic change to the stem cell compartment upon topical treatments. Quantifying the degree of proliferation and Creb stimulation after treatment in the epidermis showed that both Creb activity and a marker of proliferation were strongly induced in all parts of the epidermis, including the

bulge, where HFSCs reside (Fig 3B). This is probably due to the fact that the application of the stimulators was topical and therefore all epidermal cells had access to the drugs. We also assessed whether stimulation of Creb signaling by any of these molecules led to an increase in inflammation, which is known to strongly influence the hair cycle. Staining for several markers of inflammatory cells following each of the indicated treatments did not yield strong evidence for inflammation (Supp Fig 1).

Based on the fact that topical application of isoproterenol, procaterol, forskolin, PDE inhibitors, or cAMP led to Creb activation in most of the cells of the epidermis, it was critical to understand whether activation of Creb specifically in HFSCs was important for regulation of the hair cycle, or whether it was a general activation of the epidermis. Therefore, we designed a molecular genetic approach to activate GPCR/Creb signaling strictly in HFSCs. Taking advantage of animals with an inducible DREADD allele that couples to GαS (and includes a GFP tracer in the polycistron), we crossed animals with K15CrePR1, which upon treatment with Mifepristone would allow for expression of the DREADD allele just in hair follicle cells. In addition, the DREADD receptor is not active without its artificial ligand Clozapine (CNO). Therefore, we were able to conditionally express an experimentally activatable GαS-coupled-GPCR just in HFSCs at distinct timepoints (Fig 4A). First, we confirmed that the K15 system we employed induced expression of the DREADD allele just in hair follicles as shown by restriction of GFP expression to the hair follicle stem cell compartment during telogen (Fig 4B). Induction of the DREADD protein complex with CNO during the second adult telogen (resting phase) led to an acceleration of the hair cycle (Fig 4C), akin to what was observed with topical application of Creb stimulating molecules. In Fig 4D, we quantified the time to hair cycle initiation as measured by pigmentation across 6 independent experiments, and the DREADD positive animals consistently showed an accelerated timeline. Combined with data showing that activation of AC

and cAMP could accelerate the hair cycle (Fig 2), we concluded that activation of the canonical pathway downstream of GPCRs, namely GαS/AC/Creb in hair follicle stem cells is sufficient to activate them and induce a new hair cycle. This was also consistent with the effect of loss of Adrb2 specifically in stem cells, which blocked their activation (Fig 1).

To characterize the downstream mechanisms by which activation of Creb led to acceleration of the hair cycle, we performed an RNA-seq experiment on total epidermis following three treatments with either a PDE inhibitor (#44) or cAMP (Fig 5A). With replicates for both treatments, we assessed the genes that were altered in response to both different treatments and in both replicates. This identified 859 genes that were consistently altered by Creb stimulation, strikingly, nearly all of them were induced by these treatments (Fig 5B). Gene ontological analyses clearly demonstrated upregulated responses related to metabolism (mitochondrial dysfunction, oxidative phosphorylation, cholesterol biosynthesis, TCA cycle, fatty acid oxidation, etc), therefore we delved deeper into this observation (Fig 5C). A second analysis uncovered p53 and Myc as the top transcriptional networks disrupted by activation of Creb signaling in the epidermis (Fig 5D). This is interesting as several stress response related pathways came from the GO analysis, and Myc is a well-established regulator of cellular metabolism. In fact, many metabolic enzymes are directly regulated by MYC binding at their promoters. We validated many of these transcriptional responses to Creb activation at the protein level by western blot as shown in Fig 5E.

The alteration of metabolic genes in response to Creb activation was so striking that in mapping those changes to a chart of metabolic enzymes important for glycolysis and the TCA cycle, we found that nearly every enzyme was induced in response to PDE inhibition of cAMP

administration (Fig 6A). We validated some of these changes at the protein level by immunohistochemistry for Glut1, Hk2 and Pkm2, and all were strongly induced throughout the epidermis (Fig 6B). We previously showed that endogenous lactate dehydrogenase activity could be measured in situ with a colorimetric assay (Flores, Jelinek), and applying that assay to animals treated with forskolin, cAMP or PDE inhibitors demonstrated a strong induction of activity of this key glycolytic enzyme (Fig 6C). This was validated in a quantifiable plate-reader assay on isolated epidermis as well (Fig 6D). Finally, we performed metabolomics on skin treated with cAMP. By first pulsing animals with c13-labeled glucose, we were able to identify metabolic flux of glucose and determine the relative level of glucose utilization by mass spectrometry. These data clearly showed that glycolytic intermediates were being produced at a higher rate in cAMP treated animals relative to control (Fig 6E). Together, these data are consistent with the idea that cAMP/Creb signaling can promote glycolytic flux while promoting HFSC activation and accelerating the hair cycle.

Discussion

Others have shown that the HFSC niche is innervated by the sympathetic nervous system, and in response to stimulation by environmental factors such as cold exposure, activated nerves promote HFSCs to initiate a new hair cycle. Here our data argue the idea that piloneural and sympathetic nervous system interaction(s) such as adrenergic signaling regulate intracellular mechanisms of hair growth via the Adrb/cAMP/Creb pathway. Regardless of the systemic mechanism, the current study focused downstream of the adrenergic receptor signaling system in HFSCs. This study explains the interesting observations made previously by the Paus and Hsu groups(Botchkarev, Peters *et al.*, 1999; Peters, Maurer *et al.*, 1999), and links this signaling cascade to cellular metabolism. Several recent studies have shown that alterations of metabolism can influence the rate at which HFSCs are activated to initiate a new hair

cycle(Flores, Schell *et al.*, 2017; Miranda, Christofk *et al.*, 2018). The synthesized interpretation is that increased glycolytic metabolism in HFSCs can prime them for activation. Since many of the established growth factor signaling pathways are known to activate glycolytic signaling as well (such as Wnt, Fgf, Egf), it is possible that the combination of these signaling events lowers the threshold for activation of HFSCs by raising the glycolytic capacity. We can now add Adrenergic signaling to the list of pathways capable of stimulating glycolysis as shown in Fig 5 and 6, whereby Creb activation directly stimulated the expression of various glycolytic enzymes. Whether glycolytic metabolism is indeed the common denominator in HFSC activation signaling remains to be determined.

The skin is one of the most densely innervated organs in mammals, reaching its peak in density during anagen, thereby underscoring the mechanism presented here and its promise in pharmacological manipulations of HFSCs through a neuroepithelial-metabolic-dependent fashion. It is conceivable other adult stem cell populations possess this kind of regulation machinery. Many adult stem cells regulate homeostasis in other tissues, being able to cycle between quiescence and activation with the appropriate milieu of signals. The current study provides evidence of GPCR signaling-to activate stem cells in the hair follicle.

However, this ability can also implicate them in cancer due to their highly proliferative capacity and relative dormancy in comparison to other cells in a tissue. HFSCs are one such example, previously shown to generate hair shafts, contribute to wound healing, and indeed act as a cancer cell of origin for squamous cell carcinoma (SCC) in a murine model(Lapouge, Youssef *et al.*, 2011). Upon active hair cycling, SCC can be initiated with the presence of oncogenic stimuli, such as activated Kras. CREB is also implicated in epidermal cancers when mutated in murine

skin. In the absence of CREB, epidermal papilloma formation is shown to be dramatically reduced, suggesting CREB may promote SCC in activated HFSCs(Rozenberg, Rishi *et al.*, 2009). Another consideration is that there is evidence that HFSCs only initiate SCC upon activation by the hair cycle(White, Khuu *et al.*, 2014). Therefore, any disruption of HFSCs or the hair cycle will alter tumor initiation by HFSCs. As a result, it is possible that reduced SCC in the absence of Creb, was due to the blockage of the hair cycle, and not a direct role for Creb in tumorigenesis initiated by HFSCs. Regardless, future efforts will address a potential role for innervation of the hair follicle during tumor initiation or progression, as many neoplasia in other tissues have been shown to be highly innervated.

In summary, by harnessing GPCR/GαS/cAMP/Creb signaling, this multifaceted approach highlights the immense promise for the development of neuropharmacological compounds in regenerative medicine and anti-cancer therapeutics.

Materials and Methods

Animals & Strains. Wildtype male and female 49-day old C57BL/6 mice were obtained from Jackson Laboratories for all topical experiments. All animals were maintained in UCLA's Division of Laboratory Medicine (DLAM)-approved pathogen-free barrier facilities and procedures were performed using protocols that adhere to the standards of the UCLA Animal Research Committee (ARC), Office of Animal Research Oversight (OARO), and the National Institutes of Health (NIH).

Topical Inhibitor Treatments. Isoproteranol (Sigma I5627) and proceterol (Sigma P9180) were purchased through a commercial vendor. Soluble cAMP, forskolin were also purchased from a commercial vendor (Sigma B5386; Sigma F6886) along with PKA inhibitor H89 (Sigma 371963-

M EMD Millipore). Phosphodiesterase inhibitor compounds 44 and 61 were discovered in a Lowry Lab drug screen and then small molecule stock was ordered from Asinex for topical use. All drugs were suspended in DMSO and aliquoted at approximately 5 times IC_{50} or EC_{50} for the purposes of penetrating the epidermal barrier upon *in vivo* application. Aliquots were then mixed with the appropriate volume of Premium Lecithin Organogel (PLO) Base (Transderma Pharmaceuticals Inc.) or Norwegian Formula Concentrated Hand Cream (Neutrogena) and topically applied onto shaved dorsal skin of 49 day old telogen-stage mice. Three experimental timepoints were used: acute treatment (two doses across 48 hours), week-long treatment (three doses across five days), or long-term studies (one dose three times a week for approximately 1.5 weeks). Full-thickness dorsal skin was collected for histological analysis, cryosectioning, protein isolation, RNA isolation, and/or for epidermal stem cell isolation according to well-established FACS protocol.

Hair Cycle Analysis. Hair cycles were assessed macroscopically by observational and photographic documentation. A scale was established to grade hair cycle stage: 1) telogen (pink, white skin when dorsally shaved); 2) pigmentation (broad blue/grey pigment spots/patches on shaved dorsal area); 3) hair growth (dark pigmentation coupled with small patches of fur); 4) anagen (dark, full patches of fur within dorsal area) in relation to number of doses and elapsed time of treatment. H&E images of all treatment conditions were imaged at 20x magnification to assess morphological changes in control and treated skin. Hair cycle stages were also evaluated by follicular morphology into respective telogen, telogen-to-anagen transition, or anagen categories.

Epidermal Cell Isolation. Experimental mice were humanely euthanized with CO2 and adminstered secondary euthanasia via cervical dislocation. Dorsal skin was briefly shaved, dissected, and the underlying fat layer was scraped using a surgical scalpel. Scraped skin pelts

were then put on petri dishes containing TrypLE Express Enzyme; no phenol red (Gibco), dermis side down, for overnight incubation and dissociation at 4C.

Protein Isolation. After overnight dissociation, total epidermis was obtained by mechanical separation using a surgical scalpel and filtered through 70um and 40um filters into cold 5% BCS. Single cell suspensions were then centrifuged for 10 minutes at 300g at 4C, followed by a brief PBS wash, and spun down for an additional 5 minutes at 350g at 4C. Cell pellet was then resuspended in RIPA with HALT protease/phosphatase inhibitors (ThermoFisher Scientific) to generate protein lysate. Protein concentration(s) were quantified using Pierce BCA assay (ThermoFisher Scientific) according to standard protocol.

Western Blotting. Protein concentrations were determined using Pierce BCA assay and approximately 9ug of protein were loaded into 4-12% Bis-Tris PAGE gels (Invitrogen) and run for 1 hour at 80V, then 30 minutes at 120V until ladder was adequately separated. Proteins were transferred onto a nitrocellulose membrane for 90 minutes at 370 mAh, and then blocked with 5% milk/0.1% tween for 1 hour at room temperature. The following primary antibodies were used: rabbit β-actin (Santa Cruz, 1:1000), rabbit Glut1 (Abcam 115730, 1:1000), rabbit Txnip (CST 14715, 1:1000), rabbit Hk2 (CST 2867, 1:1000), rabbit Pkm2 (CST 4053, 1:1000), rabbit Ldha (CST 3582, 1:1000). Membranes were washed the following day with 0.1% TBST and incubated with rabbit secondary HRP-labeled polymer (Invitrogen 31460, 1:1000) for 1 hour at room temperature. Pico PLUS Chemiluminescent ECL (ThermoFisher Scientific) reagent was added to membranes and subjected to film exposure.

Histology and Immunohistochemistry. Two sets of full-thickness skin samples per animal were obtained from post-mortem tissue harvesting; one sample was freshly embedded upright in OCT (Sakura Finetek) and flash-frozen with dry ice for cryosectioning, the other sample was fixed overnight in 4% paraformaldehyde, and then dehydrated for paraffin embedding and slide

generation; hematoxylin and eosin staining according to standard protocol. For immunohistochemistry, formalin-fixed, paraffin-embedded tissue slides section at 4um were cleared and rehydrated through a series of ethanol washes. Antigen retrieval (20 minutes in pressure cooker, microwaved at 100 power) was performed with 10mM citrate. Slides were incubated in hydrogen peroxide (30 minutes at 4C) and then blocked with 10% goat serum/0.1% tween for 1 hour at room temperature. Primary antibodies were added and incubated overnight. The following antibodies were used: rabbit pCreb (CST 9198, 1:800); rabbit Sox9 (Abcam 185966, 1:800); rabbit Ki67 sp6 (Abcam 16667, 1:50); rabbit cFos (Abcam 7963, 1:100); rabbit Glut1 (Abcam 115730, 1:500), rabbit Hk2 (CST 2867, 1:500), Pkm2 (CST 4053, 1:500). Sections were washed the following day with 0.1% PBST and incubated with rabbit secondary HRP-labeled polymer (Dako) for 1 hour at room temperature, and then quickly washed with 0.1% PBST and PBS. AEC chromogen (Vector) was used for the colometric development reaction. Slides were then briefly counterstained with hematoxylin, mounted with Faramount Aqueous Mounting Media (Dako) and sealed with clear nail polish for subsequent visualization by light microscopy.

Immunofluorescence. Samples embedded in OCT were sectioned at a thickness of 7um on a Leica 3200 Cryostat. Slides were briefly fixed in 4% formalin and then washed twice in PBS. Slides were blocked with 10% goat serum/0.1% Tween for 1 hour at room temperature. Primary antibodies were diluted into blocking buffer, added to samples, and incubated overnight. The following primary antibodies were used: chicken K5 (Covance SIG3475, 1:700), rabbit pCreb (CST 9198, 1:500), rat CD11b (Catalog, dilution?), and rabbit pEGFR (Catalog, dilution?). The next day, slides were washed in PBST. Secondary antibodies are added at 1:500 dilution, with DAPI (Invitrogen) at 1:1000 dilution, and incubated on slides at room temperature for two hours. Slides were then washed in PBST, mounted with Prolong Gold with DAPI (Invitrogen), and

sealed with clear nail polish. Images were collected at 20x and 40x oil magnifications unless otherwise specified.

Microscopy. Bright-field immunohistochemistry and hematoxylin/eosin-stained images were captured using an Olympus BX51 light microscope using a 40x oil immersion lens. Fluorescence images were generated with a Zeiss Model Axio5 Imager M1 Upright Fluorescence Microscope at respective magnifications.

LDH in situ assay. Slides with OCT sections were prepared by fixing mouse skin sections in 4% formalin for 5 minutes at room temperature. The sections were then washed with PBS for 10 minutes, and then incubated at 37C with staining solution until they reached desired intensity. Staining solutions were prepared with 50mM Tris pH 7.4 (Fisher), 750uM NAD (Sigma), 80uM phenazine methosulfate (Sigma), 600uM nitrotetrazolium blue chloride (Sigma), 10mM $MgCl_2$ (Sigma), and 10mM of lactate (Sigma). The slides were then counterstained with Brazilliant reagent (Anatech 861) and briefly washed with MilliQ water. Slides were mounted with Faramount Aqueous Mounting Media (Dako) and sealed with clear nail polish for subsequent visualization by light microscopy.

LDH plate reader assay. Protein lysate was obtained from cell pellets and suspended in RIPA buffer with HALT protease (ThermoFisher Scientific 87785) and phosphatase inhibitors (ThermoFisher Scientific 78420). Staining solutions for lactate dehydrogenase (LDH) were prepared with Tris buffer pH 7.4, XTT formazan, NAD, PMS, substrate (lactate), and reagent-grade water and held at 37C until use. Solution was added directly onto samples prepared in triplicate across a 96-well plate. A microplate reader held at 37C measured 457nm absorbances every 3 minutes across a 30 minute period to assess enzyme kinetics, using a Synergy-MX plate reader (Biotek Instruments). LDH activity was determined by calculating the change in slope of absorbance levels at all timepoints for each condition.

Metabolomics. The experiments were performed as described in (Miranda et al., 2017). Briefly, cells were washed with cold 150 mM ammonium acetate (pH 7.3) and a two-phase extraction was performed: addition of 400uL cold 100% MeOH, 400uL cold sterile H20, 10 nmol D/L-norvaline (internal standard), 400uL of cold chloroform. After mixing and pelleting centrifugation at 4C, the aqueous layer of the supernatant was moved to glass vials, dessicated under vacuum, and resuspended in 70% acetonitrile. 5ul of sample(s) were injected onto a Luna NH2 (150mm x 2mm, Phenomenex) column. Samples were analyzed by an UltiMate 3000RSLC (Thermo Scientific) coupled to a Q Exactive mass spectrometer (Thermo Scientific). The Q Exactive ran with polarity switching (+3.50 kV / -3.50 kV) in full scan mode with an m/z range of 65-975. Separation was performed using A) 5mM NH_4AcO (pH 9.9) and B) ACN. The gradient ran from 15% to 90% over 18 minutes, followed by an isocratic step for 9 minutes and reversal to the initial 15% A) for 7 minutes. Metabolites were quantified with TraceFinder 3.3 using accurate mass measurements (≤ 3 ppm) and retention times.

RNA Extraction and RT-PCR. Total RNA was extracted from whole epidermal cells using a Qiagen RNeasy Micro Kit. RNA was measured using a NanoDrop One Microvolume UV-Vis Spectrophotometer. The SuperScript™ III First-Strand Synthesis SuperMix (Invitrogen) was then used to generate cDNA for RT-PCR experiments. Semi-quantitative real time PCR was performed using SYBER Green (Roche 04707516001) on a Roche Lightcycler480 System, and Ct values were normalized to mouse beta-actin housekeeping gene.

Library Preparation. RNA samples were delivered to UCLA Microarray Core for processing. Briefly, libraries for RNASeq were prepared with Illumina stranded mRNA seq. The workflow consisted of mRNA enrichment, cDNA generation, and end repair to generate blunt ends, A-tailing, adaptor ligation, and PCR amplification. Different adaptors were used for multiplexing samples. The data was sequenced on HiSeq3000 using a single-read 50bp read run. Data

quality check was done on Illumina SAV. Demultiplexing was performed with Illumina Bcl2fastq2 v 2.17 program.

RNA-sequencing and IPA Analysis. According to the UCLA Microarray Core Project Report, the Partek flow and Ingenuity Pathway Analysis (IPA) were used for bioinformatics methods and data analysis, respectively. The trimming of bases was performed based on From 5' end, the bases to be trimmed was 5. The reads were mapped to the latest UCSC transcript set using STAR - 2.6.1d. The Partek E/M was used to quantify reads to an annotation model. After obtaining transcript counts, the counts were normalized by CPM (counts per million), 1.0E-4. The Principal Component Analysis (PCA) was applied to the transcript counts. The differential gene expression was examined between all conditions and control. For all results of differential gene expression analysis, the p-values, FDR, and fold changes (FC) filtered were applied. It was p<.01, FDR<.01, and |FC|>2 for all differential gene expression results. After applying the filter, the selected lists of genes were examined among lists pairing all conditions. The numbers of common transcripts were expressed as a Venn diagram. Using the list of significantly differentially expressed genes, the Canonical pathway analysis, Disease & Function analysis, and Networks analysis were performed by IPA. The results were included for each directory named by the comparison.

Statistical Analysis. Data were analyzed in Microsoft Excel, formatted in GraphPad Prism and error bars represent +/- SEM. An unpaired, two-tailed student's t-test determined significance, with values $P < 0.05$ considered statistically significant, denoted by asterisks ($^{*}P < 0.05$; $^{**}P <$ .01).

DATA availability statement

All data in this manuscript can be made available to interested parties. The RNA-seq data is currently being submitted to NIH-GEO for wide availability.

CRediT statement

MM, IA, JE collected and quantified all the data in the manuscript. JS and YCH provided critical tissue samples. RB provided a critical transgenic animal strain. MM and WEL generated the figures and wrote the manuscript.

Figures and Legends

Figure 1. Adrenergic receptor inputs and Creb signaling influence HFSC activation

(**A**) Hair cycle histogram of topical treatment with Adrb2 agonists isoproterenol, procaterol and vehicle control in telogen stage male mice. (**B**) Representative macroscopic images of vehicle control and treated dorsal areas. (**C**) **Top row**, pathological H&E examination of hair cycle stage over time points, where D50 indicated 50 days after birth of the animal. The first morphological signs of a telogen-anagen transition occur at D63. **Lower rows**, Immunohistochemistry with the indicated stains show the timing of activation of Creb (pCreb), the location of HFSCs (Sox9), and proliferation (Ki67). Scale bars, 50um top row, 25um bottom three rows. (**D**) Quantification of pCreb-positive and Ki67-positive cells in various murine hair follicle compartments. (**E**) Transcriptional levels of Adrb1 and Adrb 2 expression in human hair follicle compartments. ORS, outer root sheath; mat/cor/me, matrix/cortex/medulla; seb/apo, sebaceous/apocrine glands; IRS (Huxley/Henley) H/H, ORS Suprabasal (SB) (**F**) Analysis of Adrb gene expression in telogen-stage murine HFSCs. (**G**) Left, immunofluorescence of control and Adrb2 cKO hair follicles with DAPI in blue, pCreb in red, K5 in green, and Ki67 in white. Right, quantification of pCreb-positive and Ki67 positive cells in various murine hair follicle compartments of control and cKO skin tissue samples.

Figure 2. Stimulation of GPCR/cAMP/Creb signaling can accelerate the hair cycle

(**A**) Schematic of various topical pharmacological manipulations of the GPCR/cAMP/Creb signaling pathway in HFSC homeostasis. (**B**) Hair cycle histogram of topical treatment with adenylyl cyclase (AC) stimulant forskolin, and vehicle control in telogen stage male mice. (**C**) Hair cycle histogram of topical treatment with phosphodiesterase (PDE) inhibitors #44 and #61, and vehicle control in telogen stage male mice. (**D**) Hair cycle histogram of topical treatment with cyclic-AMP (cAMP) and vehicle control in telogen stage male mice. (**E**) Macroscopic images of long-term topical treatments. Mice were shaved at D45 and then treated every 48 hours with vehicle, or vehicle + the indicated treatment to stimulate Creb activity. In vehicle-treated animals, pigmentation and hair growth did not start until at least D76, whereas Pde inhibitor #44 or cAMP successfully stimulated accelerated this process by up to 14 days.

Figure 3. The effect of acute stimulation of Creb signaling on HFSCs.

(**A**) Immunohistochemistry of acute topical treatments with Creb stimulators. Tissues were probed for markers of active Creb (pCreb), HFSCs (Sox9), proliferating cells (PCNA), and Creb target gene protein expression (cFos). Scale bars, 25um. (**B**) Quantification of pCreb-positive (upper row) or PCNA-positive (lower row) cells in various hair follicle compartments. IFE = interfollicular epidermis. Data are mean +/- SEM.

Figure 4. A targeted, inducible K15-DREADD system for genetic stimulation of GPCR/cAMP/Creb signaling in HFSCs.

(**A**) Schematic depicting molecular genetics for targeting artificially activatable GPCR/Creb signaling exclusively in HFSCs via a DREADD-inducible GαS system. Cre-LoxP recombination is mediated by mifepristone, for the expression of DREADD allele in HFSCs. Topical CNO induction is sufficient to transdermally activate DREADD and polycistronic GFP expression. (**B**) K15 specific targeting of DREADD and GFP expression upon recombination and CNO induction

shows signal restricted to the hair follicle stem cell compartment during telogen in double (+/+) and single (+/wt) mutant DREADD HFSCs. (**C**) Representative macroscopic pictures of littermate controls, double mutant DREADD, and single mutant DREADD transgenic mice subjected to mifepristone-dependent recombination and CNO induction. (**D**) Quantification of time to hair cycle initiation was measured by initial macroscopic pigmentation and showed DREADD-positive animals consistently had accelerated hair cycling.

Figure 5. Transcriptome analyses suggest Creb signaling influences downstream glycolysis and metabolism in HFSCs.

(**A**) Schematic of RNA sequencing experimental workflow. (**B**) Venn diagram of overlapping genes in treated whole epidermis, identifying 859 genes consistently altered by Creb stimulation. (**C**) Top Canonical Pathways as revealed by transcriptome analysis of forskolin and cAMP treatment in total epidermis. (**D**) Top Upstream Regulators uncovered by RNA-seq and Gene Onotology (GO) enrichment analysis, revealing alteration of stress response pathways and key metabolic genes regulated glycolysis. (**E**) Western blot analysis verifying transcription analysis of Creb-related and glycolysis genes elevated in response to Creb activation.

Figure 6. Creb activation drives stimulation of Ldh activity through upregulation of Ldha protein and glycolytic metabolism

(**A**) Schematic of glycolysis pathway, intermediate metabolites, and related enzymes found in topical acute forskolin and cAMP treatments of total epidermis. Red arrows indicate approximate level of transcriptional upregulation according to RNA-sequencing results. (**B**) Immunohistochemistry of acute topical treatments with Creb stimulators. Tissues were probed for markers of glycolytic proteins Glut1, Hk2, and Pkm2. Scale bars, 25um. (**C**) Colorimetric *in situ* assay for Ldh enzyme shows robust activity in the bulge niche and epidermis of skin tissue topically treated with Creb stimulators. Subcutaneous muscle layer serves as an internal

positive control. Ldh activity is indicated by a deep purple color; light pink is a nuclear counterstain. Note thickening of epidermal layers with Creb treatment relative to control. Scale bar, 50um. (**D**) left, Plate reader-based colorimetric assay for Ldh enzyme further confirms results of increased Ldh enzyme behavior in acutely treated total epidermis. Right, RNA was extracted from whole epidermis and respective cDNA was generated for semi-quantitative RT-PCR. RT-PCR analysis revealed transcriptional changes in glycolysis-related enzymes Ldha and Txnip upon forskolin and cAMP treatment. A paired t-test was used to evaluate statistical significance, where * $p < 0.05$, ** $p < 0.01$, *** $p < 0.001$. (**E**) Mice were topically treated with either vehicle or cAMP for two days and then injected with C13-Glucose just prior to sacrifice. Punch biopsies were acquired and dissociated for preparation for mass spectrometry. Shown are the relative proportions of each metabolite in the glucose utilization pathway that was labeled with C13.

References

Uncategorized References

Botchkarev VA, Peters EM, Botchkareva NV, Maurer M, Paus R (1999) Hair cycle-dependent changes in adrenergic skin innervation, and hair growth modulation by adrenergic drugs. *J Invest Dermatol* 113:878-87.

Carmon KS, Gong X, Lin Q, Thomas A, Liu Q (2011) R-spondins function as ligands of the orphan receptors LGR4 and LGR5 to regulate Wnt/beta-catenin signaling. *Proc Natl Acad Sci U S A* 108:11452-7.

Cinkornpumin J, Roos M, Nguyen L, Liu X, Gaeta X, Lin S, *et al.* (2017) A small molecule screen to identify regulators of let-7 targets. *Sci Rep* 7:15973.

Cleale RM, Ingling JM, Search DJ, Hadcock JR, Pausch MH (1998) Effects of alpha2-adrenoceptor antagonists on metabolic processes of swine: I. Effects on nonesterified fatty acid and plasma urea nitrogen concentrations in jugularly catheterized pigs. *J Anim Sci* 76:1838-48.

Flores A, Schell J, Krall AS, Jelinek D, Miranda M, Grigorian M, *et al.* (2017) Lactate dehydrogenase activity drives hair follicle stem cell activation. *Nat Cell Biol* 19:1017-26.

Fuchs E, Merrill BJ, Jamora C, DasGupta R (2001) At the roots of a never-ending cycle. *Dev Cell* 1:13-25.

Hathirat S, Himathongkam T, Triyanond K, Lochaya S (1980) Cardiac arrest and alopecia induced by beta-blocker. *J Med Assoc Thai* 63:621-4.

Iglesias-Bartolome R, Torres D, Marone R, Feng X, Martin D, Simaan M, *et al.* (2015) Inactivation of a Galpha(s)-PKA tumour suppressor pathway in skin stem cells initiates basal-cell carcinogenesis. *Nat Cell Biol* 17:793-803.

Lapouge G, Youssef KK, Vokaer B, Achouri Y, Michaux C, Sotiropoulou PA, *et al.* (2011) Identifying the cellular origin of squamous skin tumors. *Proceedings of the National Academy of Sciences of the United States of America* 108:7431-6.

Lavker RM, Sun TT, Oshima H, Barrandon Y, Akiyama M, Ferraris C, *et al.* (2003) Hair follicle stem cells. *J Investig Dermatol Symp Proc* 8:28-38.

Meinkoth JL, Alberts AS, Went W, Fantozzi D, Taylor SS, Hagiwara M, *et al.* (1993) Signal transduction through the cAMP-dependent protein kinase. *Mol Cell Biochem* 127-128:179-86.

Miranda M, Christofk H, Jones DL, Lowry WE (2018) Topical Inhibition of the Electron Transport Chain Can Stimulate the Hair Cycle. *J Invest Dermatol* 138:968-72.

Morris RJ, Potten CS (1999) Highly persistent label-retaining cells in the hair follicles of mice and their fate following induction of anagen. *J Invest Dermatol* 112:470-5.

Peters EM, Maurer M, Botchkarev VA, Gordon DS, Paus R (1999) Hair growth-modulation by adrenergic drugs. *Exp Dermatol* 8:274-81.

Plikus MV (2012) New activators and inhibitors in the hair cycle clock: targeting stem cells' state of competence. *The Journal of investigative dermatology* 132:1321-4.

Plikus MV, Mayer JA, de la Cruz D, Baker RE, Maini PK, Maxson R, *et al.* (2008) Cyclic dermal BMP signalling regulates stem cell activation during hair regeneration. *Nature* 451:340-4.

Rozenberg J, Rishi V, Orosz A, Moitra J, Glick A, Vinson C (2009) Inhibition of CREB function in mouse epidermis reduces papilloma formation. *Molecular cancer research : MCR* 7:654-64.

Shelley ED, Shelley WB (1985) Alopecia and drug eruption of the scalp associated with a new beta-blocker, nadolol. *Cutis* 35:148-9.

Shwartz Y, Gonzalez-Celeiro M, Chen CL, Pasolli HA, Sheu SH, Fan SM, *et al.* (2020) Cell Types Promoting Goosebumps Form a Niche to Regulate Hair Follicle Stem Cells. *Cell* 182:578-93 e19.

Sun Y, McGarrigle D, Huang XY (2007) When a G protein-coupled receptor does not couple to a G protein. *Mol Biosyst* 3:849-54.

Syrovatkina V, Alegre KO, Dey R, Huang XY (2016) Regulation, Signaling, and Physiological Functions of G-Proteins. *J Mol Biol* 428:3850-68.

Tatu AL, Elisei AM, Chioncel V, Miulescu M, Nwabudike LC (2019) Immunologic adverse reactions of beta-blockers and the skin. *Exp Ther Med* 18:955-9.

White AC, Khuu JK, Dang CY, Hu J, Tran KV, Liu A, *et al.* (2014) Stem cell quiescence acts as a tumour suppressor in squamous tumours. *Nat Cell Biol* 16:99-107.

White AC, Tran K, Khuu J, Dang C, Cui Y, Binder SW, *et al.* (2011) Defining the origins of Ras/p53-mediated squamous cell carcinoma. *Proc Natl Acad Sci USA* 108:7425-30.

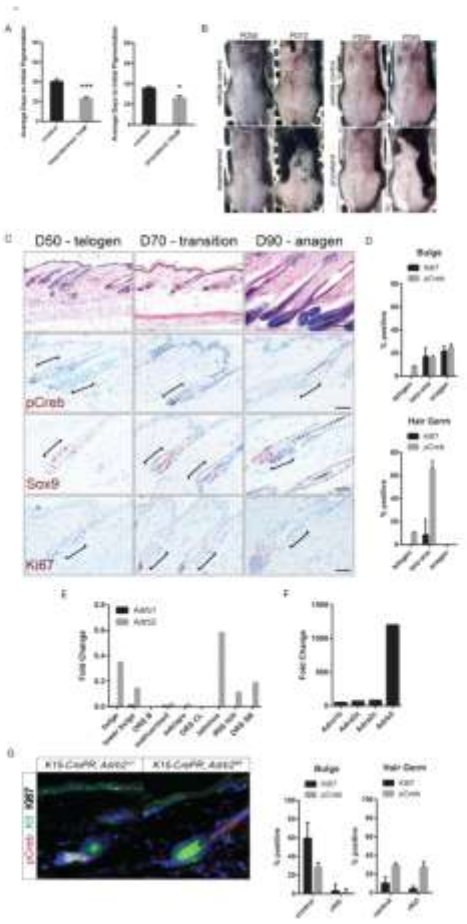

Figure 1. Adrenergic receptor inputs and Creb signaling influence HFSC activation
(A) Hair cycle histogram of topical treatment with Adrb2 agonists isoproterenol, procaterol and vehicle control in telogen stage male mice. (B) Representative macroscopic images of vehicle control and treated dorsal areas. (C) Top row, pathological H&E examination of hair cycle stage over time points, where D50 indicated 50 days after birth of the animal. The first morphological signs of a telogen-anagen transition occur at D63. Lower rows, Immunohistochemistry with the indicated stains show the timing of activation of Creb (pCreb), the location of HFSCs (Sox9), and proliferation (Ki67). Scale bars, 50um top row, 25um bottom three rows. (D) Quantification of pCreb-positive and Ki67-positive cells in various murine hair follicle compartments. (E) Transcriptional levels of Adrb1 and Adrb 2 expression in human hair follicle compartments. ORS, outer root sheath; mat/cor/me, matrix/cortex/medulla; seb/apo, sebaceous/apocrine glands; IRS (Huxley/Henley) H/H, ORS Suprabasal (SB) (F) Analysis of Adrb gene expression in telogen-stage murine HFSCs. (G) Left, immunofluorescence of control and Adrb2 cKO hair follicles with DAPI in blue, pCreb in red, K5 in green, and Ki67 in white. Right, quantification of pCreb-positive and Ki67 positive cells in various murine hair follicle compartments of control and cKO skin tissue samples.

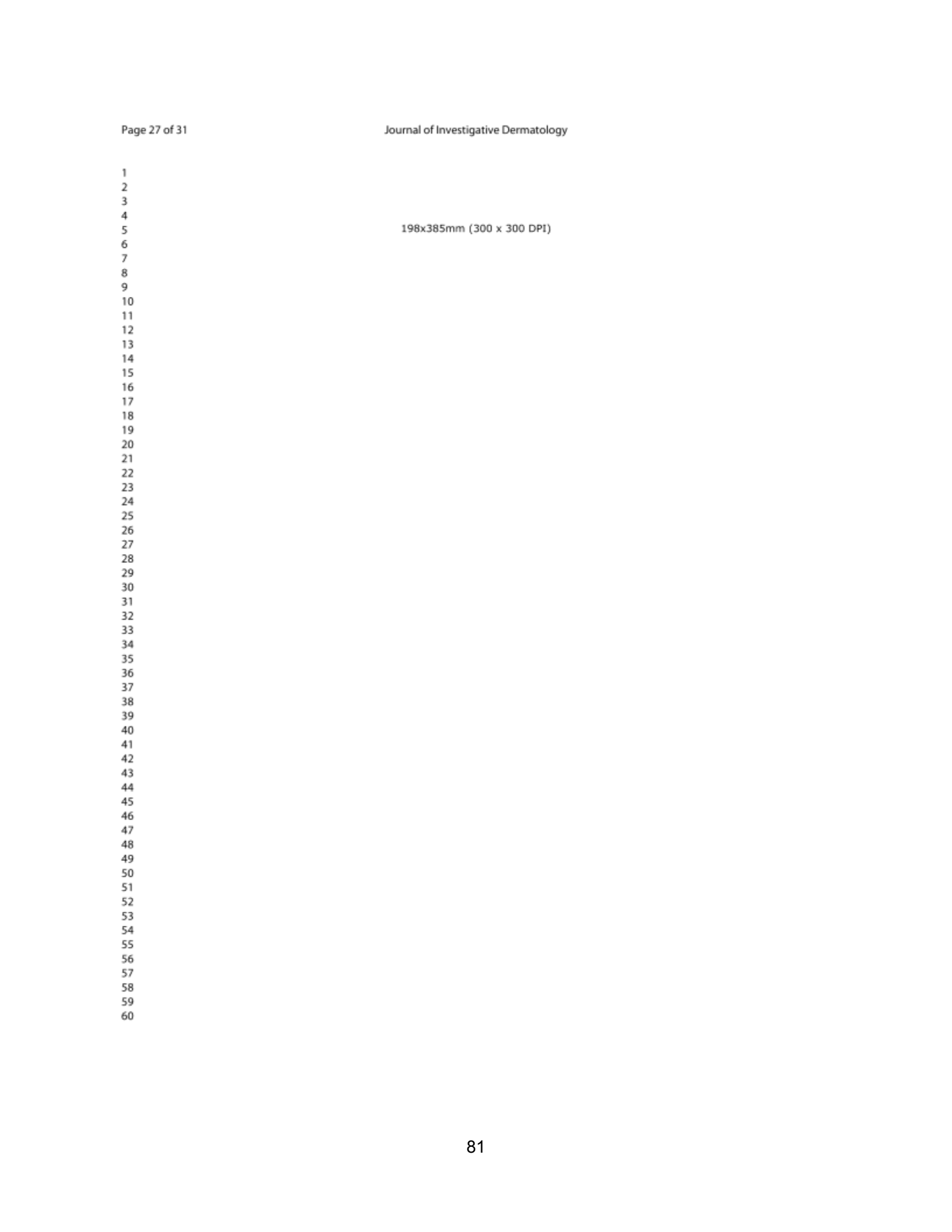
198x385mm (300 x 300 DPI)

Figure 2

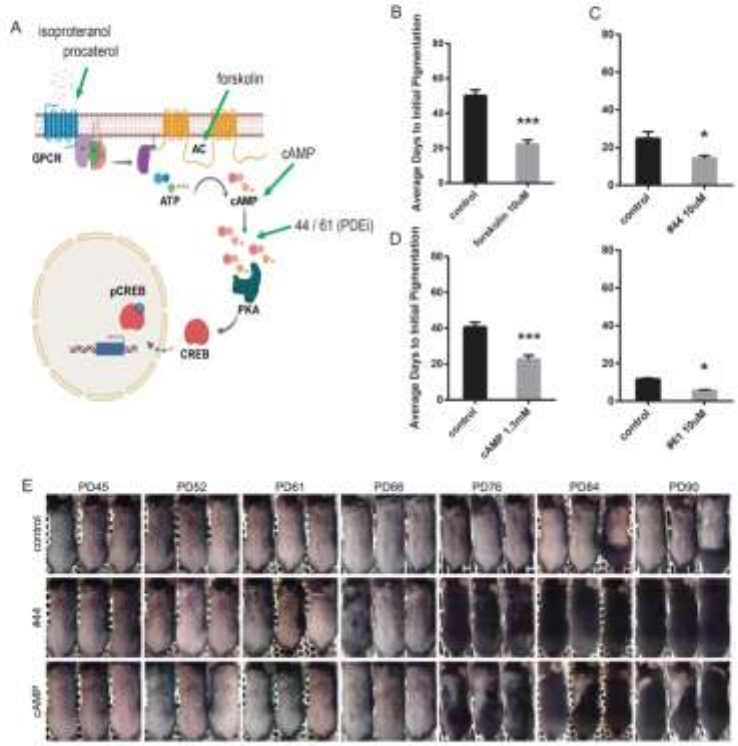

Figure 2. Stimulation of GPCR/cAMP/Creb signaling can accelerate the hair cycle
(A) Schematic of various topical pharmacological manipulations of the GPCR/cAMP/Creb signaling pathway in HFSC homeostasis. (B) Hair cycle histogram of topical treatment with adenylyl cyclase (AC) stimulant forskolin, and vehicle control in telogen stage male mice. (C) Hair cycle histogram of topical treatment with phosphodiesterase (PDE) inhibitors #44 and #61, and vehicle control in telogen stage male mice. (D) Hair cycle histogram of topical treatment with cyclic-AMP (cAMP) and vehicle control in telogen stage male mice. (E) Macroscopic images of long-term topical treatments. Mice were shaved at D45 and then treated every 48 hours with vehicle, or vehicle + the indicated treatment to stimulate Creb activity. In vehicle-treated animals, pigmentation and hair growth did not start until at least D76, whereas Pde inhibitor #44 or cAMP successfully stimulated accelerated this process by up to 14 days.

192x193mm (300 x 300 DPI)

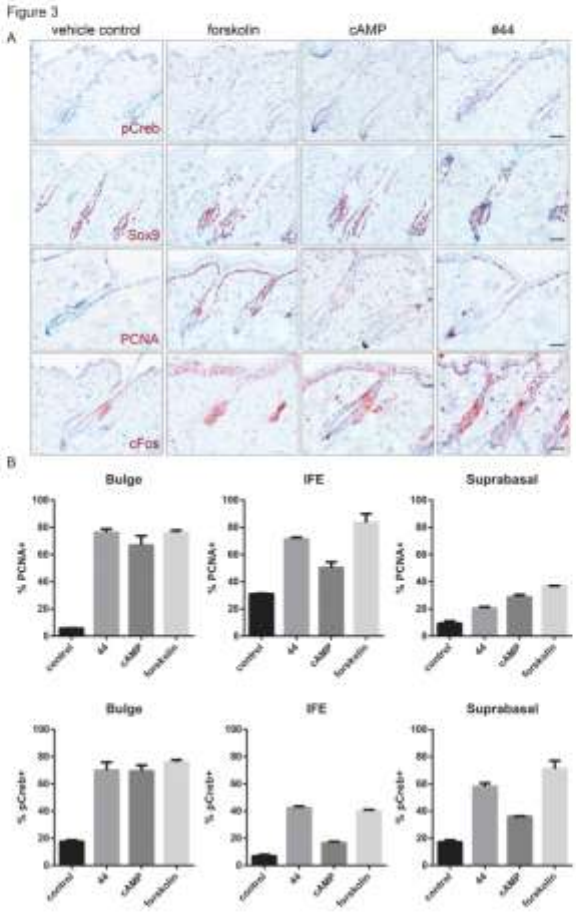

Figure 3. The effect of acute stimulation of Creb signaling on HFSCs.
(A) Immunohistochemistry of acute topical treatments with Creb stimulators. Tissues were probed for markers of active Creb (pCreb), HFSCs (Sox9), proliferating cells (PCNA), and Creb target gene protein expression (cFos). Scale bars, 25um. (B) Quantification of pCreb-positive (upper row) or PCNA-positive (lower row) cells in various hair follicle compartments. IFE = interfollicular epidermis. Data are mean +/- SEM.

174x274mm (300 x 300 DPI)

Figure 4

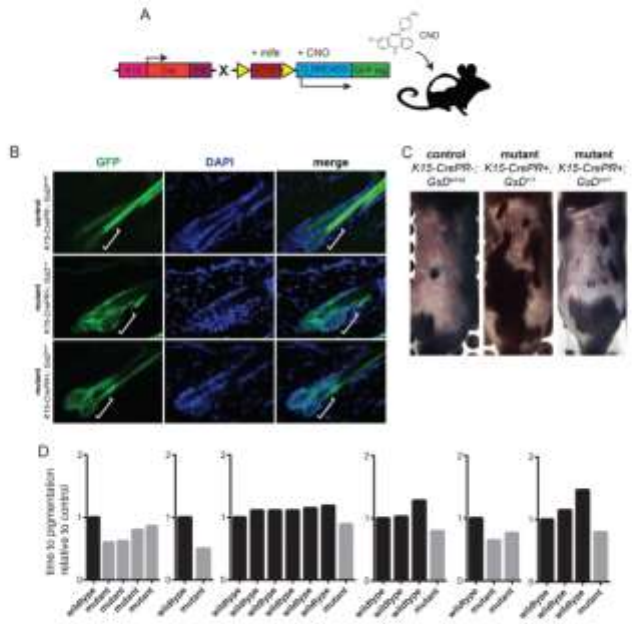

Figure 4. A targeted, inducible K15-DREADD system for genetic stimulation of GPCR/cAMP/Creb signaling in HFSCs.

(A) Schematic depicting molecular genetics for targeting artificially activatable GPCR/Creb signaling exclusively in HFSCs via a DREADD-inducible G□S system. Cre-LoxP recombination is mediated by mifepristone, for the expression of DREADD allele in HFSCs. Topical CNO induction is sufficient to transdermally activate DREADD and polycistronic GFP expression. (B) K15 specific targeting of DREADD and GFP expression upon recombination and CNO induction shows signal restricted to the hair follicle stem cell compartment during telogen in double (+/+) and single (+/wt) mutant DREADD HFSCs. (C) Representative macroscopic pictures of littermate controls, double mutant DREADD, and single mutant DREADD transgenic mice subjected to mifepristone-dependent recombination and CNO induction. (D) Quantification of time to hair cycle initiation was measured by initial macroscopic pigmentation and showed DREADD-positive animals consistently had accelerated hair cycling.

204x180mm (300 x 300 DPI)

Figure 5

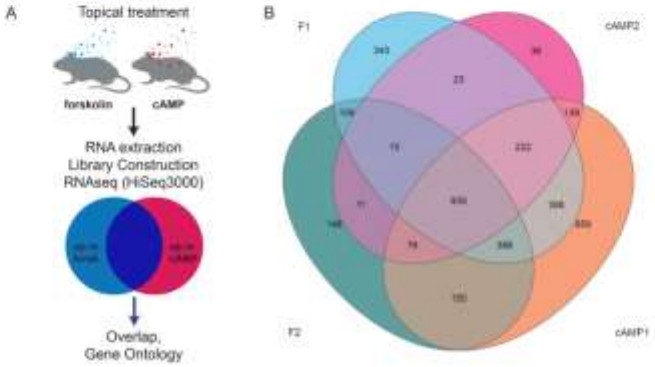

C

Top Canonical Pathways	
Name	-log(p-value)
Unfolded protein response	15.2
Mitochondrial Dysfunction	13.1
Sirtuin Signaling Pathway	11.4
Oxidative Phosphorylation	9.28
EIF2 Signaling	9.27
Superpathway of Cholesterol Biosynthesis	9.16
TCA Cycle II (Eukaryotic)	8.68
Huntington's Disease Signaling	7.48
Epithelial Adherens Junction Signaling	7.37
Fatty Acid β-oxidation I	7.26

D

Top Upstream Regulators	
Name	p-value
TP53	2.45E-42
MYC	1.64E-29
CD 437	1.34E-28
1,2-dithiol-3-thione	2.64E-27
NFE2L2	1.55E-26

Figure 5. Transcriptome analyses suggest Creb signaling influences downstream glycolysis and metabolism in HFSCs.

(A) Schematic of RNA sequencing experimental workflow. (B) Venn diagram of overlapping genes in treated whole epidermis, identifying 859 genes consistently altered by Creb stimulation. (C) Top Canonical Pathways as revealed by transcriptome analysis of forskolin and cAMP treatment in total epidermis. (D) Top Upstream Regulators uncovered by RNA-seq and Gene Onotology (GO) enrichment analysis, revealing alteration of stress response pathways and key metabolic genes regulated glycolysis. (E) Western blot analysis verifying transcription analysis of Creb-related and glycolysis genes elevated in response to Creb activation.

175x239mm (300 x 300 DPI)

Figure 6

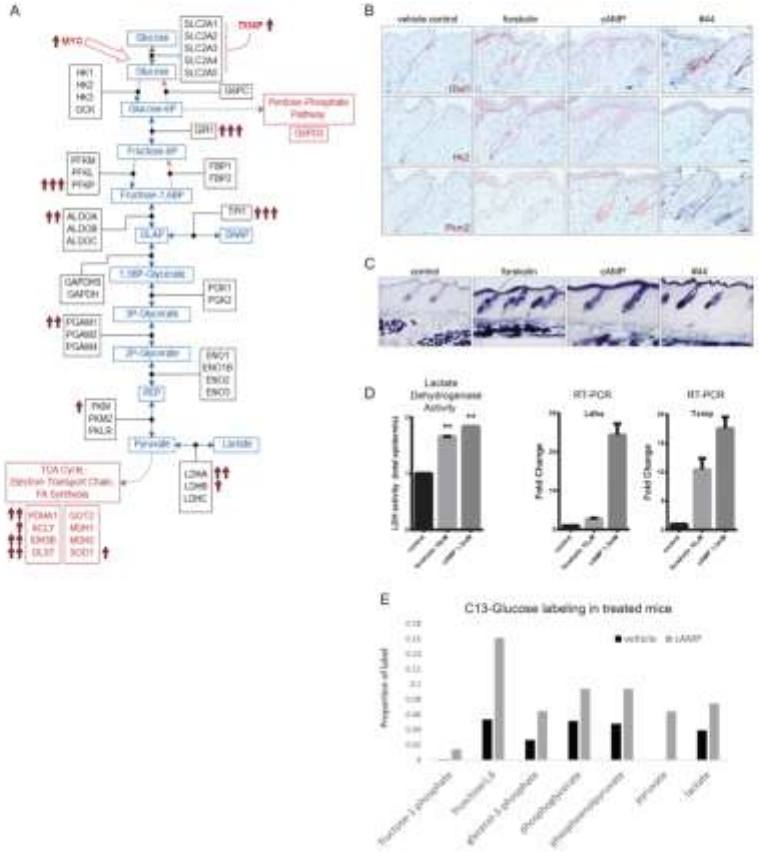

Figure 6. Creb activation drives stimulation of Ldh activity through upregulation of Ldha protein and glycolytic metabolism

(A) Schematic of glycolysis pathway, intermediate metabolites, and related enzymes found in topical acute forskolin and cAMP treatments of total epidermis. Red arrows indicate approximate level of transcriptional upregulation according to RNA-sequencing results. (B) Immunohistochemistry of acute topical treatments with Creb stimulators. Tissues were probed for markers of glycolytic proteins Glut1, Hk2, and Pkm2. Scale bars, 25um. (C) Colorimetric in situ assay for Ldh enzyme shows robust activity in the bulge niche and epidermis of skin tissue topically treated with Creb stimulators. Subcutaneous muscle layer serves as an internal positive control. Ldh activity is indicated by a deep purple color; light pink is a nuclear counterstain. Note thickening of epidermal layers with Creb treatment relative to control. Scale bar, 50um. (D) left, Plate reader-based colorimetric assay for Ldh enzyme further confirms results of increased Ldh enzyme behavior in acutely treated total epidermis. Right, RNA was extracted from whole epidermis and respective cDNA was generated for semi-quantitative RT-PCR. RT-PCR analysis revealed transcriptional changes in glycolysis-related enzymes Ldha and Txnip upon forskolin and cAMP treatment. A paired t-test was used to evaluate

statistical significance, where * $p < 0.05$, ** $p < 0.01$, *** $p < 0.001$. (E) Mice were topically treated with either vehicle or cAMP for two days and then injected with C13-Glucose just prior to sacrifice. Punch biopsies were acquired and dissociated for preparation for mass spectrometry. Shown are the relative proportions of each metabolite in the glucose utilization pathway that was labeled with C13.

211x255mm (300 x 300 DPI)

Chapter 5: Conclusions

Closing Remarks:
Finding the Root(s) of Molecular Regulation of Hair Growth

Future Directions

Skin is a deceptively simple organ. The associated hair follicle will still be a source of mystery for many researchers to come. Despite all the established mechanisms of hair follicle regulation, not one signaling pathway is revered to reign supreme for HFSC activation/quiescence. While hair research has certainly advanced with uncovering pathway after pathway, the idea of a "master regulator" of hair cycling remains elusive. Is there really one signal to rule them all? Might it be as simple as raising glycolytic capacity to nourish growing hair follicle progenitors? More work is certainly needed to uncover the common denominator in HFSC activation. This information will be useful as it may extend to other adult stem cell niches.

The source of the stimulus that shifts HFSCs from telogen to anagen is a controversial topic; there is evidence that signals can originate from the DP, from the adjacent epidermal tissue, from supportive tissues such as adipocytes, and (as of recently) even through sympathetic innervations, as we propose in our work[1-13]. What we would like to highlight is that both adrenergic signaling and metabolism intersect for adult stem cell maintenance in tissues and organs. To date, we are the first to report GPCR signaling and metabolism in hair follicle cycling. It is conceivable that dysregulation of these processes occurs in skin aging and aging-associated alopecia. As a matter of fact, studying the molecular biology of metabolism and GPCR/cAMP/Creb signaling in the context of aging has always captured my interest, but that is work for the next eager Lowry Lab member.

One large question that has gone unanswered is if Lgr5 in HFSCs functions through classical GPCR signaling. Several reports show it works in concert with Wnt

signaling to accelerate the hair cycle[14], so it would be worthwhile to validate any shared target genes upon Lef and Creb transcriptional activity.

My mechanistic work of GPCR/cAMP/Creb signaling in HFSC homeostasis also can be explored in the molecular development of epidermal cancers. Many adult stem cells provide the service of regulating homeostasis in particular organs, being able to cycle between quiescence and activation with the appropriate milieu of signals. However, this ability can also implicate them in transformation due to their highly proliferative capacity and relative dormancy in comparison to other cells in a tissue. Hair follicle stem cells are one such example – and have indeed been shown as a cancer cell of origin for squamous cell carcinoma (SCC) in a murine model[15, 16]. This is also the case with basal cell carcinoma (BCC) development and Gα overexpression or PKA deletion[17]. SCC is an extremely invasive, non-melanoma skin cancer with a high risk of metastasis; metastatic SCC usually predicts a poor prognosis. Previous work performed in the Lowry lab identified murine HFSCs as a cell of origin for SCC[15], in addition to listing the genetic hits necessary for inducing SCC. To experimentally induce SCC, one can introduce oncogenic stress (via active Ras signaling and *p53* ablation) during telogen-to-anagen transition or use a two-step chemical carcinogenesis technique to activate HFSCs and coax tumor development. However, quiescent HFSCs are unable to develop into squamous cell carcinoma even in this context. Previous work also performed in the Lowry lab states quiescence may in fact function as a tumor suppressor in the face of SCC tumorigenesis[18]. It is highly possible that controlling the hair cycle also controls skin cancer sensitivity in respect to SCC initiation. It would also be interesting to test this theory with upstream approach to test if adrenergic signaling

functions in carcinogenesis. In fact, I am currently performing this experiment; we are using Adrb1,2 null mice subjected to DMBA/TPA chemical carcinogenesis protocol. We are also testing if deletion of one or both alleles of Adrb2 might yield protection from epidermal cancer(s). Results are forthcoming.

Creb is implicated in epidermal cancers when mutated in murine skin. If a dominant negative or nonfunctional Creb is present in epidermal stem cells, papilloma and consequent SCC development is significantly reduced in spite chemical carcinogenesis treatment[19]. Papillomas are benign, hyperplastic growths on the skin that can sometimes develop into *bona fide* SCC. This means that Creb may function in the early stages of papilloma formation/SCC, thus implicating another player in SCC development. Notwithstanding, our lab aims to implicate canonical GPCR/Creb signaling as one of (perhaps, the) master regulators of hair follicle control that also has connections to initiating epidermal cancers.

Advances in SCC treatment will therefore highly benefit from elucidating the cell biology and molecular processes that transform homeostatic activities into malignant disorders. The extensive characterization of GPCR/Creb signaling in hair follicle cycling will ultimately yield translational impacts such as discovering novel methods to not only regulate the hair cycle but to also provide a mechanism by which Creb is able to promote or prevent epidermal tumors.

References

1. Blanpain, C. and E. Fuchs, *Epidermal homeostasis: a balancing act of stem cells in the skin.* Nature reviews Molecular cell biology, 2009. **10**(3): p. 207-217.
2. Chen, C.-L., et al., *Functional complexity of hair follicle stem cell niche and therapeutic targeting of niche dysfunction for hair regeneration.* Journal of Biomedical Science, 2020. **27**(1): p. 1-11.
3. Houschyar, K.S., et al., *Molecular mechanisms of hair growth and regeneration: Current understanding and novel paradigms.* Dermatology, 2020: p. 1-10.
4. Hsu, Y.-C., L. Li, and E. Fuchs, *Emerging interactions between skin stem cells and their niches.* Nature medicine, 2014. **20**(8): p. 847-856.
5. Itami, S., et al., *Mechanism of action of androgen in hair follicles.* Journal of dermatological science, 1994. **7**: p. S98-S103.
6. Lee, J. and T. Tumbar. *Hairy tale of signaling in hair follicle development and cycling*. in *Seminars in cell & developmental biology*. 2012. Elsevier.
7. Leiros, G.J., A.I. Attorresi, and M.E. Balaña, *Hair follicle stem cell differentiation is inhibited through cross-talk between Wnt/β-catenin and androgen signalling in dermal papilla cells from patients with androgenetic alopecia.* British Journal of Dermatology, 2012. **166**(5): p. 1035-1042.
8. Lin, S.-J., et al., *Hair Follicle Stem Cells and Hair Regeneration.* Cell Engineering and Regeneration, 2020: p. 265-296.
9. Plikus, M.V. and C.-M. Chuong, *Macroenvironmental regulation of hair cycling and collective regenerative behavior.* Cold Spring Harbor perspectives in medicine, 2014. **4**(1): p. a015198.
10. Schneider, M.R., R. Schmidt-Ullrich, and R. Paus, *The hair follicle as a dynamic miniorgan.* Current Biology, 2009. **19**(3): p. R132-R142.
11. Stenn, K. and R. Paus, *Controls of hair follicle cycling.* Physiological reviews, 2001.
12. Miranda, M., et al., *Topical Inhibition of the Electron Transport Chain Can Stimulate the Hair Cycle.* The Journal of investigative dermatology, 2018. **138**(4): p. 968.

13. Shwartz, Y., et al., *Cell Types Promoting Goosebumps Form a Niche to Regulate Hair Follicle Stem Cells.* Cell, 2020. **182**(3): p. 578-593. e19.
14. Barker, N., S. Tan, and H. Clevers, *Lgr proteins in epithelial stem cell biology.* Development, 2013. **140**(12): p. 2484-2494.
15. White, A.C., et al., *Defining the origins of Ras/p53-mediated squamous cell carcinoma.* Proceedings of the National Academy of Sciences, 2011. **108**(18): p. 7425-7430.
16. Lapouge, G., et al., *Identifying the cellular origin of squamous skin tumors.* Proceedings of the National Academy of Sciences, 2011. **108**(18): p. 7431-7436.
17. Iglesias-Bartolome, R., et al., *Inactivation of a Gα s–PKA tumour suppressor pathway in skin stem cells initiates basal-cell carcinogenesis.* Nature cell biology, 2015. **17**(6): p. 793-803.
18. White, A., et al., *Stem cell quiescence acts as a tumour suppressor in squamous tumours.* Nature cell biology, 2014. **16**(1): p. 99-107.
19. Rozenberg, J., et al., *Inhibition of CREB function in mouse epidermis reduces papilloma formation.* Molecular Cancer Research, 2009. **7**(5): p. 654-664.